



**UNIVERSIDAD NACIONAL AUTÓNOMA DE MÉXICO
PROGRAMA DE POSGRADO EN ASTRONOMÍA
INSTITUTO DE ASTRONOMÍA**

**LA CONEXIÓN GALAXIA-HALO:
RELACIONES DE ESCALA**

TESIS

**QUE PARA OPTAR POR EL GRADO DE:
MAESTRA EN CIENCIAS (ASTRONOMÍA)**

**PRESENTA:
BRISA LLANETH MANCILLAS VAQUERA**

**TUTOR:
DR. VLADIMIR ANTÓN ÁVILA REESE,
INSTITUTO DE ASTRONOMÍA-UNAM**

MÉXICO, D.F., OCTUBRE 2014



UNAM – Dirección General de Bibliotecas

Tesis Digitales
Restricciones de uso

DERECHOS RESERVADOS ©
PROHIBIDA SU REPRODUCCIÓN TOTAL O PARCIAL

Todo el material contenido en esta tesis está protegido por la Ley Federal del Derecho de Autor (LFDA) de los Estados Unidos Mexicanos (México).

El uso de imágenes, fragmentos de videos, y demás material que sea objeto de protección de los derechos de autor, será exclusivamente para fines educativos e informativos y deberá citar la fuente donde la obtuvo mencionando el autor o autores. Cualquier uso distinto como el lucro, reproducción, edición o modificación, será perseguido y sancionado por el respectivo titular de los Derechos de Autor.

Resumen

A través de un modelo donde se cargan discos en equilibrio centrífugo en halos de materia oscura fría y considerando su contracción adiabática por la galaxia formada, exploramos de manera (semi)empírica las relaciones de escala y otras correlaciones de la población de galaxias de disco en el Universo local. El modelo considera también la formación de bulbos y la transformación de gas en estrellas por inestabilidades del disco. Las simulaciones cosmológicas numéricas proveen las condiciones iniciales: la distribución de masa y los parámetros de giro λ y concentración C de los halos. La condición inicial astrofísica la da la relación de la fracción bariónica con la masa del halo, $f_{\text{bar}}-M_h$. Esta relación contiene información de los principales procesos de incorporación y pérdida de bariones por parte de las galaxias. Nuestro objetivo es explorar los efectos de esta relación sobre las correlaciones globales y distribuciones internas de masa de las galaxias de disco en función de su escala.

Se generó un catálogo sintético de decenas de miles de galaxias formadas en halos de masas entre 10^{10} y $10^{14} M_\odot$. Las relaciones estelares y bariónicas de radio-masa y Tully-Fisher (TF) predichas, así como correlaciones de los cocientes de masa bulbo/total (B/T) y gas/estrellas (R_{gas}) con M_* , reproducen bien las observaciones correspondientes que hemos compilado, pero sólo hasta $M_* \approx 3 - 5 \times 10^{10} M_\odot$; para masas mayores en promedio los radios y V_{max} son muy grandes, B/T muy bajo y R_{gas} muy alto. Esto es debido a que f_{bar} disminuye considerablemente con M_h . No obstante, hay que tomar en cuenta que halos muy masivos ensamblan fracciones importantes de sus masas en fusiones lo cual implica que sus galaxias sufrirán también fusiones e interacciones.

Introduciendo artificialmente el efecto de inestabilidad por las fusiones, los bulbos son mayores y el contenido de gas y el parámetro de giro disminuyen. Nuestro enfoque es heurístico ya que el efecto artificial es afinado para reproducir las relaciones observadas de radio- M_* , B/T- M_* y $R_{\text{gas}}-M_*$ a las altas masas. El método ofrece

entonces una sofisticada herramienta para estimar el parámetro de giro inicial de los bariones de los que se forman las galaxias de disco, λ_{bar} . Hasta $\log(M_h/M_\odot) \sim 11.5$, λ_{bar} promedio y su dispersión son las mismas que las de los halos, pero a masas mayores λ_{bar} promedio disminuye con M_h (y M_* por ende). Las relaciones predichas de TF estelar y bariónica concuerdan con las observaciones. No hay un problema con el punto cero, siendo que por construcción nuestros modelos están de acuerdo con la función de masa bariónica (y estelar) observada. A bajas masas, la TF estelar sufre un doblez que aparentemente también lo muestran las galaxias enanas; a nivel de TF bariónica este doblez es menor. A altas masas, los modelos muestran también un cierto doblez. La dispersión intrínseca de los modelos es mayor a la que presentan las observaciones. Este podría ser un potencial problema. La dispersión de la relación radio– M_* es alta y producida por la dispersión "cosmológica" del parámetro λ_{bar} así como por las dispersiones de f_{bar} y C . En el caso de la relación TF, la dispersión es menor y producida principalmente por la dispersión "cosmológica" de C . Se encuentran también algunas tendencias débiles de los residuales de las relaciones de escala con propiedades de las galaxias como R_{gas} , B/T y la densidad superficial Σ_e . Los residuales de la relación $M_{\text{bar}}-M_h$ muestran una mayor correlación con estas propiedades.

El modelo nos permite explorar el efecto de la relación global $f_{\text{bar}}-M_h$ y su dispersión sobre la distribución interna de masas de halo, disco y bulbo. Encontramos que el cociente de velocidades de disco a total a 2.2 radios de escala es siempre del tipo submáximo. La fracción de masa "luminosa" a un radio efectivo ($1R_e$) de las galaxias tiene su máximo (alrededor de 0.5 en promedio) para galaxias con $V_{\text{max}} \approx 200 \text{ km/s}$, $\Sigma_e \approx 500 \text{ M}_\odot/\text{pc}^2$, y $M_* \approx 5 \times 10^{10} \text{ M}_\odot$. Para valores menores que estos, las galaxias de disco ($B/T \leq 0.5$) son más y más dominadas por materia oscura a $1R_e$, pero para valores mayores, también; es una clara huella de la forma de la relación $f_{\text{bar}}-M_h$. Esta huella se ve también en las correlaciones con M_* o Σ_e de los cocientes de velocidad del disco (o disco + bulbo) a velocidad total o de la pendiente del perfil externo de las curvas de rotación. Estas correlaciones se podrán obtener con resultados de futuros catastros espectroscopicos que barran un amplio intervalo de masas y densidades superficiales de galaxias de disco.

Contents

1	Introduction	1
1.1	Antecedentes y planteamiento	1
1.2	Objetivos y Metodología de la Tesis	7
1.3	Contenido	9
2	Observational correlations of disk galaxies	11
2.1	The (semi-empirical) baryonic-to-halo mass relation	12
2.2	The size-stellar mass relation	19
2.3	The Tully-Fisher relation	24
2.4	The bulge-to-total mass ratio vs M_*	26
2.5	The gas-to-stellar mass ratio vs. stellar mass	28
3	The Semi-empirical Method	30
3.1	The static model	30
3.1.1	A disk-halo model	30
3.1.2	A disk-bulge-halo model	34
3.1.3	Stellar and gas fractions	39
3.2	The procedure	43
4	Disk galaxy correlations: the case of isolated galaxies	47
4.1	Results	48
4.2	Summary and discussion	57
5	A semi-empirical picture of local disk galaxy correlations	59
5.1	Disk galaxy correlations	61

5.1.1	The size–mass relation and inference of the spin parameter of galaxies	61
5.1.2	The B/T– M_* , $R_{\text{gas}}–M_*$ and $\Sigma_{\text{e}}–M_*$ correlations	66
5.1.3	The Tully–Fisher relations	71
5.1.3.1	The intrinsic scatter around the TF relations	75
5.2	The source of scatter in the disk scaling relations	76
5.3	On the scatter of the $M_{\text{bar}}–M_h$ and $M_*–M_h$ relations	82
5.4	Correlations among the residuals of the scaling relations	83
6	The inner mass distributions of the semi-empirical disk galaxies	86
6.1	Galaxy-to-total maximum velocity ratios	86
6.2	The inner baryon and dark matter mass fractions	91
6.3	The outer slope of the circular velocity curves	93
7	Summary and conclusions	97
A	The empirical HI-to-M_* and H₂-to-M_* correlations for local late- and early-type galaxies	104

Chapter 1

Introduction

1.1 Antecedentes y planteamiento

Las galaxias de disco son el tipo más frecuente de estos objetos en el Universo local y todo apunta a que fueron aún más abundantes en el pasado (v.gr. Bruce et al., 2012; Buitrago et al., 2013; Mortlock et al., 2013, ver predicciones teóricas en Avila-Reese et al. 2014 y más referencias ahí). Una serie de evidencias observacionales sugieren que la formación de discos es el proceso genérico de ensamblaje de las galaxias, mientras que las componentes esferoidales se desarrollan a partir de los discos en procesos violentos de fusiones e interacciones, así como producto de su evolución secular. Como resultado de las fusiones se espera la formación de esferoides (bulbos) prominentes del tipo "clásicos" (por ejemplo las galaxias elípticas), mientras que el segundo tipo de mecanismos lleva a los así llamados pseudobulbos, mismos que lucen como prolongaciones del disco interno, compartiendo propiedades con el mismo (ver una reseña en Kormendy and Kennicutt, 2004).

Desde la perspectiva teórica, la formación y evolución de galaxias requiere del marco cosmológico. El vertiginoso desarrollo de la cosmología en los últimos lustros ofrece ahora un contexto maduro y cimentado en un gran cuerpo de observaciones para calcular la evolución de las galaxias (ver reseñas al respecto en Avila-Reese, 2006; Frenk and White, 2012). El paradigma cosmológico actual se resume en el así llamado modelo de materia oscura fría con constante cosmológica Λ (Λ CDM por sus siglas en inglés). De acuerdo al mismo, las estructuras cósmicas emergen de tenues perturbaciones en densidad que a su vez provienen de las fluctuaciones

cuánticas del universo inflacionario. Estas perturbaciones evolucionan gravitacionalmente hasta separarse de la expansión y colapsan en estructuras autogravitantes que llamamos halos. En el contexto del modelo Λ CDM se propone que la materia está dominada por una componente invisible (no interactúa con la radiación) pero que produce gravedad, llamada "materia oscura". La materia oscura, según sondeos cosmológicos y astronómicos es ≈ 5 veces más abundante que la materia ordinaria, llamada bariónica. Y ambas son sólo el 30% de lo que está actualmente compuesto el Universo; el restante 70% es la así llamada energía oscura, un medio repulsivo que produce la expansión acelerada del Universo; la determinación más reciente de los parámetros cosmológicos fueron dados por la misión *Planck* y una combinación de varios sondeos (Planck Collaboration et al., 2013). La dinámica de la energía oscura se describe bien por la constante cosmológica aunque su explicación física es aún un gran reto.

En el contexto del modelo Λ CDM, el gas bariónico es atrapado gravitacionalmente en los pozos de potencial de la materia oscura; el gas se enfriá radiativamente precipitándose hacia el centro de los halos oscuros. Debido al (pequeño) momento angular que adquieren los halos por torcas de marea, el gas que disipa y cae al centro conservando parcialmente ese momento angular, caerá hasta que entre en equilibrio centrífugo: una galaxia de disco nace entonces. El disco gaseoso es susceptible de instabilidades mismas que disparan la formación estelar (por ejemplo las que describe el sencillo criterio de Toomre) y/o las interacciones y fusiones aceleran este proceso. Las estrellas a su vez inyectan energía y momento al medio interestelar, en especial cuando éstas explotan como Estallidos de Rayos Gamma y Supernovas (SNs). Este proceso de retroalimentación frena la formación estelar hasta que el gas disipe nuevamente su energía o en muchos casos, el gas es incluso completamente expulsado del sistema en los vientos galácticos; esto ocurre más eficientemente mientras menos masivo es el halo (desde halos de masa $< 10^{12} M_{\odot}$). El gas también puede ser expulsado por efectos del Núcleo Galáctico Activo (NGA) que desarrollan las galaxias más masivas. Además, en los halos más masivos el gas difícilmente llega a la galaxia central debido a que se calienta por choques a decenas de millones de grados en el proceso de colapso del halo; por esto y por la retroalimentación de los NGAs es que hay un límite superior en la masa bariónica de las galaxias.

Una cuestión clave del escenario descrito es la *conexión galaxia-halo*, misma que resume gran parte de los procesos físicos y evolutivos de las galaxias que se

ensamblan en los halos oscuros en crecimiento. En los últimos años se han hecho importantes progresos en constreñir esta conexión en todo el espectro de masas de las galaxias a través de enfoques semi-empíricos que hacen uso de las distribuciones estadísticas de las galaxias observadas y de los halos simulados. En la tesis reciente de Rodríguez-Puebla (2014) se describen a fondo estos enfoques y se da una extensa lista de referencias. La fig. 1.1 es una reproducción de dicha tesis donde se ilustra la esencia de estos enfoques. Como se puede apreciar, el cociente de masa estelar (M_*) a masa de halo (M_h) de las galaxias cambia brúscamente con la masa de halo: hacia $M_h \approx 10^{12} M_\odot$ la eficiencia de ensamblaje de masa estelar parece tener su máximo; hacia masas menores y mayores la masa estelar con relación a la del halo es cada vez menor lo cual indica que los procesos de retroalimentación y enfriamiento del gas descritos en el párrafo anterior están en acción, haciendo la eficiencia de ensamblaje de la masa estelar cada vez menor.

Las determinaciones de la relación $M_* - M_h$ se han hecho en promedio para toda la población de galaxias/halos (ver trabajos recientes Behroozi et al., 2010; Guo et al., 2011; Behroozi et al., 2013; Moster et al., 2013; Rodríguez-Puebla et al., 2013) así como separadas en galaxias centrales y satélites (Rodríguez-Puebla et al., 2012, 2013). Más recientemente, Rodriguez-Puebla et al. (2014) han logrado inferir la relación $M_* - M_h$ de galaxias centrales separadas en azules y rojas. Sorpresivamente éstas resultaron ser diferentes, siendo, a paridad de masa estelar, la masa de halo de las rojas siempre mayor a las de las azules. A muy grosso modo se pueden asociar las galaxias azules y rojas con las galaxias de tipo tardío y temprano respectivamente. Entonces podemos contar ahora con la conexión galaxia-halo para estos dos tipos por separado.

Las galaxias están compuestas también por gas neutro en forma atómica (HI) y molecular (H_2); el gas ionizado es generalmente una fracción despreciable y el He y metales constituyen cerca del 28.5% del gas neutro. Mientras más pequeñas las galaxias, mayor fracción de gas tienen. La suma del gas (considerando He y metales) y las estrellas constituyen la *masa bariónica* de las galaxias, M_{bar} . Recientemente, en la tesis de R. Calette (2014, en prep.), en base a una extensa compilación de la literatura y a la conexión entre la función de masa estelar de galaxias rojas y azules y las relaciones de masa de gas– M_* para ambas poblaciones, se ha logrado determinar la función de masa bariónica de las galaxias rojas y azules. A través de la técnica de correspondencia de abundancias (abundance matching), se logró

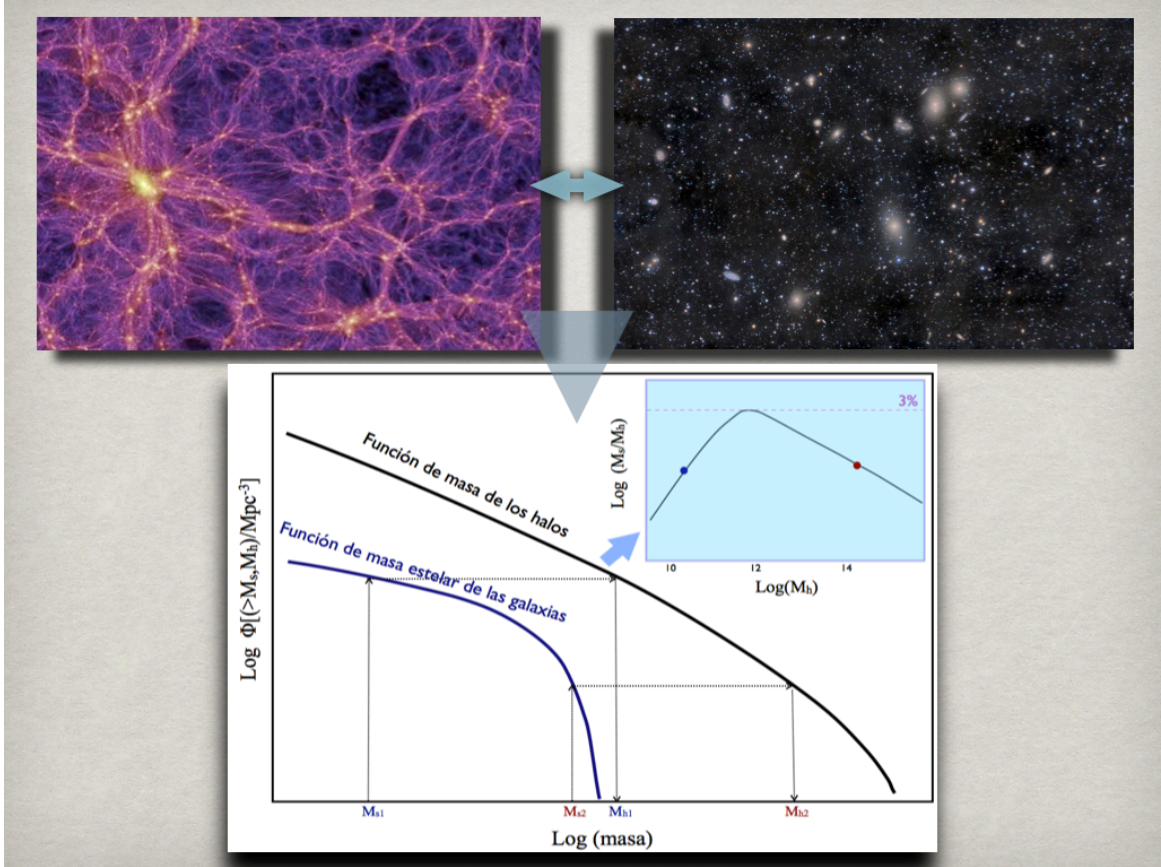


Figure 1.1: Conexión semiempírica entre el halo y la galaxia: la población de halos de materia oscura fría obtenida en simulaciones numéricas cosmológicas es confrontada estadísticamente con la población observada de galaxias bajo la suposición de que en cada halo/subhalo existe una galaxia central/satélite. Por ejemplo, empatando las funciones de masa acumulativas de galaxias y halos se infiere la masa de halo M_h que le corresponde a una dada masa estelar de galaxia M_* y se puede calcular el cociente M_*/M_h (eficiencia de crecimiento de la masa estelar) en función de la masa del halo; como se aprecia en la figura, este cociente a $z \sim 0$ tiene un pico de máxima eficiencia alrededor de $M_h \sim 10^{12} M_\odot$ e incluso en el pico el valor es mucho menor que la fracción bariónica universal, que es 15–17%. La conexión galaxia–halo se puede afinar más introduciendo modelos de ocupación de satélites en los halos y de función condicional de M_* , para lo cual se requiere más restrictores observacionales, como sería la función de correlación de dos puntos (ver por ej. Rodríguez-Puebla et al., 2013).

entonces calcular la relación $M_{\text{bar}} - M_h$ de las galaxias azules y rojas por primera vez. El cociente M_{bar}/M_h se conoce en la literatura como la fracción bariónica, f_{bar} . Del trabajo de Calette et al. (2014, en prep.) contamos ahora con la fracción bariónica en función de M_h , tanto para galaxias azules como rojas. Incluso al pico, el valor de f_{bar} es más de un factor dos menor al de la fracción bariónica universal, es decir el cociente entre densidades de fondo de bariones y materia total, Ω_b/Ω_m . Esto nos muestra que hay una gran cantidad de bariones en el Universo que en realidad no están en las galaxias.

La fracción bariónica es un parámetro importante en modelos de galaxias; varias de las propiedades de las galaxias dependen de la cantidad de bariones asignados a la galaxia que habita el centro de un dado halo. Este tipo de estudios se ha hecho principalmente para galaxias de disco, tanto con modelos evolutivos de tipo semi-numérico (v. gr. Firmani and Avila-Reese, 2000; Avila-Reese and Firmani, 2000; van den Bosch, 2000a) como *modelos estáticos donde un disco es cargado dentro de un halo Λ CDM* (v.gr. Mo et al., 1998; Gnedin et al., 2007; Dutton et al., 2007). En todos estos y otros trabajos se usaban aproximaciones burdas para f_{bar} en función de M_h , como ser valores constantes o que dependen de M_h como una simple ley de potencias. Los parámetros de entrada que generalmente tienen estos modelos son:

1. la masa del halo M_h ,
2. la fracción bariónica f_{bar} ,
3. el parámetro de giro λ que cuantifica el momento angular del halo y
4. la concentración c del halo cuyo perfil es descrito por la función Navarro-Frenk-White (o la historia de agregación del halo en el caso de los modelos evolutivos).

En el caso de los modelos estáticos, se define una época (p. ej. la actual, $z = 0$) para generar una población de galaxias a esa época, entonces para diferentes M_h 's se asigna el λ y c a cada halo (tomados de las distribuciones probabilísticas de estos parámetros que se miden en las simulaciones cosmológicas) y se asigna f_{bar} . El valor de este último parámetro (y su dispersión) depende en realidad de los procesos astrofísicos de caída y enfriado del gas en los halos así como de los procesos de eyeción del gas conducido por los mecanismos de retroalimentación

de la galaxia. En simulaciones cosmológicas o en modelos semi-analíticos, f_{bar} es calculado deductivamente (*ab initio*) pero no está libre de grandes incertidumbres relacionadas con los esquemas sub-malla o las recetas usadas, respectivamente. En el enfoque semi-empírico, en cambio, f_{bar} es constreñido (en función de la masa) sin importar los procesos físicos que la producen. Y el uso de esta inferencia en los modelos estáticos nos permite explorar los efectos del $f_{\text{bar}}(M_h)$ encontrados sobre las distribuciones de masa internas del sistema galaxia-halo en equilibrio virial y centrífugo.

Los trabajos con el modelo estático de Dutton et al. (2007), Gnedin et al. (2007) y otros exploraron a fondo los efectos en las relaciones de escala (y sus dispersiones) de galaxias de disco por parte de parámetros como λ y C , así como de procesos intermedios de la formación de galaxias de disco como ser la contracción/expansión del halo interno por la presencia del disco. El escenario cosmológico en estos trabajos es siempre el Λ CDM. Entre las principales conclusiones de estos trabajos están que:

- La relación de Tully-Fisher es reproducida de manera robusta en el sentido de que variaciones de estos parámetros poco la afectan; no obstante, para los valores explorados y dependencia con M_h de f_{bar} el punto cero de esta relación está desfasado en el sentido de que a paridad de masa o luminosidad, la máxima velocidad de rotación, V_{max} , es mayor en promedio a lo que se observa; Dutton et al. (2007) propusieron entonces que el aparente problema se resuelve si el interior de halo se expande en vez de contraerse por la formación de disco.
- La relación radio-masa estelar (o luminosidad) de las galaxias modeladas reproduce aproximadamente las observaciones pero se requieren valores de λ algo menores al promedio medido en las simulaciones, así como valores muy bajos de f_{bar} .
- La dispersión de la relación radio-masa estelar de las galaxias modeladas es significativamente mayor a la que se observa para la población de galaxias de disco.

Ahora contamos con inferencias más precisas de $f_{\text{bar}}(M_h)$ y su dispersión, de tal forma que, a diferencia de previamente, son una entrada bien constreñida para los modelos. Es de interés explorar el efecto de estas recientes inferencias sobre las galaxias de disco modeladas. Al mismo tiempo, entonces responder preguntas que

los trabajos previos desencadenaron, como ser: ¿El Λ CDM es consistente con las relaciones de TF estelar y bariónica, en particular con sus puntos ceros, sin introducir una expansión interna del halo? ¿Existe un problema de radio en las galaxias de disco formadas en halos Λ CDM? ¿Es el λ original de los halos consistente con el tamaño de las galaxias observadas? ¿Existe un problema a nivel de las dispersiones de las relaciones de TF y masa-radio?

Además, siguiendo un enfoque heurístico, se pueden usar los modelos estáticos para hacer inferencias sobre el rol de los procesos astrofísicos intermedios entre formación de halos y formación de galaxias. Por ejemplo, un problema estudiado en la literatura es el de si los radios de escala de las galaxias de disco son consistentes con el parámetro de giro λ medido en las simulaciones cosmológicas (e.g., Cervantes-Cota et al., 2007; Berta et al., 2008). En estos estudios, los autores infieren para muestras nutridas de galaxias de catastros como el SDSS, cuál es el λ_{bar} que tuvo el halo de estas galaxias. Encuentran que λ_{bar} decrece con la masa o luminosidad de la galaxia, lo cual podría estar asociado a procesos de transporte de momento angular durante la formación de la galaxia masiva, principalmente por fusiones que son comunes en las galaxias más masivas (e.g., Zavala et al., 2008).

1.2 Objetivos y Metodología de la Tesis

El principal objetivo de esta tesis es explorar los efectos de la relación $f_{\text{bar}}-M_h$ determinada empíricamente para galaxias tardías sobre las relaciones de escala y correlaciones diversas de la población de galaxias de disco (incluyendo bulbo) a la luz de un modelo donde las galaxias son insertadas en halos de Λ CDM para formar un sistema en equilibrio centrífugo, tomando en cuenta la deformación central del halo por el jaloneo gravitacional de la galaxia. Alrededor de este objetivo principal, se plantearon varios objetivos específicos:

- Constatar si las propiedades de los halos Λ CDM (perfil de densidad, concentración, parámetro de giro λ) proveen las condiciones necesarias para que las galaxias de disco ensambladas en su interior reproduzcan las relaciones de escala y sus dispersiones observadas; en caso de que se obtengan desviaciones, explorar los cambios que se requieren introducir así como los procesos físicos que explicarían dichos cambios.

- Estudiar las condiciones de formación de bulbos y explorar el efecto de los bulbos sobre la curvas de velocidad circular en función de propiedades globales.
- Mapear la relación global $M_{\text{bar}}-M_h$ y su dispersión en la distribución interna de masas oscura, de disco y de bulbo de las galaxias. Estudiar las predicciones obtenidas, como ser el cociente de velocidades máximas de disco-bulbo a total o de masa bariónica a oscura a 2.2 radios de escala, en función de las propiedades globales de las galaxias. Comparar con observaciones disponibles y sondear si los halos Λ CDM enfrentan o no problemas a este nivel de correlaciones de distribuciones internas con propiedades globales.
- Estudiar el comportamiento de la parte externa de las curvas de velocidad circular de las galaxias formadas en los halo Λ CDM en función de propiedades globales de las galaxias y confrontar con evidencias observacionales. ¿Hay un potencial problema?

Para realizar el estudio y abordar los objetivos planteados, se usará el modelo estático basado en el enfoque de Mo et al. (1998) pero extendido aquí para incluir (a) la formación de un bulbo, (b) la generalización del invariante adiabático usado para el jaloneo gravitacional del halo por la galaxia y (c) la transformación de gas en estrellas (formación estelar de acuerdo al criterio de Toomre). *El código fue escrito por Aldo Rodríguez-Puebla*, quien amablemente lo proporcionó para realizar modificaciones, como ser la inclusión de un bulbo y su adaptación para la estrategia heurística (semiempírica) que se seguirá en esta tesis.

La estrategia a seguir trata siempre de estar apegada a un enfoque semi-empírico. Inicialmente, como ya lo hicieron autores previos, se busca generar una población de galaxias de disco usando las propiedades tal cual de los halos de Λ CDM (condiciones iniciales “cosmológicas”) y bajo la suposición en el modelo de que las galaxias evolucionan aisladamente. Posteriormente se confrontan correlaciones globales obtenidas con las observaciones; en caso de haber diferencias, se explora qué suposiciones iniciales son sensatas de relajar, como p. ej. el que las galaxias evolucionan aisladas y sólo secularmente (las evidencias muestran que una fracción de las galaxias, en particular las más masivas, sufrieron en el pasado fusiones mayores). Se opera sobre los parámetros pertinentes para “emular” la acción de fusiones/interacciones sobre las propiedades finales de la galaxia de tal manera que haya consistencia con ciertas

correlaciones observacionales relacionadas con el efecto de las fusiones/interacciones. Lograda esta consistencia, quedan constreñidos entonces los parámetros en cuestión. De esta manera el modelo hace predicciones de otras correlaciones y de las distribuciones internas de masa de las galaxias. En este sentido, el modelo se convierte en un paso intermedio para mapear ciertas correlaciones globales (como la $M_{\text{bar}} - M_h$ y la masa-radio) sobre otras correlaciones (como la de Tully-Fisher) y sobre las distribuciones internas de materia oscura, disco y bulbo.

1.3 Contenido

El contenido de esta tesis está dividido en capítulos.

- En el Capítulo 2 se presenta la relación $f_{\text{bar}}(M_h)$ para galaxias tardías a ser usada aquí, así como una recopilación de la literatura observacional de las relaciones de escala y correlaciones pertinentes a las galaxias de disco.
- En el Capítulo 3 se describe a fondo el modelo estático de galaxia-halo usado en esta tesis para obtener poblaciones de galaxias de disco. Primero se describe el modelo originalmente presentado en Mo et al. (1998) y Dutton et al. (2007) y luego se presentan las actualizaciones que se hicieron sobre el código numérico de Aldo Rodríguez a fin de tomar en cuenta la formación secular de bulbos. Se describe también la manera en que se toma en cuenta la posibilidad de las fusiones en la evolución de las galaxias, especialmente las masivas. Se presenta la estrategia a seguir a fin de generar un catálogo sintético de galaxias de disco.
- En el Capítulo 4 se presentan las relaciones de escala que se obtienen del catálogo sintético generado con las condiciones iniciales de los halos oscuros tal cual como se obtienen en simulaciones cosmológicas y bajo la suposición de sólo evolución secular, sin presencia de fusiones. Se muestra que las relaciones de escala predichas concuerdan con las observadas hasta masas estelares del orden de $M_* = 3 - 5 \times 10^{10} M_\odot$. Para galaxias más masivas, los radios efectivos y las V_{max} a paridad de M_* son sistemáticamente mayores en los modelos que en las observaciones.
- Mientras que en el Capítulo 5, mismo que junto al Capítulo 6 se presentan los principales resultados de la tesis. En este Capítulo se introduce el efecto

de las fusiones en las galaxias masivas de tal manera que se reproduzcan las relaciones observadas de radio– M_* , B/T– M_* y cociente de gas a masa vs. M_* . Se estudia a fondo las relaciones de Tully-Fisher estelar y bariónica predichas y sus dispersiones. Se infiere la dependencia del parámetro de giro inicial del gas del que se forman las galaxias de disco con la masa del halo y de la M_* de la galaxia. Se explora también: (1) el rol que juegan las condiciones iniciales sobre las dispersiones de las relaciones de escala, (2) la posible correlación de los residuales de estas relaciones con ciertas propiedades galácticas, (3) la posible correlación de las relaciones $M_{\text{bar}}-M_h$ y M_*-M_h con propiedades galácticas, y (4) las correlaciones entre los residuales de las relaciones de TF y radio–masa. Todos estos estudios permiten sondear la viabilidad de la formación de galaxias de disco en halos oscuros en el contexto de las cosmología Λ CDM.

- En el Capítulo 6 se presentan las distribuciones espaciales internas de masa de las diferentes componentes de los sistemas generados en el catálogo sintético: bulbo, disco y halo; las fracciones de masa luminosa a masa total a diferentes radios son estudiados en función de la masa estelar, V_{\max} y la densidad superficial estelar de las galaxias. Se presentan también varios cocientes de velocidades a $2.2R_D$ o al máximo de los mismos en función de estas propiedades globales con el fin de comparar con las escasas inferencias observacionales que hay al respecto. Se presenta también la dependencia de la pendiente externa de las curvas de rotación en función de estas propiedades globales.
- Finalmente en el Capítulo 7 se discuten los principales resultados y conclusiones obtenidos en la tesis.

Chapter 2

Observational correlations of disk galaxies

Disk galaxies follow several correlations among their global properties (luminous, stellar and baryonic). The most known are those called "scaling relations", as the Tully-Fisher (TF) and the radius–mass relations (e.g., Gnedin et al., 2007; Courteau et al., 2007; Avila-Reese et al., 2008, and more references therein). These relations enclose key aspects of the formation, evolution and dynamics of disk galaxies, as well as of the properties of dark matter. An interesting question is whether these relations are directly related (or at least are consistent) to the initial conditions of the cosmological scenario, in particular the Λ CDM scenario, which is the most popular one (see the Introduction).

On the other hand, if we have a model for the structure and dynamics of the population of disk galaxies, this model allows us to "map" some correlations into other ones, including the scatters. For example, given that the model reproduces the radius–mass relation of observed galaxies, we can explore how is, within the context of this model, the TF relation and compare with observations. We can also explore what are the effects of the global $M_{\text{bar}}-M_h$ relation (semi-empirically inferred) on these and other relations. As discussed in the Introduction, this relation resumes the galaxy–halo connection, which includes several key aspects of the galaxy assembly process. Moreover, the disk galaxy model to be used here (see Chapter 3) allows to constrain the mass distribution of the bulge, disk, and halo. Therefore, the global galaxy–halo connection can be mapped into the inner structural and

dynamical properties of disk galaxies, which are related to empirical quantities as the maximum circular velocity or the circular velocities of the bulge, disk and halo at a given radius like 2.2 scale radii; therefore, one can pass from the $M_{\text{bar}}-M_h$ or M_*-M_h relations to, for instance, the $V_{\text{max}}-M_{\text{bar}}$, $V_{\text{max}}-M_*$, $(V_D/V_T)_{2.2}-M_*$ and other galaxy correlations. In the same way, once generated a population of disk galaxies through our model, we can explore whether the galaxy stellar mass function or the V_{max} function are consistent or not with, e.g., the TF and radius-mass relations. This is a very instructive mapping of galaxy correlations to abundance distributions and viceversa (see e.g., Blanton et al., 2008).

Following, we describe the relevant empirical or semi-empirical correlations that will be used in our work, either for constraining the model or for comparing with its predictions.

2.1 The (semi-empirical) baryonic-to-halo mass relation

The galaxy $M_{\text{bar}}-M_h$ relation will be used as input in our static model of disk galaxies. As mentioned in the Introduction, this relation summarizes most of the relevant galaxy evolutionary processes. The change of the baryonic fraction $f_{\text{bar}} \equiv M_{\text{bar}}/M_h$ with M_h tell us about the ability of the halo of mass M_h to capture and cool gas, to transform the cold gas into stars, as well as about the role that play the stellar (mainly through SNe) and AGN feedbacks and the processes of gas loss from the galaxy. The determination of the $f_{\text{bar}}-M_h$ (or $M_{\text{bar}}-M_h$) relation is not an easy task mainly due to the difficulty in measuring directly the mass at the virial radius (see the Introduction for a discussion). Besides the few and yet limited direct studies, the galaxy-halo connection has been established through statistical approaches that combine the observed galaxy distribution functions and spatial correlation with the halo/subhalo distributions measured in large cosmological simulations.

In recent years, the new generation of galaxy surveys have provided us with uniform and precise measures of properties for a large number of galaxies, complete in magnitude or volume. Simultaneously, the impressive progress made in cosmological N-body simulations, allows us to have precise predictions for the evolution, properties, and distributions of the Λ CDM halos (see a recent review in Knebe et al.,

2013). In the light of these advances, several statistical approaches have recently emerged for connecting galaxy properties, such as luminosity, M_* , M_g , M_{bar} , etc., to their dark matter halos in a semi-empirical way. Among them, the abundance matching technique (AMT) is one the most popular (see the Introduction and references therein). In its most simple form, the observed cumulative galaxy number density at a given property is matched against the theoretical halo plus subhalo cumulative number density (see Fig. 1.1). As a result, one obtains the relation between M_* and the halo mass, without requiring knowledge of the underlying physics of galaxy evolution. Instead, the results of this kind of connections allow us to infer semi-empirically which are the key physical processes of galaxy evolution.

In its most basic form, however, the AMT assumes that galaxy properties are determined only by halo mass, M_h , in such a way that exists a univocal relation between e.g., M_* (or M_{bar}) and M_h . In reality, the galaxy properties, like M_* and M_{bar} , are expected not being determined by only M_h but other halo properties and evolutionary features also play a role. For example, as it was stated in the pioneering works of Mo et al. (1998); Avila-Reese et al. (1998); Firmani and Avila-Reese (2000), the scaling relations of galaxies are actually coined by the mass, spin parameter, and concentration of the halos (the latter on its own is determined by the halo mass aggregation history). The mass is probably the most relevant factor because it establish the gravitational potential and the scaling properties of the galaxy. However, for a fixed mass, there are other halo properties that are also relevant for the galaxy. For instance, the halo spin parameter, λ , regulates the galaxy size, and it plays some role also on the values of M_* , the gas fraction, and M_{bar} . The halo mass aggregation history, quantified mainly by the halo concentration, C , is expected to influence on intensive properties as the galaxy color and gas fraction but also partially on M_* and M_{bar} .

As the result of the effects of different halo parameters on the galaxy properties, the connection between M_* or M_{bar} and M_h is expected to have some intrinsic scatter, i.e. the galaxy stellar or baryonic masses do not depend only on M_h but they can be affected also by λ , concentration, mass aggregation history, etc. This has led to different authors to take into account an intrinsic scatter around the M_* – M_h (or $M_{\text{bar}}-M_h$) relation. Commonly, previous studies have found that the width of this scatter is small and essentially constant with halo mass, but see Rodriguez-Puebla et al. (2014). An interesting question is whether the scatter around the

galaxy-halo relation correlates or not with a given galaxy property. Recent studies, from both direct and indirect probes of halo masses, have found that on average red galaxies reside in more massive halos than blue galaxies. Potentially, this difference is showing that galaxy and halo properties are correlated in a non-trivial way. This is an important point in studies focused to study a particular sample of galaxies, like late-type galaxies, as it is the case in this Thesis.

Since the $M_* - M_h$ relation of blue galaxies segregates from the average (Rodriguez-Puebla et al., 2014), then *it is important to determine also the $M_{\text{bar}} - M_h$ relation of blue galaxies in order to correctly study the structural and dynamical correlations of disk galaxies, which tend to have namely bluer colors.* This has been done in Calette (2014), who used a modification of the abundance matching technique to include information on gas masses and able to separate the galaxy population into two groups: blue, disk-dominated and red, bulge-dominated galaxies; the method was called Multi-Abundance matching Technique Constraints in Halos, MATCH.

By using MATCH, a population of 3×10^6 galaxies that follow the observed galaxy stellar mass function (GSMF) down to $M_{*,\text{lim}} = 10^7 M_\odot$ at $z \sim 0.1$ and agree with the empirical atomic gas- M_* and molecular gas- M_* relations was generated. The GSMF was constructed from joining two observational determinations, both based on the NYU-VAGC SDSS catalog: one by Baldry et al. (2008) from the DR4, corrected to be approximately complete in volume down to $M_* \sim 10^7 M_\odot$, and other by Rodriguez-Puebla et al. (2014), from DR4 for a larger volume and complete for masses above $M_* \sim 10^9$. Rodriguez-Puebla et al. (2014) corrected their stellar masses in order to take into account that the galaxy surface brightness profiles extends further away than the commonly used aperture limits in the SDSS, specially for central massive galaxies, see e.g., Bernardi et al. (2013); Kravtsov et al. (2014). This implies larger stellar masses, specially for the most massive (mostly central) galaxies. Baldry et al. (2008) applied some corrections to volume completeness at low masses, this is why their GSMF could be extended down to $M_* \sim 10^7 M_\odot$. However, at the high-mass end the Rodriguez-Puebla et al. (2014) GSMF is more suitable due to the larger volume of the updated SDSS data release they have used.

Galaxies in MATCH were divided into two populations, blue/late-type and red/early-type galaxies, respectively. The idea in Calette (2014, as well as in Rodriguez-Puebla et al. 2015) was to have an approximate division of the overall galaxy population into two groups, which roughly can be associated to disk-

dominated and bulge-dominated galaxies. Because for the construction of the GSMF, an updated version of the NYU-VAGC SDSS catalog (Blanton et al., 2005b) was used, where colors are reported for almost all the galaxies, then the color should be used as the property to separate galaxies into two groups. On the other hand, the empirical correlations of gas-to-stellar mass were inferred from a diverse compilation from the literature, where in some cases galaxies are characterized by their colors and in other cases, by their morphology or star formation activity. It is well known that color correlates with the galaxy morphology and star formation activity. However, it is also known that there is a fraction of galaxies that do not follow these correlations and, according to the criteria used to divide them into two groups, they can be disk-dominated but red and passive (e.g., Maller et al., 2009; Masters et al., 2010, the fraction of these galaxies is not larger than $\sim 10\%$ of the late-type ones and it is more common among massive galaxies), or bulge-dominated but blue and star forming (e.g., Schawinski et al., 2009, these galaxies are less than 6% of early-type ones and are not found among massive galaxies). The $M_* - M_h$ and $M_{\text{bar}} - M_h$ relations that Rodriguez-Puebla et al. (2014) and Calette (2014) attempted to infer are not for a fine and continuous separation of galaxies by color or morphological type, but only for two rough galaxy populations. Therefore, *the “contaminations” produced by the above mentioned (few) deviations from the general correlations are not so relevant as to change these mass relations when separated just in two groups.*

In order to separate the GSMF into blue and red galaxies, Calette (2014) used a fit to the fraction of red (blue) galaxies from the NYU-VAGC SDSS DR7 catalog used in Rodriguez-Puebla et al. (2014):

$$f_{\text{red}} = \frac{1}{1 + (M_*/M_{\text{char}})^{\gamma}}, \quad (2.1)$$

where M_{char} is the mass where $f_{\text{red}} = f_{\text{blue}} = 0.5$. The fitting to the data provides that $\log(M_{\text{char}}/\text{M}_\odot) = 10.1$ and $\gamma = -0.40$; the blue fraction is $f_{\text{blue}} = 1 - f_{\text{red}}$. Colors in Rodriguez-Puebla et al. (2014) were K-corrected to $z = 0.1$ and separated into blue and red galaxies based on the color-magnitude criteria of Li et al. (2006). The latter authors used a bi-Gaussian fitting model to separate blue and red galaxies in several absolute magnitude bins. They have used the $^{0.1}(g - r)$ color and a definition of the magnitudes at $z = 0.1$ Calette (2014) uses these fractions in order to compute the GSMFs of blue and red galaxies as: $\phi_{g,i} = f_i \times \phi_g$, where subscript

‘*i*’ refers either to blue or red galaxies. Note that for masses smaller than $\sim 5 \times 10^8 M_\odot$, the red/blue fractions are just extrapolations of the determinations mentioned above. In any case, observations suggest that most of dwarfs are indeed blue, star-forming galaxies, unless they are satellites. However, the fraction of satellite to central galaxies is small, specially at low masses.

The strategy followed in Calette (2014) consisted in generating a Monte Carlo mock catalog of 3×10^6 galaxies. Each galaxy is extracted with a stellar mass M_* from the overall GSMF described above, taking into account their error bars. For a given M_* , whether the extracted object is blue or red is randomly assigned from the probability given by eq. (2.1). Then, to each galaxy are assigned HI and H₂ masses, M_{HI} and M_{H_2} , respectively, by using the M_{HI} -to- M_* and M_{H_2} -to- M_* correlations recently constrained for blue/late- and red/early-type galaxies in Calette (2014); these correlations have intrinsic scatters, which are assumed to be lognormally distributed, and were taken into account in the Monte Carlo trials. These empirical correlations are based on a compilation and homogenization of observations of M_{HI} and M_{H_2} for local galaxies with known stellar masses and galaxy type and/or color. The correlations inferred in Calette (2014), are presented in Appendix A. Thus, galaxies in the MATCH mock catalog *reproduce by construction* the observational correlations of M_{HI} and M_{H_2} with M_* along with their scatters for both blue/late-type and red/early-type galaxies. As a direct consequence of the above, galaxies in the MATCH catalog have also defined the total cold gas mass, $M_g = (M_{HI} + M_{H_2}) + M_{(He+Z)} = 1.4(M_{HI} + M_{H_2})$, and the total baryonic mass, $M_{\text{bar}} = M_g + M_*$. The factor 1.4 is for accounting for He and metals.

The MATCH mock galaxy sample, by construction, is volume-complete in stellar mass down to $\sim 10^7 M_\odot$. By applying the abundance matching technique for blue and red galaxies, Calette (2014) inferred the $M_* - M_h$ for the blue and red galaxy populations. For this, it is necessary to know the probability of a subhalo/halo to host a blue or red galaxy. In the case of central galaxies (associated to halos), such a probability as a function of M_h has been inferred semi-empirically in Rodriguez-Puebla et al. (2014). In the case of satellite galaxies (associated to sub halos), Calette (2014) introduced an approximation, based on Peng et al. (2012), to calculate the probability of a subhalo to host a blue or red satellite, which assumes that this probability is similar to the case of central galaxies but corrected by a factor that depends on the effects of satellite quenching due to the halo environment. In any

case, have in mind that the overall population of galaxies is dominated by centrals, so that any uncertainty in the proposed approximation for satellites/subhalos, has a minor effect on the overall probability as a function of M_h .

From the abundance matching applied to the blue and red total GSMF's, the M_*-M_h relations of blue/red galaxies, including their scatters, are found. Then, a halo mass is assigned to each blue or red galaxy of mass M_* of the mock catalog by using the corresponding M_*-M_h relation and its lognormally distributed scatter. For the given M_* and color type, as mentioned above the empirical M_{HI} -to- M_* and M_{H_2} -to- M_* correlations are used to assign M_{HI} and M_{H_2} to the galaxies, taking into account the lognormal scatter distributions of these correlations. Therefore, it is possible to construct the galaxy mass functions for HI, H₂, cold gas, and baryons, separately for blue and red galaxies, which are associated to late- and early-type galaxies, respectively. The obtained total HI and H₂ mass functions agree well with direct determinations of them using surveys in radio as ALFALFA, HIPASS, and others (Calette, 2014). Note that we need many Monte Carlos trials for seeding galaxies in the halos in order to sample well the halo mass function as well as the scatter distributions of the GSMFs, the blue/red galaxy fractions, the blue/red halo mass fractions, the M_* -to- M_h relations, and the empirical $M_{HI}-M_*$ and $M_{H_2}-M_*$ relations. Finally, *the obtained relation between M_{bar} and M_h (or $f_{\text{bar}}=M_{\text{bar}}/M_h$ and M_h) and its scatter for blue/late-type galaxies will be used in our static model of disk galaxies as one of the basic input parameters.* We will use actually the best Behroozi et al. (2013) function fit to these results:

$$\log_{10}(M_{\text{bar}}/M_h) = \log_{10}(\epsilon M_1) + f(x) - f(0), \quad (2.2)$$

where

$$f(x) = -\log_{10}(10^{-\alpha x} + 1) + \frac{\delta[\log_{10}(1 + \exp(x))]^\gamma}{1 + \exp(10^{-x})}, \quad (2.3)$$

and $x = \log_{10}(M_h/M_1)$. The recent inferred parameters are: $\log_{10}M_1 = 11.69$, $\epsilon = 0.0668$, $\alpha = 1.5$, $\delta = 2.6993$, $\gamma = 0.8275$.

In Fig. 2.1 the $M_{\text{bar}}-M_h$ relation of blue galaxies (left panel) as obtained in Calette (2014) is plotted along with its intrinsic scatter in dex (lower panel). For comparison, the relation for red galaxies and the average relation of both populations are also plotted. The corresponding $f_{\text{bar}}-M_h$ relations are plotted in right panel.

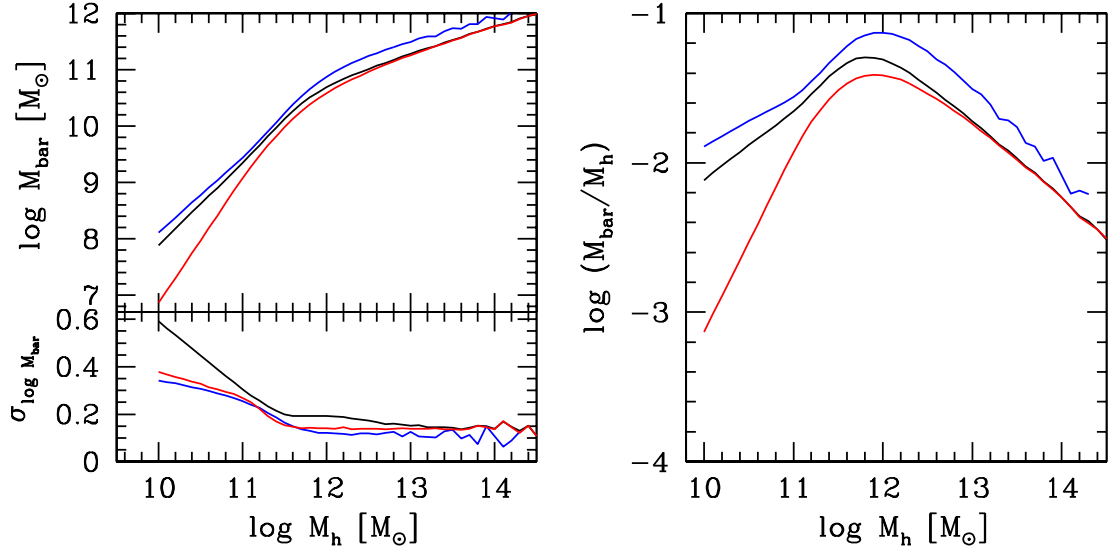


Figure 2.1: The $M_{\text{bar}} - M_h$ relations of blue and red galaxies (blue and red lines) and the average relation (black line) as obtained in Calette (2014) by the MATCH semi-empirical approach. The intrinsic scatters around these relations are shown in the lower panel. The corresponding $f_{\text{bar}} - M_h$ relations are plotted in the right panel.

In Fig. 2.2, we plot the best Behroozi function fit for blue/late-type galaxies with its respective intrinsic scatter. The $f_{\text{bar}} - M_h$ relation and its scatter are inputs of our static model. For the intrinsic scatter, we have fitted two linear functions in the log-log plots to the scatter reported in Calette (2014) (blue line in the lower panel of Fig. 2.1).

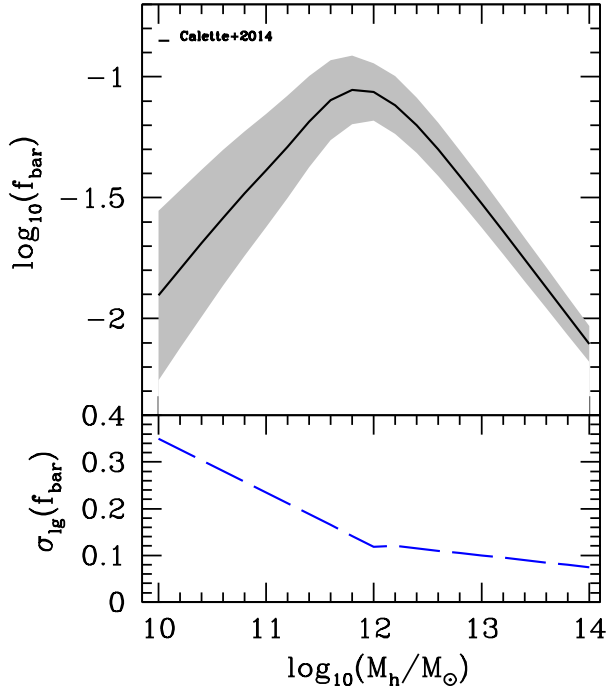


Figure 2.2: The mean with its scatter (gray shaded area) are plotted for the $f_{\text{bar}}-M_h$ relation for the blue galaxies. The black solid line is the Behroozi-like function that best fits the MATCH result for the blue $M_{\text{bar}}-M_h$ relation.

2.2 The size-stellar mass relation

One of the most important scaling relation is the one between size and mass of a galaxy. The size of the galaxies is related to the overall scale of the system (given for instance by the mass) and to the angular momentum. Therefore, it is expected that the scatter around the mean size-mass relation is associated mainly to the spin parameter λ : for a given mass, the larger the λ , the more extended is expected to be the disk. The size-mass relation is a key observational constrain in our approach. Since the size of galaxies for a given mass depends mainly on the spin parameter, this relation will be important for constraining namely the spin parameter.

For late-type disk galaxies, their surface brightness (density) profiles are typically

well fitted by an exponential distribution, characterized by the scale radius, R_D . For a perfect exponential disk, the radius where half of the luminosity (mass) is contained is given by $R_e=1.68R_D$. However, the presence of a bulge, which is typically more concentrated than a exponential disk, can alter this equality for real galaxies, more as larger is the bulge-to-disk ratio. Because the bulge-to-disk decomposition is not an easy task, specially when applied to large surveys, the most common reported characteristic radius of galaxies in these surveys is R_e .

Following, we report and discuss several R_e-M_* relations for blue or late-type galaxies obtained from large surveys with different methods. These relations will be compared to our model results and, eventually, they will help to constrain the model.

- **Shen et al. (2003, S03):** From the DR1 SDSS survey, these authors separated galaxies into late- and early-type by using the photometric concentration index C and index Sérsic n . The former were assigned to those with $C < 2.86$ and $n < 2.5$; the latter to those with $C > 2.86$ and $n > 2.5$. The stellar masses are obtained from the Max-Planck-Institute for Astrophysics–Johns Hopkins University (MPA-JHU) catalog (Kauffmann et al. (2003b); Salim et al. (2007)). The R_e-M_* relations of both groups are different, with low-concentration galaxies being larger for a given M_* than high-concentration ones. The low-concentration galaxies follow the mean and intrinsic scatter relations:

$$R_e[kpc] = \gamma \left(\frac{M_*}{M_\odot} \right)^\alpha \left(1 + \frac{M_*}{M_0} \right)^{\beta-\alpha} \quad (2.4)$$

and

$$\sigma_{lnR_e} = \sigma_2 + \frac{(\sigma_1 - \sigma_2)}{1 + (M_*/M_0)}, \quad (2.5)$$

respectively, where α , β , γ and M_0 are free fitting parameters. α and β represent the slopes of the relation, and M_0 , the characteristic mass, which determines the stellar mass at which the slope of the relation change. The values of these parameters are: $\alpha = 0.14$, $\beta = 0.39$, $\gamma = 0.10$, $M_0 = 3.98 \times 10^{10} M_\odot$, $\sigma_1 = 0.47$ and $\sigma_2 = 0.34$. The corresponding relation with its scatter, are plotted in Fig. 2.3 (black solid line with the dotted lines for the scatter); note that the scatter in the figure is in dex.

- **Mosleh et al. (2013):** These authors present their size-stellar mass relation from the New York University Value-Added Galaxy Catalog (NYU-VAGC; Blanton

et al. (2005c)) updated with the DR7 data from the SDSS (Abazajian et al. (2009)). The stellar masses are also obtained from MPA-JHU catalog updated to the DR7. The galaxies are classified into different sub-samples based on their color, morphology and specific star-formation rate (sSFR). We use the sub-sample based in color. Following Blanton et al. (2005c), the criterion to separate galaxies into red and blue objects is: $(g - r) = 0.68 - 0.032(M_r + 20)$. To measure the effective radii, they used two methods: (a) "parametric", where the half-light radius of galaxies is calculated by using best-fit, two-dimensional analytic models, and (b) "non-parametric", where the observed one-dimensional light profiles and the total flux are used. They use the same functional form employed for late-type (low-concentration) galaxies in S03 (see eq. 2.4 and 2.5 above) for their $R_e - M_*$ and intrinsic scatter relations. The corresponding fitting parameters for the sample selected by color are $\alpha = 0.185 \pm 0.081$, $\beta = 0.329 \pm 0.164$, $\log(\gamma) = -1.406 \pm 0.750$, $M_0 = 10.325 \pm 0.299$, $\sigma_1 = 0.574 \pm 0.059$ and $\sigma_2 = 0.056 \pm 0.122$. The mean relation for this parameters are plotted in Fig. 2.3 (magenta dots connected with solid line).

- **Cebrian & Trujillo (2013).** These authors considered the effect of environment where galaxies are. As in Mosleh et al. (2013), the sample is taken from SDSS-DR7. The estimates of stellar mass are obtained from (Blanton and Roweis (2007)) using a Chabrier (2003) Initial Mass Function (IMF) with population synthesis model from Bruzual and Charlot (2003). The size of the galaxies were determined using a Sersic (1968) fit to the radial intensity profile obtained using circular apertures (Blanton et al. (2005a)). This relation is studied in different large scale environments, considering whether the galaxies are in a high-density or a low-density region. The galaxies are segregated by their morphology (using the Sérsic index as we describe above). Consequently, it is applied a "Maximum Likelihood estimator" to obtain the most likely values for the mean size and the scatter of the distribution, for a given mass bin. Thus, using this method, it can be estimated the more likely mean size $\bar{R}(M)$, dispersion $\sigma_{lnR}(M)$ and their 1σ -errors. We use the data given in tables A1 and A2 of Cebrian and Trujillo (2014) for the $R_e - M_*$ relation and its dispersion, which is displayed in Fig.2.3 (green dots connected with solid line and dashed lines for the corresponding scatter).

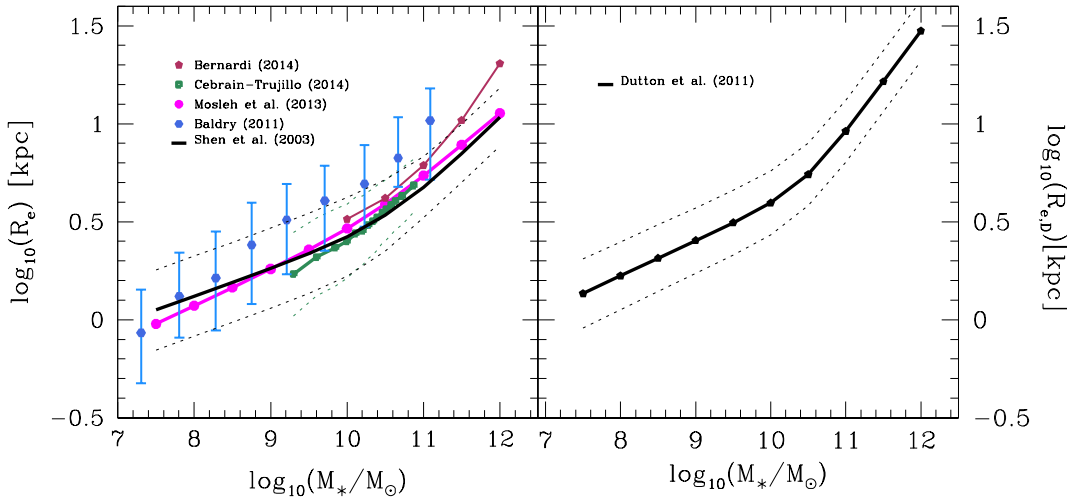


Figure 2.3: Stellar mass-size relation of observed galaxies in different samples. In left panel, are plotted the relations for total effective radius. The relation inferred by Shen et al. (2003) are plotted with black solid and dashed lines for the mean and its intrinsic scatter. The same relation and scatter but with parameters inferred for blue galaxies in Mosleh et al. (2013) are plotted with magenta dots connected with solid line. The green dots connected with solid line corresponding to the observations of Cebrian and Trujillo (2014). The sample studied in Bernardi et al. (2012) are represented with brown dots connected with solid line. The blue dots with error bars correspond to observations from Baldry et al. (2012). In right panel are plotted with black solid and dashed lines, the relations for disk effective radii, assuming that R_e is $1.68R_D$, from Dutton et al. (2011).

- **Bernardi et al. (2012):** These authors obtain their stellar mass-size relation using a sample from SDSS DR7 (as both previous authors). The estimated stellar masses come from Bernardi et al. (2010), assuming a Chabrier IMF. To quantify stellar mass-size is performed fits to the Main Galaxy Sample images using the PyMorph package. This algorithm is used to fit single component deVaucouleurs and Sérsic profiles, and two component exponential + deVaucouleurs (deVExp) and exponential + Sérsic (SerExp) profiles to each image. As a result of their analysis, they find that the reductions of the SerExp model to return the least biased estimates

of R and M_* , and hence the $R - M_*$ relation, finding the following relation:

$$\langle \log_{10} R_e / [kpc] | O \rangle = p_0 + p_1 O + p_2 O^2, \quad (2.6)$$

where $O = \log_{10}(M_*/M_\odot)$ and p_0 , p_1 and p_2 are the fitting parameters. We use the values of parameter for late-type galaxies presented in the tables 3 and 4 from Bernardi et al. (2012): $p_0 = 11.2699$, $p_1 = -2.3026$ and $p_2 = 0.1227$. In Fig. 2.3 the corresponding relation is plotted with brown dots connected with solid line.

All the relations presented above *are for the total effective radius, R_e , i.e., they do not take into account any bulge-disk decomposition.* If the bulge-disk decomposition is applied, then in principle it can be obtained the scale radius, R_D , of the exponential disk. In this case, $R_e = 1.68R_D$. The next authors present the size-mass relations inferred for only the disks.

- **Dutton et al. (2011)** present R_e obtained as $1.68R_D$ for the SDSS DR7 sample, where R_D was measured from 2D bulge+disk decompositions, using GIM2MD simultaneously on g and r images. For this sample, the stellar masses are calculated using the relation between the r -band mass-to-light ratio and $(g - r)$ color from Bell et al. (2003) with an offset of -0.1 dex to correspond to a Chabrier (2003) IMF. They select blue-cloud galaxies for this study. The criterion to select blue galaxies is by requiring that $(g - r) < 0.71 - 0.067(\log_{10} M_* - 10)$. The median of the relation between $R_e = 1.68R_D$ and M_* found in Dutton et al. (2011) is given by:

$$R_e = R_0 \left(\frac{M_*}{M_0} \right)^\alpha \left[\frac{1}{2} + \frac{1}{2} \left(\frac{M_*}{M_0} \right)^\gamma \right]^{(\beta-\alpha)/\gamma}, \quad (2.7)$$

where α is the slope at low masses $M_* \ll M_0$, β is the slope at high masses $M_* \gg M_0$, γ control the sharpness of the transition between the two slopes, M_0 is the transition mass, and R_0 is the value of the R at this M_0 . They find that $\log_{10}(M_0/[M_\odot]) = 10.44$, $\log_{10}(R_0/[kpc]) = 0.72$, $\alpha = 0.18$, $\beta = 0.52$ and $\gamma = 1.8$ provide a good fit to the data. The scatter around the mean relation is assumed as lognormal distributed with $s = \sigma_{\ln R|M}$, given by following relation:

$$s = s_2 + (s_1 - s_2) / [1 + (M_*/M_0)^\gamma]. \quad (2.8)$$

Here s_1 is the scatter at low masses, s_2 is the scatter at high masses, M_0 is the transition mass and γ control the sharpness of the transition. They find that $s_1 = 0.47$, $s_2 = 0.27$, $\log_{10}(M_0/[M_\odot]) = 10.30$ and $\gamma = 2.2$ give a good fit to the data.

In the right panel of Fig. 2.3, we plot the mean relation and its scatter as given in Dutton et al. (2011) for blue galaxies. Recall that, though it is given for R_e , it was actually obtained for R_D , by using disk-bulge decomposition, and R_e was just assumed to be $1.68R_D$. Therefore, in this case R_e is actually the effective or half-mass radius of the disk and not of the total (bulge+disk) galaxy.

2.3 The Tully-Fisher relation

The relation between the maximum rotation velocity, V_{\max} , and the luminosity (or stellar mass) of disk galaxies is called the Tully-Fisher (TF) relation. This is probably the tightest correlation in Extragalactic Astronomy and it was subject of hundreds of observational studies since it was established (Tully and Fisher, 1977). The stellar and baryonic TF relations are predicted in the static model of disk galaxies. Therefore, we need observational TF relations (both stellar and baryonic) in order to compare with the predictions of our static model.

In Avila-Reese et al. (2008), the authors compiled a sample of disk galaxies larger than $M_* \sim 10^9 M_\odot$ with the observational information necessary to obtain the stellar masses, V_{\max} , radii, colors, gas masses, etc. including the uncertainties. The sample is not pruned to minimize the scatter in the TF relation, as usually was done in the literature in order to use this relation as a distant estimator. The intrinsic scatter of the TF relation contains valuable information related to galaxy formation and evolution and we will also compare it with our model predictions.

Since the compiled sample of galaxies by Avila-Reese et al. (2008) contains information on stellar mass and cold gas masses, they determined both the stellar and baryonic TF relation with their respective intrinsic scatters (the latter, after resting the observational uncertainties). The compiled sample is presented in Fig. 2.4 for both the stellar and baryonic cases. The authors carried out several line fittings to the log-log data. We reproduce in Fig. 2.4 their orthogonal fits including the intrinsic scatters. These are the fits that we will use to compare with our model predictions.

The determination of the TF relation for dwarf galaxies is difficult due to observational limitations. It seems that the intrinsic scatter strongly increases as smaller are the masses. There are some pieces of evidence that the main relation bends slightly at $M_* \sim 3 - 5 \times 10^9 M_\odot$ in the sense that at a given V_{\max} smaller galaxies have lower stellar masses than the corresponding to the extrapolation of the TF relation established at larger masses. This has been also found in cosmological N-body+Hydrodynamics simulations (e.g., de Rossi et al., 2010, see for observational references therein). In Fig. 2.4 we plot individual estimates of V_{\max} and M_* for dwarf galaxies as reported in McGaugh (2005) and Geha et al. (2006).

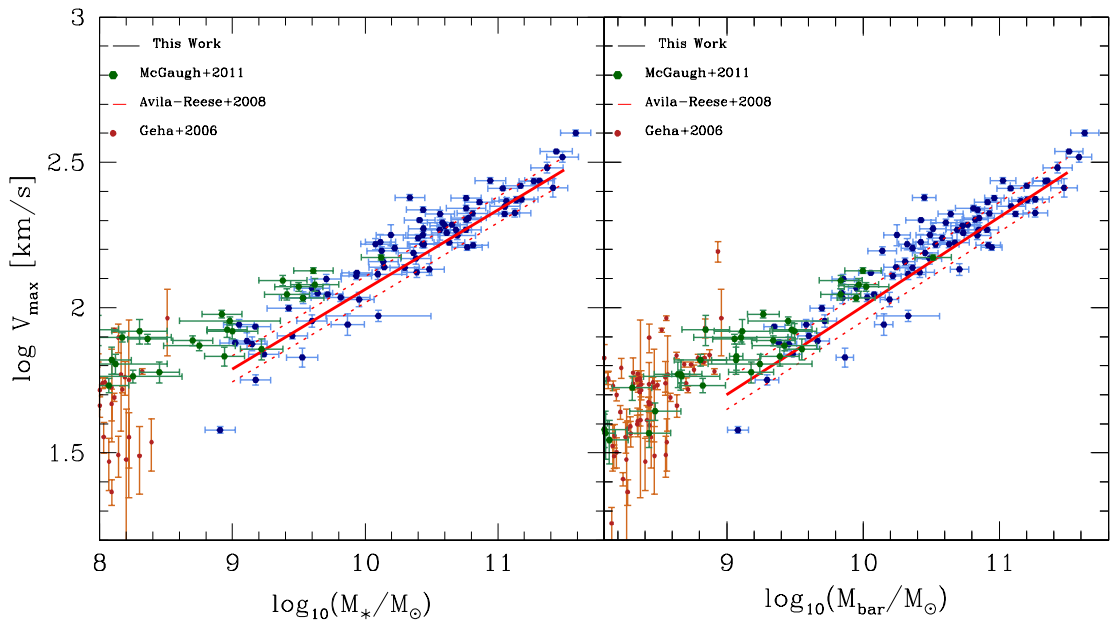


Figure 2.4: Observational dependence of V_{\max} as a function of stellar mass (left panel) and baryonic mass (right panel) for several samples. The blue dots with error bars and the orthogonal fits with 1σ intrinsic scatter (red solid and dotted lines) in both panels represent a compiled sample of disk galaxies by Avila-Reese et al. (2008). The brown dots and its error bars, are the the observed dwarf galaxies from the compiled sample by Geha et al. (2006). The observed dwarf galaxies from McGaugh (2011) are the green dots with corresponding error bars.

2.4 The bulge-to-total mass ratio vs M_*

The bulges contain important clues to galaxy formation and evolution. It is believed that the bulges are the result of dynamical processes. Those called classical seem to have formed through violent processes, such as hierarchical clustering via major mergers. Those formed through longer time-scales, via disks instabilities and secular evolution processes are called pseudo-bulges (e.g., Wyse et al., 1997; Kormendy, 2013).

- **Gadotti (2009).**- The data used for the bulge-to-total mass ratio by this author are taken from the SDSS. He performed 2D bulge/bar/disk decompositions using g , r and i -band images of a representative sample of 1000 galaxies. He finds that the Petrosian concentration index is a better proxy for the bulge-to-total ratio than the global Sérsic index. He also finds that the pseudo-bulges can be distinguished from classical bulges as outliers in the Kormendy relation. The sample is composed by all objets spectroscopically classified as galaxies in the SDSS DR2, applying the following criterion. First, all galaxies with redshift in the range $0.02 \leq z \leq 0.07$ are selected. Secondly, all galaxies with stellar masses below $10^{10} M_\odot$ are excluded. Galaxy stellar masses were obtained from Kauffmann et al. (2003a), having then a volume-limited sample, i.e., a sample which includes all galaxies more massive than $10^{10} M_\odot$ in the volume defined by redshifts cuts and the DR2 footprint. Finally, galaxies with an axial ratio $b/a \geq 0.9$ are selected, where a and b are the semi-major and semi-minor axes of the galaxy, respectively, taken from the SDSS data base (these are measured at the 25 mag arcsec $^{-2}$ isophote in the g band).
- **Fisher and Drory (2011).**- These authors present an inventory of non-edge-on galaxies, from elliptical galaxies to galaxies with classical and pseudo-bulges and bulgeless galaxies, in a volume-limited sample within the local 11 Mpc sphere complete down to $M_B < -15.2$, using *Spitzer* 3.6 μm and *Hubble Space Telescope* (HST) data. They studied the abundance of pseudo-bulges and classic bulges. The sample is taken from the Kennicutt et al. (2008) local survey, requiring Galactic latitudes of $|b| > 20^\circ$. The final sample contains 320 galaxies. The full sample and measured quantities are listed in their Table 1.

Their galaxies are decomposed into a Sérsic bulge and an exponential disk, where the decompositions are taken from Fisher and Drory (2010). The Sérsic index, n , is used to diagnose bulges into pseudo- ($n < 2$) and classical ($n > 2$) Fisher and Drory (see 2008). For those bulges with $n \sim 2$, is supplemented bulge identification with nuclear morphology from (HST) images. Ellipticals are assigned $B/T = 1$. Galaxies in which the decomposition yields $B/T < 0.01$ are assigned $B/T = 0$ and are called "bulgeless". The total luminosity is determinate by integrating the near-IR SB profile and convert to stellar mass using RC3 B-V color as described in Fisher et al. (2009) following Bell and de Jong (2001).

- **Weinzirl et al. (2009).**- The data set analyzed by these authors are derived from the 182 H -band images from the public data release of the Ohio State University Bright Spiral Galaxy Survey (OSUBSGS; Eskridge et al. (2002)). OSUBSGS is a magnitude-limited survey with objects whose distance range up to ~ 60 Mpc. The sample is reasonably complete for bright ($M_B \leq -19.3$ or $L_B > 0.33L^*$) galaxies. To derive global stellar masses for most of the OSUBSGS sample galaxies is used the relation between stellar mass and rest-frame $B - V$ color from Bell et al. (2003). Using population synthesis models, the latter study calculates the stellar M/L ratio as a function of color using functions of the form $\log_{10}(M/L) = a_\lambda + b_\lambda \times Color + C$, where a_λ and b_λ are bandpass dependent constants and C is a constant that depends on the stellar initial mass function (IMF). For the V band, Bell et al. (2003) find $a_\lambda = -0.628$ and $b_\lambda = 1.305$; assuming a Kroupa et al. (1993), they find $C = -0.10$. The Weinzirl et al. (2009) sample is limited to only disk galaxies, which they assume to be those with $B/T < 0.5$. The bulge-to-disk decomposition is carried out using several algorithms for two-dimensional luminosity decomposition, including GIM2D (Simard et al. (2002)), GALFIT (Peng et al. (2002)) and BUDDA (deSouza et al. (2004)).
- **Cibinel et al. (2013).**- The data and B/T ratios presented by these authors are taken from the Zurich Environmental Study (ZENS; Carollo et al. (2013)), which is based on a sample of 1484 galaxies, members of 141 galaxy groups extracted from the 2-degrees Field Galaxy Redshift Survey (2dFGRS; Colless

et al. (2001), Colless et al. (2003)), and specifically from the Percolation-Inferred Galaxy Group (2PIGG) catalog Eke et al. (2004). The group halo mass, the distance from the center of the group, the rank within the group (i.e., whether the galaxy is the central or a satellite) and the location on the large-scale structure (LSS) are given for each galaxy. The bulge-disk decomposition is carried out by using the Galaxy IMage 2D (GIM2D) software package (Marleau and Simard (1998); Simard et al. (2002)).

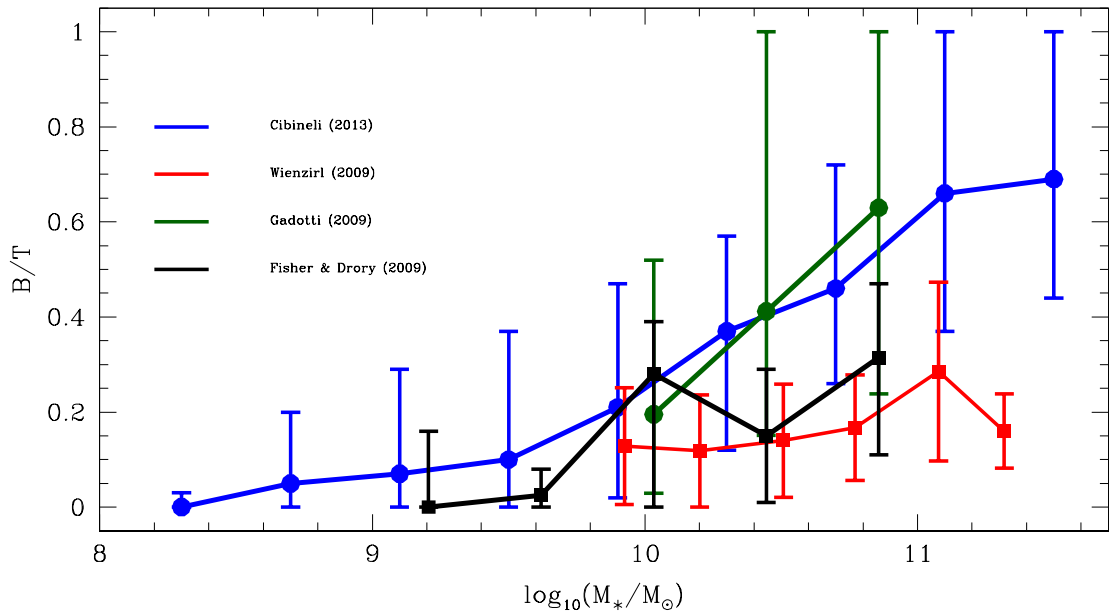


Figure 2.5: The observationally inferred B/T mass ratio as a function of stellar mass. The blue filled circles with error bars are from the groups sample of Cibinel et al. (2013). The red filled squares with error bars are from Weinzirl et al. (2009) and refer only to disk-dominated galaxies ($B/T < 0.5$). The green dots with error bars are from Gadotti (2009). The black filled squares with error bars are from the local 11-Mpc volume study of Fisher and Drory (2011).

2.5 The gas-to-stellar mass ratio vs. stellar mass

The determination of the gas fractions for large samples of galaxies is not an easy task since it requires of dedicated campaigns of observations in radio, both for the atomic HI and molecular H₂ gas contents. For the latter, a tracer of H₂ should be

used for massive studies, for example the CO emission lines. Besides, in order to infer the gas fractions or the gas-to-stellar mass ratios, observations in the optic that provide the data to infer M_* are necessary.

A recent compilation and homogenization of data from the literature of samples that contain information on M_* and M_{HI} and/or M_{H_2} was presented in Calette (2014). The total cold gas mass is calculated as $M_g = (M_{\text{HI}} + M_{\text{H}_2}) + M_{(\text{He+Z})} = 1.4(M_{\text{HI}} + M_{\text{H}_2})$, where the factor 1.4 accounts for helium and metals. In Calette (2014), blue/late-type and red/early-type galaxies were treated separately because the gas fractions in both populations are quite different. The author determined the $M_{\text{HI}}-M_*$ and $M_{\text{H}_2}-M_*$ correlations, and from them inferred the M_g-M_* correlation, all the time by separate for blue/late-type and red/early-type galaxies.

In Fig. 2.6, the M_g/M_*-M_* correlation for blue/late-type galaxies as inferred from observations in Calette (2014) is plotted. The dashed lines correspond to the 1σ scatter.

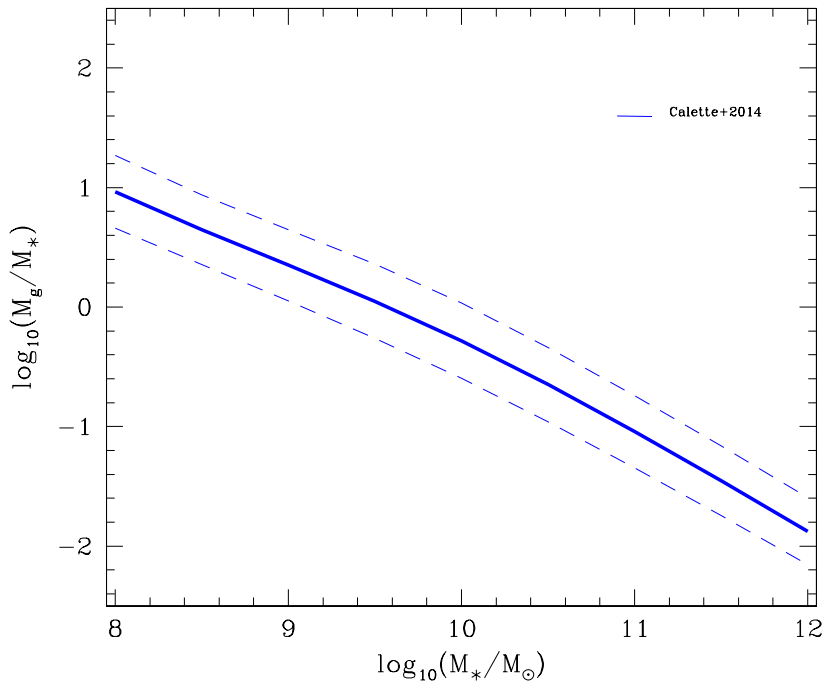


Figure 2.6: Cold gas-to-stellar mass ratio of blue/late-type galaxies as a function of M_* as inferred in Calette (2014). The dashed lines are the 1σ scatter.

Chapter 3

The Semi-empirical Method

3.1 The static model

3.1.1 A disk-halo model

As already mentioned above, the "static" model introduced by Mo et al. (1998) (hereafter MMW98) became a powerful tool for probing the correlations of disk galaxies formed inside CDM halos. We call "static" this model in order to differentiate it from those where the evolution of the galaxy is followed (e.g., Firmani and Avila-Reese, 2000; Avila-Reese and Firmani, 2000; van den Bosch, 2000b; Dutton and van den Bosch, 2009). In the static model, a disk is loaded instantaneously into the gravitational potential of a Λ CDM halo, and the dynamics is solved in order the disk settled into centrifugal equilibrium, taking into account its drag onto the inner halo. The halo is assumed to be spherical and with an initial NFW density profile (Navarro+1997):

$$\rho = \frac{4\rho_s}{(r/r_s)(1+r/r_s)^2}, \quad (3.1)$$

where r_s is the characteristic radius at which the logarithmic slope of the density distribution $d\ln\rho/d\ln r = -2$ and $\rho_s = \rho(r_s)$. We define the virial radius, R_{vir} , as the radius that encloses a mean density equal to Δ_{vir} times the mean density of the universe, where Δ_{vir} is obtained from the spherical top-hat collapse model. The

halo mass profile obtained by integrating equation (3.1) is:

$$M(r) = 8\pi\rho_s r_s^3 \left[\frac{1}{1+Cx} - 1 + \ln(1+Cx) \right], \quad (3.2)$$

where $x \equiv r/R_{vir}$ and

$$C = \frac{R_{vir}}{r_s} \quad (3.3)$$

is the NFW concentration parameter. We also define the virial velocity V_{vir} as the circular velocity at the virial radius, $V_{vir}^2 = GM_{vir}/R_{vir}$, where G is the gravitational constant, M_{vir} is the virial mass and R_{vir} is the virial radius.

The angular momentum of the halo is expressed through the so-called spin parameter λ :

$$\lambda = \frac{J_{vir} |E|^{\frac{1}{2}}}{GM_{vir}^{\frac{5}{2}}} = \frac{J_{vir}/M_{vir}}{\sqrt{2}R_{vir}V_{vir}} f_c^{\frac{1}{2}}, \quad (3.4)$$

where J_{vir} is the total angular momentum at the virial radius, E is the halo energy and

$$f_C = \frac{C}{2} \frac{1 - 1/(1+C)^2 - 2\ln(1+C)/(1+C)}{[C/(1+C) - \ln(1+C)]^2}, \quad (3.5)$$

which measures the deviation of E from that of a singular isothermal sphere with the same mass (see MMW98). The spin parameter is a measure of the centrifugal rotational support of a structure against the potential energy. For $\lambda = 1$, the structure is fully supported by rotation, while for $\lambda \ll 1$, rotation is not important for the virial equilibrium.

Due to the gravitational effects produced by forming galaxies, the halo contracts its inner regions. This happens when baryons cool and concentrate in the center of the spheroid, modifying the shape of the gravitational potential. Since this process is slow with respect to the dynamical time of the system, the halo contracts to conserve its adiabatic invariants taking into account that its spherical symmetry remains. This way, the angular momentum of individual dark matter particles, which moves on circular orbits, is conserved during contraction. Therefore, a particle that is initially (before the formation of the disk) at radius r_i , ends up at radius r_f , where

$$GM_f(r_f)r_f = GM_i(r_i)r_i. \quad (3.6)$$

Here $M_i(r_i)$ is given by equation (3.2) (NFW profile) and $M_f(r_f)$ is the total final

mass within r_f . The final mass is the sum of the dark matter mass inside the initial radius r_i and the mass of an exponential disk (Blumenthal et al. (1986)):

$$M_f(r_f) = M_d(r_f) + M_{h,f}(r_f) = M_d(r_f) + (1 - f_{\text{bar}})M_i(r_i), \quad (3.7)$$

where f_{bar} is the fraction of the total mass locked in the baryonic disk of mass M_d , that is, $f_{\text{bar}} \equiv M_d/M_h$, and

$$M_d(r) = M_d \left[1 - \left(1 + \frac{r}{R_D} \right) e^{-r/R_D} \right]. \quad (3.8)$$

Thus, from equations (3.6) and (3.7), we can find iteratively a contraction factor $\Gamma(r_i) \equiv \frac{r_f}{r_i}$, which allows us to calculate the mass distribution of the contracted dark matter halo. The relation between r_i and r_f can be generalized as

$$r_f = \Gamma^\nu r_i, \quad (3.9)$$

where ν is a free parameter and varies according the type of contraction. For example, $\nu = 1$ is the standard contraction for radial orbits from Blumenthal et al. (1986), $\nu = 0$ is for non contraction, and $\nu < 0$ corresponds to models of expansion of the inner dark matter halo instead of contraction. In Dutton et al. (2007) it was proposed that most of halos actually should expand due to galaxy formation, because of the strong effects of SN-driven outflows. In a more standard context, based on numerical cosmological hydrodynamical simulations, Gnedin et al. (2004) have found that the Blumenthal et al. (1986) adiabatic contraction formalism should be slightly corrected (the particle orbits deviate from the pure circular motion). The corrections suggested by their results is such that instead of the standard value $\nu = 1$, one should use $\nu = 0.8$. This is the value that we will use in our model.

In the static model of disk galaxies in centrifugal equilibrium loaded inside Λ CDM halos, it is assumed that the baryons initially had the same density profile and angular momentum distribution as the dark matter. Therefore, if we assume detailed angular momentum conservation (i.e., the specific angular momentum of the disk, J_{gal}/M_d remains the same as that one of the halo, J_{vir}/M_h), then the spin parameter of the baryons that will form the disk is the same than the halo one,

$\lambda_{bar} = \lambda_h$. If this assumption is relaxed, then

$$\lambda_{bar} \equiv \left(\frac{j_{gal}}{f_{bar}} \right) \lambda_h, \quad (3.10)$$

where

$$j_{gal} = J_{gal}/J_{vir}. \quad (3.11)$$

The total angular momentum for a disk with a surface density distribution $\Sigma(R)$ and a circular velocity profile $V(R)$ is

$$J_{gal} = 2\pi \int_0^{R_{vir}} \Sigma(R) R V_T(R) R dR. \quad (3.12)$$

We assume that the disk has an exponential surface density distribution $\Sigma(R) = \Sigma_0 \exp(-R/R_D)$, so that

$$J_{gal} = M_d R_D V_{vir} f_V, \quad (3.13)$$

where

$$f_V = \frac{1}{2} \int_0^{R_{vir}/R_D} e^{-u} u^2 \frac{V(uR_D)}{V_{vir}} du, \quad (3.14)$$

a factor that takes into account the gravitational effects of the disk. Assuming that the angular momentum of the disk is a fraction of the total angular momentum of the halo (i.e. $J_{gal} = j_{gal} J_{vir}$), we can combine equations (3.4) and (3.12) to obtain:

$$R_D = \frac{1}{\sqrt{2}} \left(\frac{j_{gal}}{f_{bar}} \right) \lambda_{bar} R_{vir} f_c^{-1/2} f_V^{-1}, \quad (3.15)$$

with $\lambda_{bar} = \lambda_h$ when detailed angular momentum conservation is assumed.

Once calculated the scale radius R_D , we can calculate the (total) circular velocity $V_T(R)$, which is the sum in quadrature of contributions from disk and halo:

$$V_T^2(R) = V_D^2(R) + V_H^2(R), \quad (3.16)$$

where

$$V_H^2(R) = G[M_f(R) - M_d(R)]/R, \quad (3.17)$$

and

$$V_D^2(R) = \frac{GM_d}{R_D} 2y^2 [I_0(y)K_0(y) - I_1(y)K_1(y)] \quad (3.18)$$

is the circular velocity produced by an exponential disk, where $y = r/(2R_D)$, and I_n and K_n are modified Bessel functions (Freeman, 1970). However, in order to define R_D , according to eq. (3.15), we should know the total circular velocity profile (see eq. 3.14). This circularity leads us to use an iterative approach in order to calculate the final disk scale radius R_D of the disk in centrifugal equilibrium with the potential of the cosmological halo contracted on its own by this disk.

3.1.2 A disk-bulge-halo model

In this Section, we describe the inclusion of a bulge proposed to be formed by internal instabilities of the disk, following Dutton et al. (2007, hereafter D+2007). The baryonic mass of the galaxy is now the sum of a disk and a bulge:

$$M_{\text{bar}} \equiv f_{\text{bar}} M_{\text{vir}} = M_d + M_{\text{B}}. \quad (3.19)$$

The bulge-to-disk mass ratio is defined as:

$$\theta \equiv \frac{M_{\text{B}}}{M_d} \quad (3.20)$$

and the disk mass and the bulge mass are given in terms of this ratio, so that

$$M_d = \frac{1}{1 + \theta} f_{\text{bar}} M_{\text{vir}}, \quad (3.21)$$

and

$$M_{\text{B}} = \frac{\theta}{1 + \theta} f_{\text{bar}} M_{\text{vir}}. \quad (3.22)$$

According to eq. (3.11), the fractional angular momentum of the baryons is given by $j_{\text{gal}} = J_{\text{gal}}/J_{\text{vir}}$. Let $J_b = j_b J_{\text{vir}}$ be the original angular momentum of the baryonic material out of which the bulge forms. However, during the bulge formation process this angular momentum is transferred to the disk plus the halo, and therefore the final angular momentum of the bulge is zero (D+2007). If f_t is the fraction of J_b that is transferred to the disk, then the final angular momentum of the disk is

$$J_{\text{gal}} = [j_{\text{gal}} - (1 - f_t)j_b] J_{\text{vir}}, \quad (3.23)$$

and the specific angular momentum of the final disk is

$$\frac{J_{gal}}{M_d} = (1 + \theta)(1 - f_{lost}) \left(\frac{j_{gal}}{m_{gal}} \right) \frac{J_{vir}}{M_{vir}}, \quad (3.24)$$

where the parameter f_{lost} is the fraction of the total angular momentum of the material out of which the bulge plus disk forms and which has been lost to the halo:

$$f_{lost} = (1 - f_t) \left(\frac{j_b}{j_{gal}} \right). \quad (3.25)$$

We define other important parameter:

$$f_x \equiv f_{lost} \left(\frac{1 + \theta}{\theta} \right) = (1 - f_t) \left(\frac{J_b/M_B}{J_{gal}/M_{gal}} \right), \quad (3.26)$$

which expresses the ratio of specific angular momentum that has been lost to the halo due to bulge formation to the total specific angular momentum of the material out of which the disk and bulge have formed. This parameter should be less than unity if the bulge is formed out of material with low specific angular momentum (van den Bosch et al., 2002).

We can obtain a new relation for the scale length of the disk after a bulge formed from the disk by dynamical instabilities by combining equations (3.4), (3.12), (3.11). One obtains:

$$R_D = \frac{1}{f_V \sqrt{2f_c}} [1 + (1 - f_x)\theta] \lambda_{bar} R_{vir}, \quad (3.27)$$

where λ_{bar} is now the effective initial spin parameter of the material out of which the bulge and disk form, and it is given by

$$\lambda_{bar} \equiv \left(\frac{j_{gal}}{f_{bar}} \right) \lambda, \quad (3.28)$$

where f_{bar} is the baryonic fraction. As we can see in equation (3.25), the bulge formation affects the final scale length of the disk through the parameters θ and f_x . Following D+2007, it is assumed that the material that forms the bulge has the same specific angular momentum as the disk. Here, we assume $f_x = 0.5$ (see Shen et al., 2003).

The new total circular velocity $V(R)$ is given by the equation:

$$V_T^2(R) = V_D^2(R) + V_B^2(R) + V_H^2(R), \quad (3.29)$$

the component V_B is the circular velocity of the bulge, which is derived from the mass distribution of the bulge. In principle, the instabilities are intrinsic (isolated disk), giving rise to secular evolution that ends in a pseudo-bulge (see e.g. Kormendy, 2013). Observations show that pseudo-bulges are well described by a Sérsic surface brightness (surface density) profile with index n between 0.5 and 3. A Sérsic surface density profile (Sérsic, 1963; Sersic, 1968), is given by

$$I(R) = I_{e,B} \exp \left\{ -b_n \left[\left(\frac{R}{R_{e,B}} \right)^{1/n} - 1 \right] \right\}. \quad (3.30)$$

where $I_{e,B}$ is the surface brightness at the effective radius $R_{e,B}$, which is defined as the projected radius that encloses one half of the total luminosity (mass), by adjusting the value of b_n . The conditions to sets the value of b_n is (see Graham and Driver, 2005; Ciotti, 1991):

$$\Gamma(2n) = 2\gamma(2n, b_n), \quad (3.31)$$

where Γ and γ are the Gamma and lower Incomplete Gamma Functions, respectively. Capaccioli (1989) introduced the following approximation for b_n , valid for $0.5 < n < 10$:

$$b_n \approx 2n - (1/3). \quad (3.32)$$

Assuming a spherical density distribution, the surface density profile given by equation (3.30) can be translated into a volumetric density distribution.

According to the formation mechanism, the mass distribution of bulges are expected to be different. Bulges formed by secular evolution of the disk (our starting scenario) have typically the properties of pseudo-bulges (e.g., Kormendy and Kennicutt, 2004; Avila-Reese et al., 2005), with Sérsic profiles shallower than a de Vaucouleurs profile, that is with Sérsic index $n < 4$. Here, we assume an average value of $n = 2$ for the secular bulges (see e.g., Gadotti, 2009), in which case the

mass profile is

$$\nu(R) = M_B \left\{ 1 - \exp(-\sqrt{\alpha^2 \eta}) \left[1 + \sqrt{\alpha^2 \eta} + \frac{(\alpha^2 \eta)}{2} + \frac{(\alpha^2 \eta)^{3/2}}{6} + \frac{(\alpha^2 \eta)^2}{24} + \frac{(\alpha^2 \eta)^{5/2}}{120} \right] \right\}, \quad (3.33)$$

where M_B is the total mass bulge, $\alpha = 5.67$ and $\eta \equiv R/R_{e,B}$. The corresponding circular velocity profile is:

$$V_B(R) = \sqrt{\frac{G\nu}{R}}, \quad (3.34)$$

where G is the gravitational constant.

As it will be discussed below, in the case of massive galaxies, interactions and mergers are actually common. Therefore, the massive disks are expected to undergo strong induced instabilities that end commonly with the formation of large bulges with a de Vaucouleurs profile or $n = 4$ Sérsic profile. The corresponding density profile in this case is given by the Hernquist function (Hernquist, 1990):

$$\rho_b = \frac{M_B}{2\pi} \frac{r_b}{R(R + R_b)^3}, \quad (3.35)$$

where $R_b = R_{e,B}/1.815$ is a scale length. The corresponding circular velocity is:

$$V_B(R) = \frac{\sqrt{GM_B R}}{(R + R_{e,B})}. \quad (3.36)$$

Thus, for galaxies smaller than a given mass, we will assume Sérsic distribution with $n = 2$, while for massive galaxies, $n = 4$. The corresponding circular velocities are given by equations (3.34) and (3.36). In both cases, the relevant parameters are M_B and $R_{e,b}$. Since our model is not evolutionary, we are not in conditions of calculating $R_{e,B}$ for our bulges. Instead, we use an empirical relation between $R_{e,B}$ and M_B , as given in Gadotti (2009):

$$\log R_{e,B} [\text{kpc}] = \begin{cases} -2.062 + 0.2 \log(M_B/M_\odot), & \log(M_B/M_\odot) < 10 \\ -3.057 + 0.3 \log(M_B/M_\odot), & \log(M_B/M_\odot) > 10. \end{cases} \quad (3.37)$$

Finally, we include the bulge component to the final mass budget and eq. (3.7) is then rewritten as:

$$M_f(r_f) = M_d(r_f) + M_B(r_f) + M_{DM,f}(r_f) = M_d(r_f) + M_B(r_f) + (1 - f_{bar})M_i(r_i). \quad (3.38)$$

Thus, we calculate the adiabatic invariant dark matter halo contraction by using this new mass distribution.

Bulge mass assignment

Let us first consider the case of internal dynamical instabilities produced by the secular evolution of a self-gravitating disk. For this, the critical instability parameter let be $\beta(R) = V_D(R)/V_T(R)$. According to the numerical simulations of Christodoulou et al. (1995) the disk is stable as long as $\beta(R) < \beta_{crit}$, where the value of the parameter β_{crit} falls roughly in the range $0.52 \leq \beta_{crit} \leq 0.70$. Following D+2007, we calculate the mass of the disk contained within the radius where $\beta(R)$ attains a maximum and check if $\beta_{max} > \beta_{crit}$:

$$\beta_{max} = \max_{0 \leq R \leq R_{vir}} \beta(R) < \beta_{crit}. \quad (3.39)$$

If this is the case, then all this mass is assigned to a bulge. We use $\beta_{crit} = 0.62$ for the case of an isolated disk.

However, the secular bulge formation mechanism is not suitable in the case of galaxy interactions and mergers. The mergers transfer the secondary galaxy to the bulge of the primary, and induce disk instabilities in the primary (Hopkins et al., 2010, see more references therein),. In order to take into account these effects, yet within our scheme of β_{max} , we propose that the bulge formation by mergers can be emulated by lowering the value of β_{crit} . It is well known that mergers become important in the mass assembly of only massive galaxies ($M_* \geq 2 - 3 \times 10^{10} M_\odot$, $M_h \geq 3 - 5 \times 10^{11} M_\odot$), being more frequent as more massive they are (see e.g., Gottlöber et al., 2001; Zavala et al., 2012). Therefore, one expects that β_{crit} will decrease on average with M_h . This dependence will be fixed in order our model could reproduce the observational trend of the bulge-to-disk ratio with M_* .

Note that in our scheme the bulge is formed only from stars of the primary disk.

This might not be the case when the mergers are majors because in this case most of the stars in the bulge come from the accreted secondary galaxy rather from the disk. This is why our scheme becomes somewhat uncertain for galaxies dominated by bulges.

3.1.3 Stellar and gas fractions

So far in our static model of disk galaxies in centrifugal equilibrium loaded inside Λ CDM halos, we did not make any difference between stellar and gas components in the galaxies. Since the static model is not an evolutionary model, we can not follow a star formation history as well as we can not follow the secular or major merger processes. However, as was done in the case of bulge formation, the structural and dynamical internal distributions of our "instantaneous" galaxies can be used for estimating when the conditions of large-scale star formation due to disk instabilities are fulfilled. The simple Toomre criterion (Toomre, 1964) will be used for this purpose.

First, we consider that if a fraction of the disk is converted into bulge, according to the criterion described in the previous subsection, then the bulge is composed only by stars. Second, for the remaining baryonic disk, we estimate the fraction of it that could have been transformed into stars. According to the Toomre criterion, instabilities in a gaseous disk able to drive star formation happen when $\Sigma_{crit}(R) < \Sigma_d(r)$, where

$$\Sigma_{crit}(R) = \frac{\sigma_{gas}(R)\kappa(R)}{3.36QG}. \quad (3.40)$$

Here, $\Sigma_d(r)$ is the baryonic (assumed gaseous initially) disk surface density profile, $\kappa(R)$ and σ_{gas} are the epicycle frequency and velocity dispersion radial distributions, and Q is the Toomre stability parameter. The two first distributions are given by the solution of our static model. Regarding σ_{gas} , observational studies of neutral, atomic (H_I) gas for spiral galaxies, including our galaxy, show that it lies in a range of 5–15 km/s (Tamburro et al., 2009; Petric and Rupen, 2007; van Zee and Bryant, 1999) without any clear trend with radius. We will assume a constant value of $\sigma_{gas} = 7$ km/s.

The Q stability parameter originally given in Toomre (1964) for an infinitesimal thin disk has the value of 1. However, in numerical simulations of more realistic

disks, the value found for Q is typically $1.5 - 2.5$. In the early stages of the gaseous disk, the formation of massive clumps make the disk more unstable and the value of Q can be larger (Dekel and Birnboim, 2008; Perez et al., 2013). Besides, the Toomre criterion changes a little when taking into account the coexistence of two fluids, stars and gas (Shen and Lou, 2003)). The value of Q is affected by other factors, such as the presence of a bulge; a bulge provides more dynamical support against instabilities, making the Q parameter larger. Other factors affecting Q are the height of disk, which is derived from vertical equilibrium, as well as the gas dissipation which extends the instability to small scales, producing infinitesimally thin disks unstable for all Toomre- Q values and reasonable thick disks stable at high Q , primarily because of thickness effects (Elmegreen, 2011; Romeo and Wiegert, 2011). The turbulences of gas also change Q ; the perturbations in the molecular and atomic gas have a significant effect on both the inner and outer regions of the disk. This can drive the inner gas disk to a regime of transition between two stability phases such that the outer disk is more prone to star-dominated instabilities (Hoffmann and Romeo, 2012; Shadmehri and Khajenabi, 2012).

There are also observational studies that attempted to constrain the value of Q along the disks of local galaxies. For example, Bottema (1993) conclude that Q along the disks of their analyzed spiral galaxies is around 2 and 2.5.

We will take a constant value of $Q = 2.5$ for the “secular” disks, i.e. those that are not expected to have suffered mergers. This applies on average for low-mass galaxies, let say those smaller than $M_* \approx 3 \times 10^{10} M_\odot$ ($M_h \approx 5 \times 10^{11} M_\odot$). However, as already discussed in the previous subsection, for galaxies formed in more massive halos, the major mergers become more frequent in such a way that the central galaxy likely suffers also mergers and interactions, which trigger strong disk instabilities able to produce bursts of star formation. Since our model is not evolutionary, we are not able to calculate these processes, but if we keep ourselves in the scheme of the Toomre instability criterion, such an enhanced star formation can be estimated somehow by increasing artificially the value of Q . As in the case of bulge formation in massive galaxies, we again will proceed empirically. The “artificial” value of Q as a function of M_h for the massive halos will be set in such a way that the gas fraction, R_{gas} , vs stellar mass empirical relation is reproduced. The observations show that as larger are the galaxies, the smaller gas fractions have (or larger stellar fractions have). In the next Section, it is described in more detail our procedure.

Following the Toomre instability criterion, the stellar mass contained up to the radius r along the disk is calculated as:

$$M_{d,*}(r) = 2\pi \int_0^r [\Sigma_s(r)] r' dr' \quad (3.41)$$

where $\Sigma_s(r) = \Sigma_{bar}(r) - \Sigma_{crit}(r)$ is the stellar surface mass density in the regions where the local criterion for instability is fulfilled. $M_{d,*}(r)$ is computed up to the radius where $\Sigma_b(r) = \Sigma_{crit}(r)$. The total baryonic surface density is then $\Sigma_{bar}(r) = \Sigma_d(r) + \Sigma_g(r)$. Since by construction $\Sigma_{bar}(r)$ is an exponential function, the stellar surface mass density is expected then to be deviate from an exponential distribution.

Summary

The initial parameters of our static model are the halo mass M_h (its initial distribution is assumed to follow the NFW density profile), the halo λ and C parameters, and f_{bar} . By means of iterations, a baryonic exponential disk in centrifugal equilibrium is constructed, taking into account the gravitational drag of the halo within the adiabatic invariance approach. During the iterations, the regions of the disk that obey our criterion of dynamical instability are converted into a Sérsic bulge, which has its own contribution to the gravitational potential. As the result, a bulge-disk-halo system in equilibrium is obtained; the main criterion of convergence of the iterations is when R_D changes less than a given ϵ . For the remaining disk in centrifugal equilibrium, the Toomre gas stability criterion allows us to estimate the amount of stars formed along the disk. The bulge is assumed to be made only of stars.

The main equations solved in the iterations are (3.38), (3.8), (3.20), (3.27) and (3.29). Following MMW98 and D+2007, we start with a guess for R_D by setting $f_V = 1$ in equation (3.27). Then, we obtain M_d from equation (3.8) and M_B from equation (3.20); by replacing this into equation (3.38) and using equation (3.6), we find r_i as a function of r to obtain M_f from equation (3.38). Thus, we have $V_T^2(R)$ and the bulge mass M_B for the given R_D , and we can calculate the bulge circular velocity and the new disk circular velocity from equations (3.17) and (3.29). Replacing this into eq. (3.14) and using (3.27), finally we obtain a new value for R_D and M_B and check for convergence. In Fig. 3.1 we show the total circular

velocity profile and its decomposition into bulge, disk, and halo for models of four halo masses and with the average values of λ_{bar} , f_{bar} and C corresponding to these masses. For the average λ_{bar} values, we use those ones constrained and discussed in Chapter 5. The radii are normalized to the stellar effective radius, R_e , of each model, which are indicated inside each panel. From panel (a) to panel (d), the masses are $\log(M_h/M_\odot) = 10.5, 11.5, 12.0$ and 13.5 .

In the case of the lowest halo mass model, stars nor bulge are not formed (the respective instability criteria are not obeyed at any radius); therefore, the baryonic component corresponds only to a gaseous disk. The halo component completely dominates in the circular velocity profile at all radii, whose maximum is attained at $\approx 4R_e$; at inner radii, V_c keeps increasing with radius. For the $\log(M_h/M_\odot)=11.5$ model, stars and a bulge form. However, the circular velocity continues being dominated by the the halo component, excepting at the very inner regions, where the bulge component dominates, though not too significantly as to affect the maximum of V_c ; V_{\max} is attained at $\approx 2.7R_e$. For the $\log(M_h/M_\odot)=12.0$ model, the compact bulge component is already significant enough as to produce a bumped maximum in V_c at the very center of the galaxy; at slightly larger radii, the V_c profile follows the decreasing behavior of the bulge component and at $\sim 1R_e$ it flattens and then gently decreases with radius. In the case of the $\log(M_h/M_\odot)=13.5$ model, the bulge also produces an inner bump in the V_c profile, but at larger radii, V_c again rises with radius, following the halo component which is dominant, as in the case of the low-mass systems; this is because f_{bar} is very small for this model, following the semi-empirical $f_{\text{bar}}-M_h$ relation. The V_{\max} is attained at a very external radius.

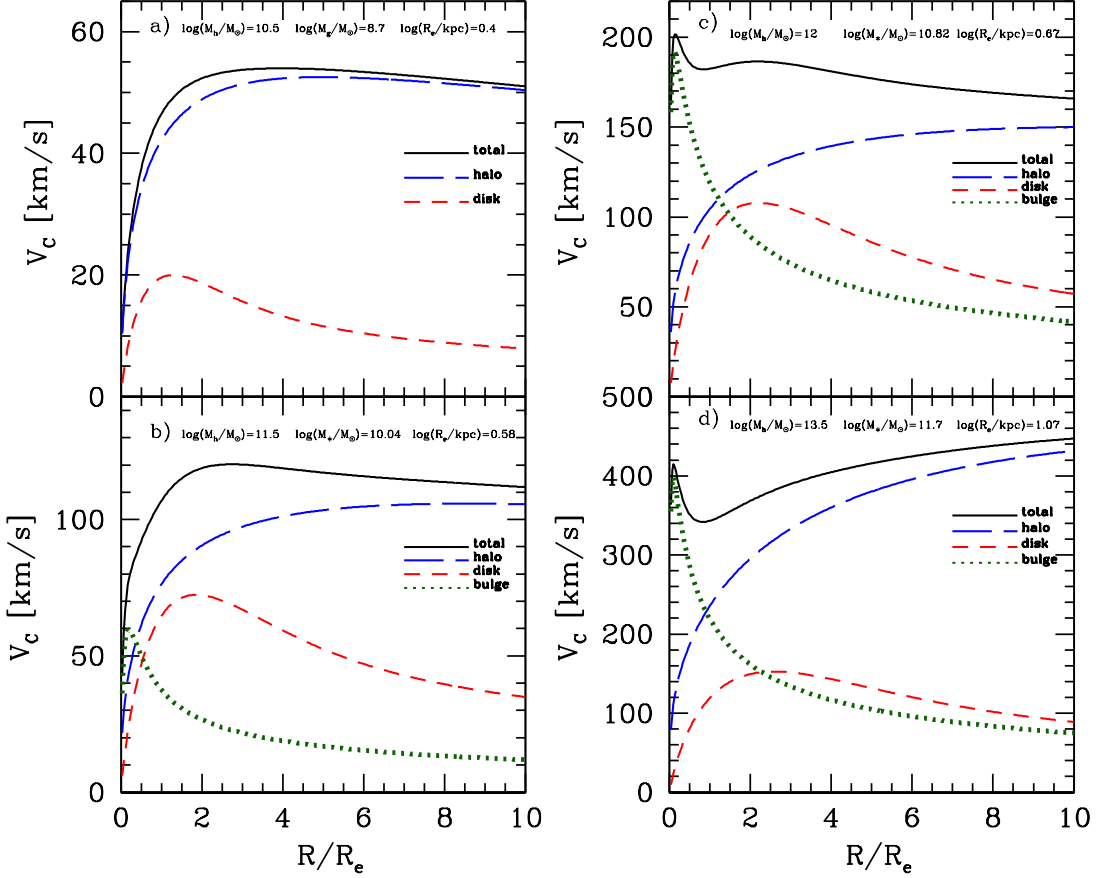


Figure 3.1: The circular velocity profiles and their decompositions into bulge, disk, and bulge (solid black, dotted green, dashed red and long-dashed blue lines, respectively). Each panel corresponds to a halo mass, indicated inside the panel. The radii are normalized to the R_e of each model. The λ_{bar} , C and f_{bar} input parameters of each model were taken as the average ones corresponding to the given M_h .

3.2 The procedure

In this Section, we describe the steps to generate a mock catalog of disk galaxies, which is our ultimate goal. We set up an uniform halo mass distribution in bins of 0.1 *dex* in $\log_{10} M_h$ in the mass range 10^{10} to $10^{14} M_\odot$. Note that the Λ CDM halo mass function (HMF) is not uniform, but in order to obtain scaling relations, we

need to sample all masses with good statics. The Λ CDM HMF strongly decreases with mass and it is described well, for example, by the Sheth-Thormen function (Sheth and Tormen, 1999). In order that our mock catalog predicted statistical distributions of the galaxy properties, we can convolve it with this function. The mock catalog is generated as follows:

For each halo mass bin of 0.1 *dex*, we assign the input parameters by taking them randomly from their corresponding distributions. These distributions are as follow:

- ★ For the spin parameter, it is a lognormal function:

$$P(\log \lambda) = \frac{1}{\sigma_\lambda \sqrt{2\pi}} \exp \left[-\frac{\log^2(\lambda/\lambda_0)}{2\sigma_\lambda^2} \right], \quad (3.42)$$

where λ_0 is the mean and σ_λ is the width. Cosmological N-body simulations show that both λ_0 and σ_λ do not depend on M_h . We use the values measured in the Millennium Simulations for unperturbed halos by Bett et al. (2007): $\lambda_0 = 0.03687 \pm 0.000016$ and $\sigma_\lambda = 0.2216 \pm 0.00012$.

- ★ For the NFW concentration parameter, C , the N-body cosmological simulations show that it follows a lognormal distribution at a fixed halo mass, with the mean of this distribution, \bar{C} , slightly decreasing with M_h , while the width, σ_{lgC} , remains roughly constant. For the mean, we use here the $\bar{C} - M_h$ relation reported for the Bolshoi Simulation in Muñoz-Cuartas et al. (2011) as

$$\log_{10} \bar{C} = a(z) \log_{10}(M_h/[h^{-1} M_\odot]) + b(z), \quad (3.43)$$

where $a(z) = wz - m$ and $b(z) = [(\alpha/z + \gamma) + (\beta/(z + \gamma)^2)]$ are the coefficients given at any redshift and the additional fitting parameters have been set equal to $w = 0.029$, $m = 0.097$, $\alpha = -110.001$, $\beta = 2469.720$ and $\gamma = 16.885$. For the width, we adopt $\sigma_{lgC} = 0.11$ dex

- ★ Regarding f_{bar} , the semi-empirical dependence of f_{bar} on M_h for blue/late-type galaxies presented and discussed in Chapter 2 is used. According to it, for a given M_h , f_{bar} follows a lognormal distribution with constant width $\sigma_{lgf_{\text{bar}}} = 0.12$ dex. The mean of this distribution depends on M_h . The results

obtained in Calette (2014), show that the mean $M_{\text{bar}} - M_h$ relation of blue/late-type galaxies is well fitted by a Behroozi et al. (2013) function:

$$\log_{10}(M_{\text{bar}}/M_h) = \log_{10}(\epsilon M_1) + f(x) - f(0), \quad (3.44)$$

where

$$f(x) = -\log_{10}(10^{-\alpha x} + 1) + \frac{\delta[\log_{10}(1 + \exp(x))]^\gamma}{1 + \exp(10^{-x})}, \quad (3.45)$$

and $x = \log_{10}(M_h/M_1)$. The fit of this function to the Calette (2014) results give the next values for these parameters: $\log_{10}M_1 = 11.69$, $\epsilon = 0.0668$, $\alpha = 1.5$, $\delta = 2.6993$, $\gamma = 0.8275$.

For each M_h and the set of initial conditions taken from the distributions above mentioned, we apply the static model of disk galaxies in centrifugal equilibrium inside Λ CDM halos described in Section 3.1, and generate the global properties and internal mass distributions of the given galaxy. As discussed above, in the case the disks evolved only secularly, without mergers and interactions, the dynamical criterion for bulge formation in isolated disks (§§3.1.2) and the Toomre criterion for disk star formation (§§3.1.3) apply normally. In both cases, the criteria are given by one parameter, β_{crit} and Q , respectively. The values we assume for these parameters are $\beta_{\text{crit}} = 0.62$ and $Q = 2.5$ (see for details the mentioned subsections).

For each halo mass bin, we perform 1000 random extractions from the distributions for λ , C and f_{bar} presented above.¹ We have checked that 1000 extractions are enough to sample well each one of these distributions. Since we cover the halo mass range from 10^{10} to 10^{14} M_\odot in bins of 0.1 dex, we have 40 mass bins. For each bin, we perform 1000 realizations of our three parameters, for a total of 40,000 models. In Chapter 5, we will show how

¹We make use of the fact that the integrals of two probability distributions are equal, $\int_0^x h(x')dx' = \int_0^y g(y')dy'$. In the case of a uniform distribution between 0 and 1, $\int_0^x U(x')dx' = x$. Therefore, a random number y from the distribution $g(y)$ can be obtained by resolving the equation $x = \int_0^y g(y')dy'$, where x is a random number from the $[0,1]$ interval. In all the three cases of the parameters λ , C , and f_{bar} , they are log normally distributed, or, that is the same, the logarithms of these parameters, are Gaussian distributed. Therefore, we solve the above equation for a Gaussian function.

well sampled are the given distributions of the parameters with our statistical realizations.

Chapter 4

Disk galaxy correlations: the case of isolated galaxies

In the previous Section, we have described our stationary model for generating a population of disk galaxies inside Λ CDM halos. This model has two sets of input parameters:

1. **Initial conditions parameters**, which define the halo-galaxy global properties. They are the halo mass, M_h , halo spin parameter, λ , halo concentration, C , and the galaxy baryon fraction, $f_{\text{bar}} = M_{\text{bar}}/M_h$. The three first parameters are related to the “cosmological” dark matter halos. The baryon fraction f_{bar} encloses the complex astrophysical processes of gas accretion and cooling into the galaxy, as well as the stellar- and AGN-driven outflows. The relationship of f_{bar} on M_h and its scatter for disk galaxies (actually, blue/late-type galaxies) has been recently determined in Calette (2014) and we use it here. The initial spin parameter out of which the galaxy forms, λ_{bar} , actually could deviate from the one of the halo; by the moment we assume detailed angular momentum conservation in which case $\lambda_{\text{bar}} = \lambda$.
2. **Disk instability parameters**, which are related to the criteria that define the amount of disk mass transformed into bulge (β_{crit}), and the amount of disk gas mass transformed into stars (the Q Toomre parameter).

All these parameters are in principle thought for distinct (“isolated”) halos, inside which formed one central disk that evolves *secularly*, i.e., the disk does not suffer mergers and external perturbations, and it is formed under detailed angular momentum conservation. In this Chapter, these will be our initial (naive) assumptions. We proceed by generating a mock disk galaxy catalog as described in subsection 3.2.

Before presenting the main results from the generated catalog, we note that there is a (small) fraction of model galaxies with some peculiarities:

- Galaxies with B/T ratios larger than 0.5. Elliptical galaxies are typically defined as those with B/T>0.5. Therefore, we exclude from our statistics models with B/T>0.5. They are actually few and mostly in the $10^{10} - 10^{11}$ M_{\odot} stellar mass range.
- Galaxies with no stellar masses, i.e., those for which the Toomre criterion never was attained. These are purely gaseous galaxies. In the lowest halo mass bins ($M_h \lesssim 3 \times 10^{10} M_{\odot}$), they are more than 50% of the cases. At higher masses, the gaseous galaxies are very rare.
- Models that did not converge. The overall fraction of not converged models is 1.8%. There is not a trend of not converged models with M_h , f_{bar} and λ ; instead, many of them happen for low values of C .

4.1 Results

In Fig. 4.1, the stellar and baryonic effective radius–mass relations are plotted (left and right upper panels, respectively). The effective radius is defined as the one inside which half of the (bulge+disk) stellar mass (R_e) or (bulge+disk) baryonic mass ($R_{e,\text{bar}}$) is contained. The solid line and shaded area correspond to the mean and standard deviation from our model results in M_* bins of 0.3 dex. The blue dashed line and the dotted lines are the mean and the 1σ scatter from observations corresponding to Shen et al. (2003), while the pink and red dots connected by long-dashed lines correspond to the studies by Mosleh et al. (2013) and Bernardi et al. (2012), respectively. See Section 2.2 for details on these observational inferences as well as on other ones; we

consider that the showed observational determinations are representative of the $R_e - M_*$ observational relation and its scatter.

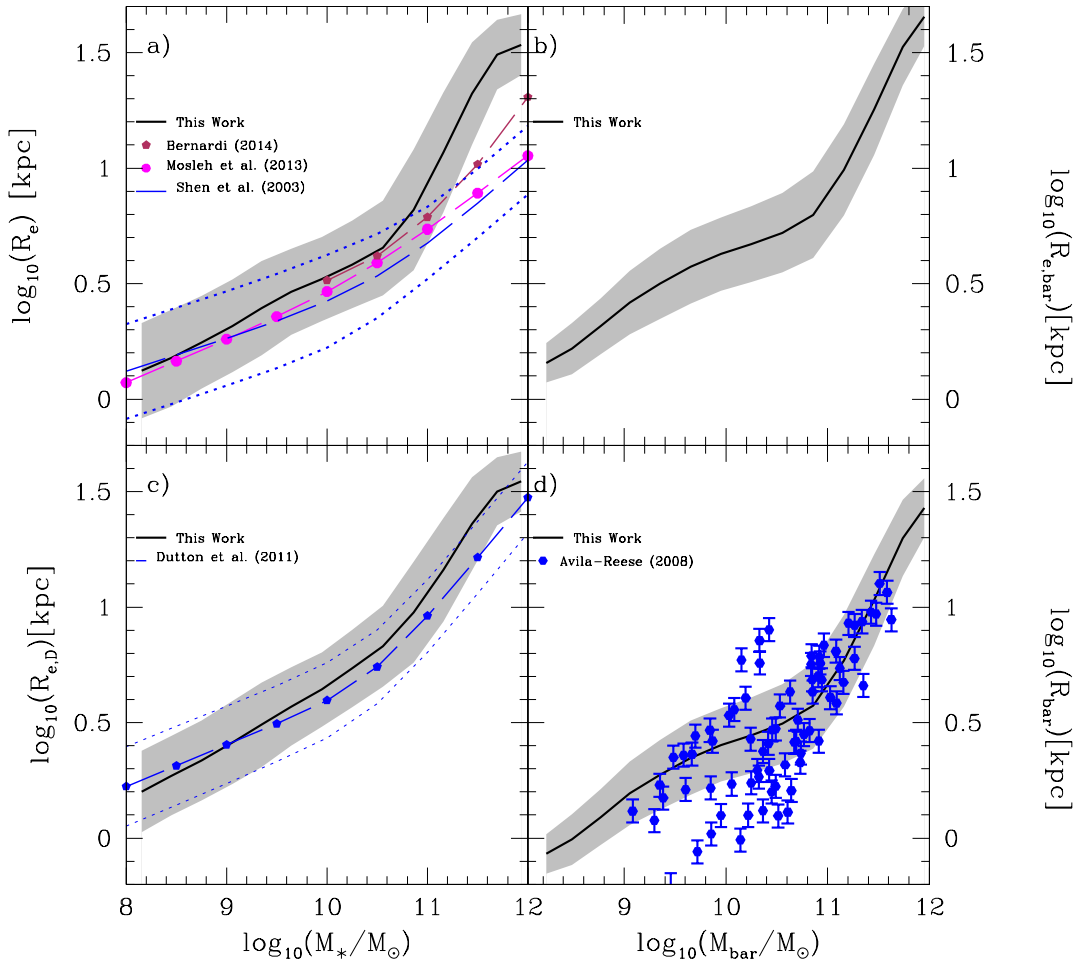


Figure 4.1: Different radius–mass relations from the models ($B/T \leq 0.5$) compared to some observational determinations (indicated inside the panels). The black solid lines and the shaded areas are the model means and standard deviations obtained in small M_* bins. *Upper left panel:* Stellar effective radius vs. M_* . *Upper left lower panel:* Disk stellar effective radius vs. M_* . Note that the observational correlation by Dutton et al. (2011) is actually for the exponential disk scale length; for this case, $R_{e,D}=1.68R_D$. *Upper right panel:* Baryonic stellar effective radius vs. M_{bar} . *Lower right panel:* Disk baryonic scale radius vs. M_{bar} .

In the left lower panel, we plot the effective radius of only the stellar disk component, $R_{e,D}$, versus the total galaxy stellar mass (black solid line and shaded area). This is compared to the fit to observations presented in Dutton et al. (2011, blue dashed and dotted lines, for the mean and 1σ scatter, respectively). These authors used bulge-disk decompositions to estimate the exponential disk scale radius; the $R_{e,D}$ they report is then $R_{e,D} = 1.68R_D$ (see Section 2.2 for details). In the right lower panel, we plot the $R_{\text{bar}} - M_{\text{bar}}$ relation, where R_{bar} is the baryonic disk scale radius, which by definition is exponential. We compare these results with the respective observational data from a compilation of disk galaxies presented in Avila-Reese et al. (2008, blue circles with error bars).

The model results agree well with the $R_e - M_*$ relation from observations up to $\log(M_*/M_\odot) \approx 10.7$; at larger masses, the trend of increasing R_e with M_* is steeper in the models than in the observations. The scatter around the relations are also similar in models but at $\log(M_*/M_\odot) \gtrsim 10.7$, the scatter is larger in the former. The recent results from Bernardi et al. (2012) show that the $R_e - M_*$ relation can be steeper at large masses than previous works. However, even in this case, the model $R_e - M_*$ relation is steeper at the high-mass. A similar situation is seen for the $R_{e,D} - M_*$ relation, though model and observations agree better than in the case of the $R_e - M_*$ relation. *This suggests that the potential problem is mainly at the level of the bulge component.* Regarding the baryonic disk radius–baryonic mass relation (lower right panel), the model results are also consistent with the observations.

As previous studies have shown, the size–mass relation of disk galaxies depends mainly on the spin parameter λ and the baryon fraction f_{bar} , and the scatter around this relation is given by the scatter in the λ distribution (see e.g., Mo et al., 1998; Firmani and Avila-Reese, 2000; Dutton et al., 2007; Avila-Reese et al., 2008). The combination of the recently determined $f_{\text{bar}} - M_h$ relation for blue/late-type galaxies and halo λ distribution measured in large cosmological simulations, produces galaxies that at masses lower than $\log(M_*/M_\odot) \approx 10.7$ have mean sizes for their masses in good agreement with observations; the agreement is also remarkable at the level of the scatter around the mean relation. However, the models disagree with observations in the size–mass relations at larger masses in the direction of being the sizes and the dispersions too

large. This suggest mainly the presence of some evolutionary mechanism(s) able to lower the angular momentum of the baryons that ultimately form the bulge-disk galaxy. In figure 4.2, we show the stellar and baryonic TF relations (V_{\max} vs. M_* and V_{\max} vs. M_{bar} , respectively). Here, V_{\max} is the maximum of the total (bulge+disk+contracted halo) circular velocity profile. The solid lines and shaded areas correspond to the means and standard deviations from our model results in M_* bins of 0.3 dex. The red solid line in each panel is the best orthogonal fit to observations reported in Avila-Reese et al. (2008, see Section 2.3); the dotted lines enclose the 1σ *intrinsic* scatters given by these authors. The data points with error bars correspond to individual observations of dwarf galaxies by Geha et al. (2006, red dots) and McGaugh (2011, green dots)(see Fig. 2.4).

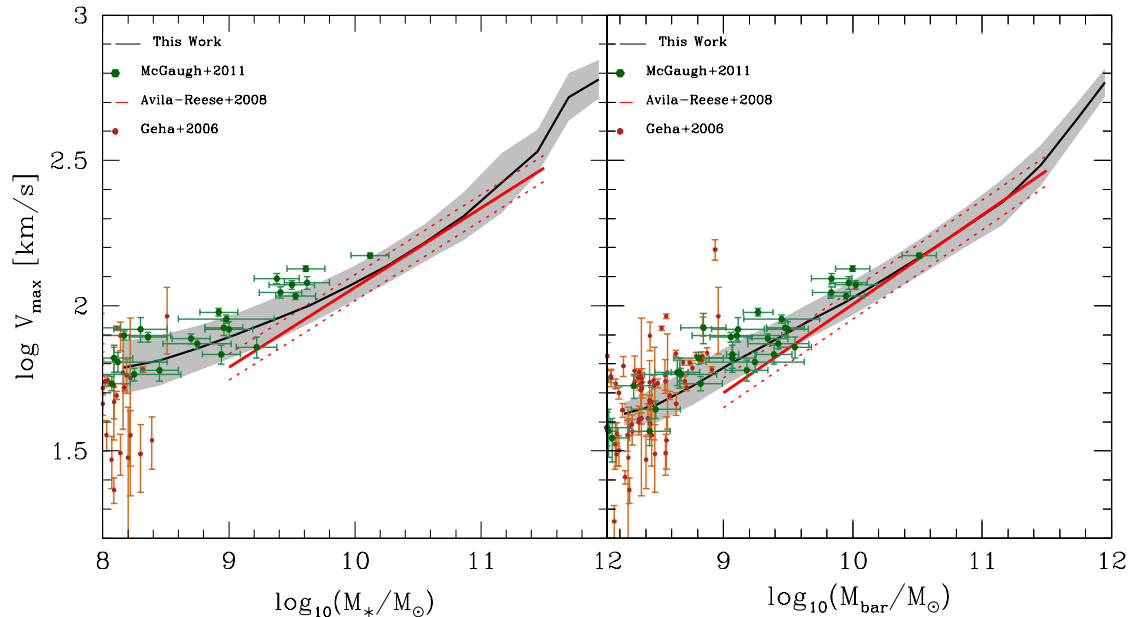


Figure 4.2: Predicted dependence of V_{\max} as a function of stellar mass (left panel) and baryonic mass (right panel) using initial cosmological parameters and the $f_{\text{bar}}-M_h$ relation inferred by Calette (2014). The average and 1σ of the model population distribution are plotted with solid lines and shaded areas. The fits and 1σ intrinsic scatter in both panels to a compiled sample of normal disk galaxies by Avila-Reese et al. (2008) are plotted with red solid and dotted lines, respectively. The red dots are for observed dwarf galaxies by Geha et al. (2006), while the green dots are from McGaugh (2011).

For intermediate masses, the model results are in rough agreement with the observations both in the stellar and baryonic TF relations; if any, the models have slightly larger values of V_{\max} than the observational fits. However, for masses larger than $\log(M_*/M_\odot) \approx 10.7$ ($\log(M_{\text{bar}}/M_\odot) \approx 11$), the models start to significantly deviate from the observations; as larger is the mass, the larger is V_{\max} in the models with respect to observations. At the low-mass side,

the models show a bending in the TF relations, though less pronounced in the case of the baryonic relation. The observations at low masses show a large scatter; a bending seems evident from the McGaugh (2011) data, while for the Geha et al. (2006) the scatter is too large. The sample of the later authors contain actually a large fraction of satellite galaxies. On the other hand, some observational studies for samples containing massive and dwarf galaxies show that indeed dwarf galaxies lie on average above the extrapolation of the stellar TF relation of massive galaxies (e.g., De Rijcke et al., 2007). For the baryonic TF relation, the observations seem to show that there is not a bending towards low masses (e.g., De Rijcke et al., 2007). The intrinsic scatters around model TF relations are significantly larger than those inferred for the observations, in particular at large masses.

The upper panel of Fig. 4.3 shows the B/T ratio vs. M_* . The mean B/T ratio and the standard deviation from our model results for M_* bins of 0.3 dex are plotted with the solid line and shaded area; recall that we excluded models with $B/T > 0.5$, since they are closer to elliptical galaxies. The observational data from Cibinel et al. (2013) and Weinzirl et al. (2009) are also reproduced in this plot; for more details and other observational reports see Section 2.4.

The scatter in the B/T– M_* relation is large in both the observations and models. Most of the models at low masses are bulgeless ($B/T < 0.1$). The B/T ratio increases with M_* but at masses larger than $\approx 5 \times 10^{10} M_\odot$, the B/T ratio decreases on average with M_* . The observations show that the B/T ratio increases on average with M_* . The sample of Weinzirl et al. (2009) includes only spiral galaxies; this is why their average B/T ratios are small and the statistics at large masses is poor (most of massive galaxies are of early type). In the case of models, galaxies that likely would be classified as S0 are actually taken into account. Therefore, we should compare with something in between the data from Weinzirl et al. (2009) and Cibinel et al. (2013). We conclude that, within the large scatter, our models present a trend of B/T with M_* in agreement with observations but at large masses, the model galaxies show B/T ratios systematically smaller as larger is M_* , in poor agreement with the observational trends.

Finally, in the lower panel of Fig. 4.3, the gas-to-stellar mass ratio, $R_{gas} \equiv$

M_g/M_* , vs. M_* is plotted. The means and the standard deviations from our model results in M_* bins of 0.3 dex are plotted with the black solid line and the shaded areas. The blue solid line is the mean relation inferred from a compilation of observations in Calette (2014, see Section 2); the blue dashed lines enclose the estimated 1σ scatter in the observations. The agreement between models and observations is remarkable until $\log(M_*/M_\odot) \approx 10.5$; at larger masses, the models have too large gas mass ratios as compared to observations.

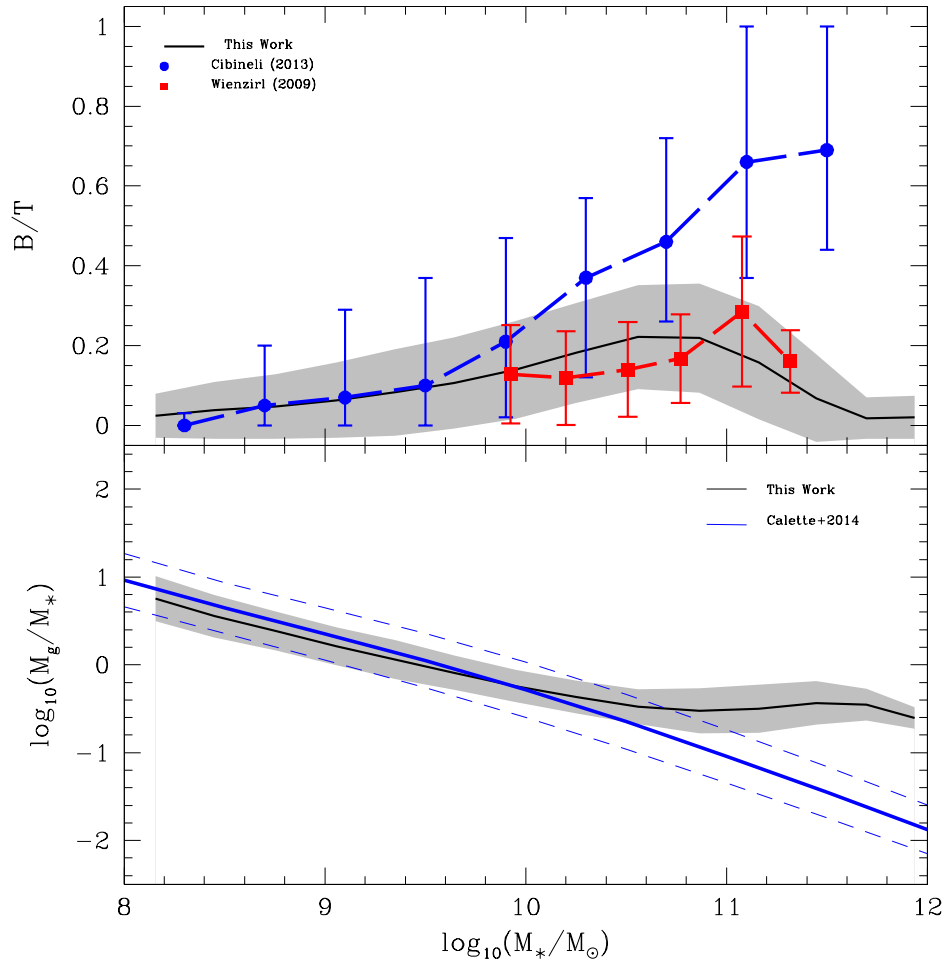


Figure 4.3: Distributions of the B/T and gas mass ratios, respectively, as a function of stellar mass. The mean values and the standard deviations of our models are plotted with the solid black lines and shaded areas, respectively. Some observational results are also plotted (see the labels inside the panels for the sources as well as Section 2).

4.2 Summary and discussion

We have obtained different galaxy correlations with the static disk galaxy model implemented here using the “cosmological” initial conditions, the semi-empirical $f_{\text{bar}}-M_h$ relation, and assuming that the galaxies are isolated. The results are in general in good agreement with observations up to stellar masses $\approx 3 - 5 \times 10^{10} M_\odot$. At larger masses, the models significantly deviate from observations:

- the size-mass relations become steeper, i.e., as larger is M_* , the larger are the model galaxy sizes with respect to observations;
- the stellar and baryonic TF relations become steeper, i.e., as larger is M_* , the larger are the model galaxy V_{max} with respect to observations;
- the B/T ratio decreases on average with M_* , opposite to what observations show;
- the gas mass ratio, R_{gas} , remains constant on average while for the observed massive galaxies, this ratio decreases with M_* .

It is encouraging that the “cosmological” halo initial conditions, the simple disk “secular” instability criteria for isolated galaxies, and the recently constrained $f_{\text{bar}}-M_h$ relation for blue/late-type galaxies are consistent with the main scaling correlations of the local disk galaxy population up to $M_* \approx 3 - 5 \times 10^{10} M_\odot$. In particular, the zero-points of the model TF and size-mass relations at intermediate masses are in agreement with observations. Recall that in our model, the inner halo suffers adiabatic contraction due to galaxy formation. Thus, at difference of Dutton et al. (2007), we find that it is not necessary to lower the spin parameter from halo to disk galaxy formation nor to invoke halo expansion instead of the standard adiabatic halo contraction. We attribute this difference with that and other studies, mainly to the new $f_{\text{bar}}-M_h$ relation and its scatter used here. It is important to remark that this relation, by construction, is in agreement with the observed local galaxy stellar and baryonic mass functions! Note also that we use the λ distribution from the Millennium Simulation reported for unperturbed halos (Bett et al., 2007),

which has the mean and scatter slightly lower than those used in Dutton et al. (2007).

Nevertheless, that the model results disagree with observations at large masses, it means that we are omitting the effects of astrophysical and evolutionary processes relevant for the properties of massive galaxies. Indeed, this is the case, since in our model it is not taken into account the role of mergers in the formation of the disk-bulge systems, the angular momentum transport, and the interaction-induced star formation. Namely for galaxies formed in halos larger than $10^{12} M_{\odot}$, the effects of mergers seem to be relevant in their evolution, more as more massive is the halo (see e.g., Zavala et al., 2012, and more references therein).

The mergers contribute directly with stars to the bulge, and make the disk more unstable to both processes of bulge growth and disk star formation. Therefore, we can not already use the values of the β_{crit} and Q parameters that apply for isolated disks. The effects of mergers during galaxy evolution affect also the behavior of the angular momentum distribution of baryons. The mergers seem to work as a mechanism of angular momentum transference from baryons to dark matter (e.g., Zavala et al., 2008). Hence, one expects that the more massive the halo, the lower will be the spin parameter of the baryons out of which the disk forms with respect to the spin parameter of the host halo, $\lambda_{bar} < \lambda$.

It is interesting that the mentioned above effects of mergers are expected to work just in the direction of improving the failures of the static model at large masses. In the next Chapter we will explore this possibility.

Chapter 5

A semi-empirical picture of local disk galaxy correlations

In the previous Chapter, we have generated a catalog of disk-bulge-halo systems by means of the static model of disk galaxies in centrifugal equilibrium loaded inside Λ CDM halos described previously in Chapter 3. As a first exploration, we have used the “cosmological” halo initial conditions and the disk “secular” instability criteria that apply for systems growing in isolation. Besides, for the parameter that contains the information about the astrophysical processes, we have used *the recently constrained $f_{\text{bar}}-M_h$ relation (and its scatter) for blue/late-type galaxies*. The static model predictions at this level are encouraging: several structural, dynamical and star formation-related correlations are in good agreement with observations from¹ $M_* \approx 10^9$ to $\approx 3-5 \times 10^{10}$ M_\odot . However, at larger masses the model galaxies deviate systematically from observations, suggesting that we have missed an important factor in the evolution of massive galaxies: the mergers.

Since the static model is not an evolutionary approach, we are not in position to follow the merger history of the halo-galaxy systems and, consequently, to estimate the merger-driven bulge growth and star formation, as well as the

¹We have set a lower limit in the masses of the halos, $M_h = 10^{10} M_\odot$, which corresponds on average to $M_* \approx 7 - 10 \times 10^8 M_\odot$. The empirical constraining of the $f_{\text{bar}}-M_h$ relation at lower masses is uncertain and it seems that the scatter turns on very large at lower masses in such a way that the methods to infer this relation are expected to fail.

merger-driven angular momentum transport processes. However, as mentioned in Chapter 3, we can attempt to emulate the effects of mergers, yet within our scheme, by artificially lowering the instability parameter β_{crit} and the spin parameter λ , and by increasing the star formation Toomre parameter Q . In order to constrain the change of these parameters with M_h , we may proceed in a heuristic way, looking for reproducing the observed scaling correlations at high masses that mostly depend on these parameters, as we will show below.

From our models and previous works, we know that the size–mass relation depends strongly on the spin parameter λ . Regarding the B/T– M_* and R_{gas} – M_* correlations, they depend mostly on the parameters β_{crit} and Q , respectively. For low masses, we leave the models to be generated in our mock catalog with the same parameters as in the previous Chapter, while for larger masses, the parameters are varied as a function of M_h in such a way these observational correlations are reproduced at high masses (at lower masses our model already reproduced them). We introduce dependences of these parameters with halo mass from $\log(M_h/M_\odot) \approx 3 - 5 \times 10^{11} M_\odot$ by using, first, a subset of models with the mean parameter values in λ , C and f_{bar} . From these experiments, we establish the functionalities that describe how the parameters λ , β_{crit} and Q should depend on M_h in order to improve the model predictions in the size–mass, B/T– M_* and R_{gas} – M_* correlations at high masses. Then, we calibrate with better accuracy the parameters of these functionalities in order the whole generated mock catalog reproduced the high-mass ends of the mentioned above observational correlations.

At this point, it should be said that our approach turned on to be less deductive (*ab initio*) and more heuristic or semi-empirical. The approach is aimed in general to generate Λ CDM-based models that are consistent with several observational scaling correlations of disk galaxies. This allows us then:

- to predict other global correlations of disk galaxies and compare them with observations in order to test the overall consistency of the model as well as of the underlying cosmological background;
- to probe the effects of the recent determinations of the M_{bar} – M_h and M_* – M_h relations (galaxy-halo connection) on the structural/dynamical properties of galaxies accesible to direct observations;

- to explore and constrain how much the initial parameters (e.g., the spin parameter) and the key assumptions (e.g., adiabatic invariant halo contraction) of the model should be modified in order to generate a disk galaxy population in agreement with observations;
- to use these constraints for speculating about the physical and evolutionary processes relevant to disk galaxy evolution at different scales, for example the role of mergers;
- to explore the inner structure and dynamics of the generated bulge-disk-halo systems as a function of global properties.

Below, we present the results obtained from our mock catalog generated as described in Section 3.2 but with a modification in some parameters for halos more massive than $3 - 5 \times 10^{11} M_{\odot}$, following the strategy mentioned above. In Section 5.1, the scaling correlations are presented and discussed. In Sections 5.2 and 5.3 we explore the origin of the scatters in the correlations, as well as whether the scatter around the $M_{\text{bar}}-M_h$ and M_*-M_h correlations are segregated or not by some galaxy properties; Section 5.4, we explore the correlations among the residuals of the scaling relations. In Chapter 6, the inner mass distributions of the different components and the implied dynamics are presented as a function of several global galaxy properties.

5.1 Disk galaxy correlations

5.1.1 The size-mass relation and inference of the spin parameter of galaxies

Similar to Fig. 4.1, in Fig. 5.1 we plot the R_e-M_* and $R_{e,\text{bar}}-M_{\text{bar}}$ relations (left and right upper panels, respectively), as well as the $R_{e,D}-M_*$ and $R_{\text{bar}}-M_{\text{bar}}$ relations (left and right lower panel). While the first two radii are calculated for the whole (disk + bulge) stellar or baryonic galaxy, the latter radii refer only to the disk stellar or baryonic component. The black solid lines and gray shaded areas are the mean and standard deviations in bins of 0.1 dex in M_* for galaxies with $B/T \leq 0.5$. The means and standard deviations for the

few galaxies with $B/T > 0.5$, are plotted with green dots and error bars, respectively. The same observations as in Fig. 4.1 are shown in Fig. 5.1. While at masses lower than $M_* \approx 3 \times 10^{10} M_\odot$, the model results are similar to those in Fig. 4.1 (Chapter 4), at higher masses, the too steep increasing of the radii with M_* is now shallower and in good agreement with the observations.

The agreement is good also at the level of the scatters around the size–mass relations, even at large masses, where the scatter was too large previously (see Fig. 5.1). In Fig. 5.2, we compare the one sigma scatter of the R_e - M_* and $R_{e,D}$ - M_* relations (showed in Fig. 5.1) from our models (black solid lines) with those of the corresponding observations (blue dashed lines). As seen both scatters are similar, in special for the $R_{e,D}$ - M_* relation. Note that in both cases the scatters decrease with mass.

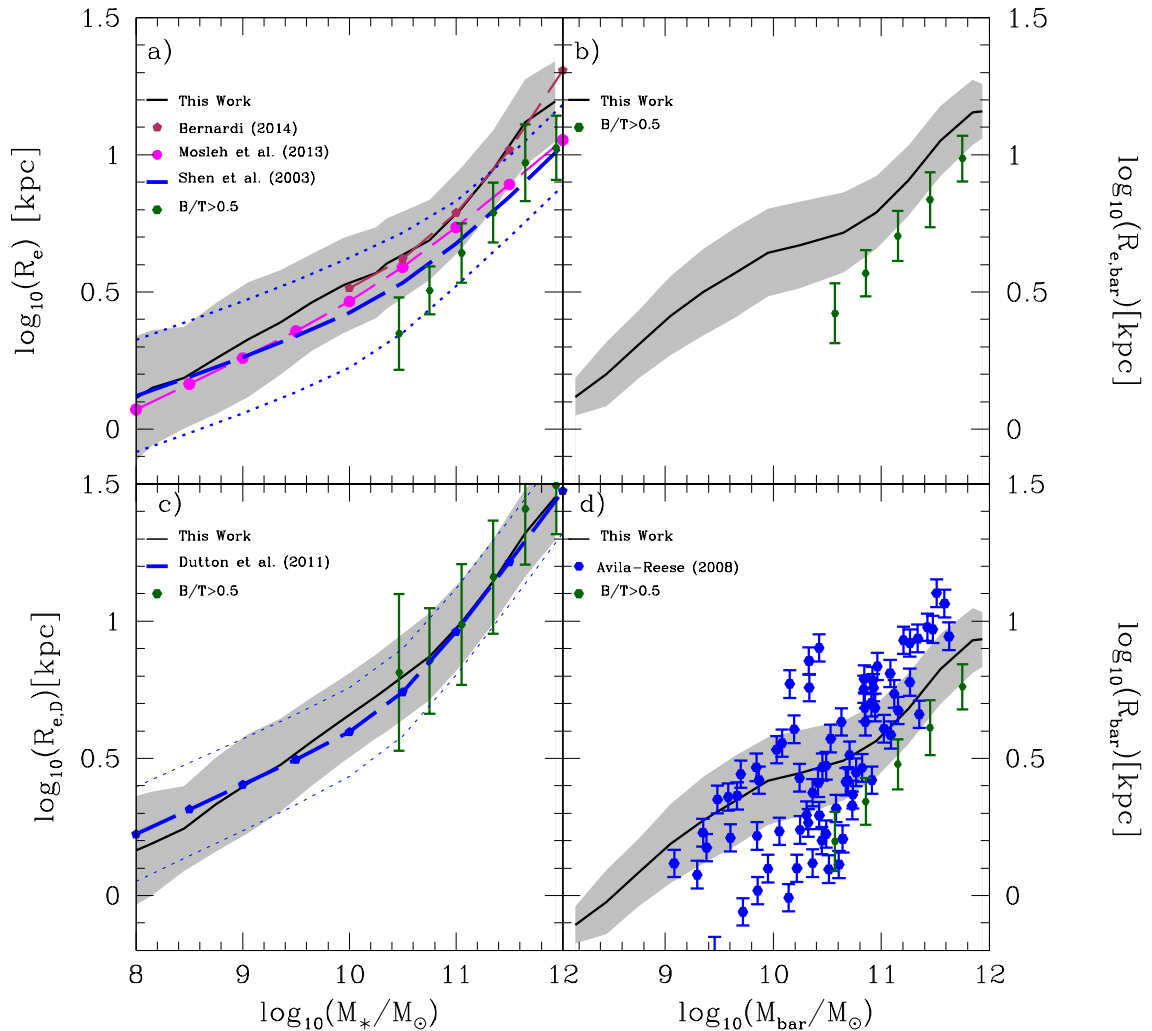


Figure 5.1: Different radius–mass relations from the semi-empirical models compared to some observational determinations (indicated inside the panels). The black solid lines and the shaded areas are the model means and standard deviations ($B/T \leq 0.5$) obtained in small M_* bins. The green dots with error bars are the means and standard deviations for models with $B/T > 0.5$. *Upper left panel:* Stellar effective radius vs. M_* . *Upper left lower panel:* Disk stellar effective radius vs. M_* . Note that the observational correlation by Dutton et al. (2011) is actually for the exponential disk scale length; for this case, $R_{e,D}=1.68R_D$. *Upper right panel:* Baryonic stellar effective radius vs. M_{bar} . *Lower right panel:* Disk baryonic scale radius vs. M_{bar} .

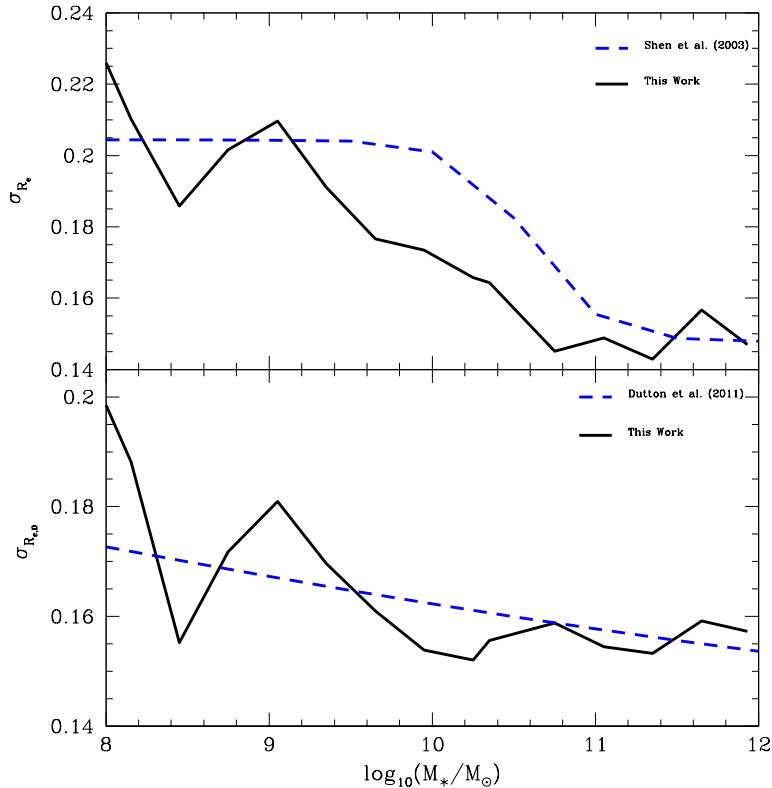


Figure 5.2: Intrinsic scatters of the R_e - M_* (upper panel) and $R_{e,D}$ - M_* (lower panel) relations showed in fig 5.1. Solid black and dashed blue lines are for the models and the observations, respectively.

As mentioned above, the parameter that most affects the size–mass relations is λ . The semi-empirical galaxies presented in Fig. 5.1 are with the same “cosmological” mean λ distributions as in Chapter 4 but with the mean of λ decreasing with M_h since $M_h = 3 \times 10^{11} M_\odot$ as:

$$\lambda_0 \rightarrow \lambda_{0,bar} = 0.145 - 0.0095 \times \log(M_h/M_\odot). \quad (5.1)$$

Therefore, our static model of disk galaxies in centrifugal equilibrium inside Λ CDM halos allows us to probe the initial spin parameter of the baryons

out of which disk galaxies formed. Different observational size–mass relations and their scatters are well reproduced if this spin parameter is log-normally distributed following the results from N-body cosmological simulations (see eq. 3.42) with $\sigma_\lambda = 0.22$ dex and a mean that is equal to that one of the simulations up to $M_h = 3 \times 10^{11} M_\odot$ ($\lambda_{0,bar} = 0.037$), and for larger masses with a mean that decreases with M_h as given in eq. (5.1).

Thus, our results show that the ratio of the mean initial spin parameter of the baryons out of which the galaxy is assembled to the one the halos had originally, $\ell \equiv \lambda_{0,bar}/\lambda_0$, is equal to one for halos smaller than $M_h = 3 \times 10^{11} M_\odot$, and it decreases with M_h from this mass as:

$$\ell = 3.955 - 0.257 \times \log(M_h/M_\odot), \quad M_h > 3 \times 10^{11} M_\odot. \quad (5.2)$$

For instance, $\ell = 0.5$ for halos of mass $\log M_h = 13.44 M_\odot$. An implication of this result is that galaxies formed in halos less massive than $M_h \approx 3 \times 10^{11} M_\odot$, on average, conserve in detail the angular momentum acquired by the Λ CDM halo, while in more massive halos, the baryons out of which galaxies form transported a fraction of their angular momentum to substructures and dark matter (see e.g., Zavala et al., 2008). This process is more efficient as more massive is the halo (eq. 5.2), consistent with the fact that more massive halos assemble larger fractions of their masses in major mergers than the less massive ones.

In the literature, there were some observational attempts to infer the spin parameters of the baryons out of which galaxies formed (e.g., Cervantes-Sodi et al., 2008; Berta et al., 2008). These inferences were done for SDSS galaxies by using very simplified approaches to estimate λ_{bar} from only the optical information. It is interesting that these studies agree in that λ_{bar} decreases on average with the luminosity or stellar mass of galaxies, with little dependence on environment. Our models of disk galaxies in centrifugal equilibrium inside Λ CDM halos offer a sophisticated way to constrain λ_{bar} and its scatter, taking into account even the effect of the halo contraction. The mock galaxy catalog we use reproduces several observational correlations of galaxies and it also agrees with the GSMF through the used $f_{bar}-M_h$ relation. Therefore, *the* λ_{bar}

values of the disk galaxy models are expected to reflect well the λ_{bar} values real galaxies should have if they were formed in Λ CDM halos.

The galaxies in our mock catalog have on average $\lambda_{0,\text{bar}} \approx \lambda_0 = 0.037$ up to $M_* \approx 3 \times 10^{10} M_\odot$ and for larger masses it decreases down to $\lambda \approx 0.02$ at $M_* = 5 \times 10^{11} M_\odot$ (see the upper left panel of Fig. 5.6 to be presented below). The scatter is basically equal to the scatter of the halo spin parameter used as input in the model, $\sigma_\lambda = 0.22$ dex (compare both shaded areas in the upper panels of Fig. 5.6). Interesting enough, the scatter around both the $R_e - M_*$ and $R_{e,D} - M_*$ observed relations was reproduced namely with this “cosmological” scatter in λ_{bar} , as shown in Fig. 5.2. Therefore, *the dispersion in the spin parameter values of the relaxed Λ CDM halos explains the dispersion in the size-mass relations of observed local disk galaxies*

5.1.2 The B/T– M_* , $R_{\text{gas}} - M_*$ and $\Sigma_e - M_*$ correlations

At large masses, the parameters related to the bulge formation (β_{crit}) and disk gas transformation into stars (Q), need to be calibrated in order to take into account the effects of the mergers. We perform this calibration by making that the predicted B/T– M_* and $R_{\text{gas}} - M_*$ correlations were in agreement with the observations. The upper panels of Fig. 5.3 show the B/T– and $R_{\text{gas}} - M_*$ correlations (solid lines surrounded by shaded areas) from the models that include a correction in the instability parameters β_{crit} and Q at large masses to take into account the effects of mergers; the correction to λ as a function of M_h discussed in the previous subsection remains the same. The green solid circles with error bars correspond to the galaxies with $B/T > 0.5$. The same observational data as in Figs. 4.3 are plotted in these figures.

As in the case of the size-mass relations, the semi-empirical models are practically the same as in the previous Chapter for $M_* \lesssim 3 - 5 \times 10^{10} M_\odot$. The corrections introduced in β_{crit} and Q (and λ) for halos larger than $M_h = 3 \times 10^{11} M_\odot$, worked namely in the direction of improving the comparison of models with observations at stellar masses larger than $M_* \approx 3 - 5 \times 10^{10} M_\odot$. As can be seen from Fig. 5.3, the agreement with observations is now good at all masses:

- The B/T ratio increases on average with M_* ; the increasing is weak for masses up to $M_* \approx 10^{10} M_\odot$ and stronger for larger masses; most of the low-mass mass galaxies are actually bulgeless, $B/T < 0.1$.
- The model galaxies with $B/T > 0.5$ are all massive galaxies. The fraction of them increases with M_* ; for $M_* > 10^{11} M_\odot$ it accounts for 10.6%. If we add to this fraction, those models that did not converge (1.8%, they are mostly too unstable), the fraction is then 12.4%. This can be considered as the fraction of early-type galaxies predicted by our semi-empirical approach.
- The (cold) gas-to-stellar mass ratio, $R_{gas} = M_g/M_*$, is on average 10 at $M_* \approx 10^8 M_\odot$ (or 91% in fraction, $M_g/(M_g + M_*)$) and it decreases with M_* ; for a Milky Way-sized galaxy, $R_{gas} \approx 0.15$ (0.13 in fraction). At larger masses, the mean R_{gas} decreases fast.
- The 1σ scatter around the $R_{gas}-M_*$ relation increases slightly as M_* is smaller; in general, the intrinsic scatter of the model $R_{gas}-M_*$ relation is slightly larger than that one of the observational inference, but it should be taken into account that the latter is very uncertain due to sample selection effects, observational errors, and non-detections. It should be said that at low masses the fraction of pure gaseous galaxies is significant; for $M_* < 10^9 M_\odot$, this fraction is 17.8%.

In order to attain a good agreement with observations of the B/T ratios at large masses, we have artificially lowered the value of β_{crit} in the criterion of bulge formation (see subsection 3.1.2 and eq. 3.39 therein) for $\log(M_h/M_\odot) > 11.5$. Lowering β_{crit} it implies that the disk is more unstable and larger bulges are formed; the source of instability is not already intrinsic, but external, produced by mergers. This parameter was lowered as:

$$\beta_{crit} = -0.0217[\log_{10}(M_h/M_\odot)]^2 + 0.4319 \log_{10}(M_h/M_\odot) - 1.4932 \quad (5.3)$$

for $\log(M_h/M_\odot) > 11.5$. Note, however, that in our scheme, the bulge is all the time formed from stars of the disk, producing this that as larger is the formed bulge, the lower is the surface density of the disk. This might not be the case when the mergers are major because in this case most of the stars in

the bulge come from the accreted galaxy rather from the disk, and the latter remains the same or even more dense due to the merger-induced instabilities. This is why our scheme is valid *only for galaxies with non-dominant bulges, let say $B/T \lesssim 0.5$.*

Similarly, in order to agree with the gas-to-stellar mass ratios of massive blue/late-type galaxies, we have increased artificially the value of the Toomre parameter Q (see subsection 3.1.3) for $\log(M_h/M_\odot) > 11.5$. For the largest masses, the increasing should be very large, to values up to $Q \sim 200$. This is because in these cases, a prominent (stellar) bulge forms; then, as mentioned above, the remaining disk is less dense and more extended than the original one, therefore it is stable against axisymmetric perturbations and it does not form stars. However, the same merger(s) that produced the bulge, likely produce strong bursts of induced star formation that we emulate by increasing Q .

Finally, the lower panel of Fig. 5.3 shows the effective stellar surface density, Σ_e , vs. M_* for the the models with $B/T \leq 0.5$ (solid line surrounded by the gray area). This effective surface density refers to half of the sum of the bulge and disk components. The semi-empirical disk galaxies show a significant correlation between Σ_e and M_* . Up to $\sim 2 \times 10^{10} M_\odot$, the slope of the correlation is ~ 0.6 and for larger masses it systematically flattens. The flattening of the $\Sigma_e - M_*$ correlation at large masses is associated to the steepening seen in the $R_e - M_*$ correlation at these masses (Fig. 5.1).

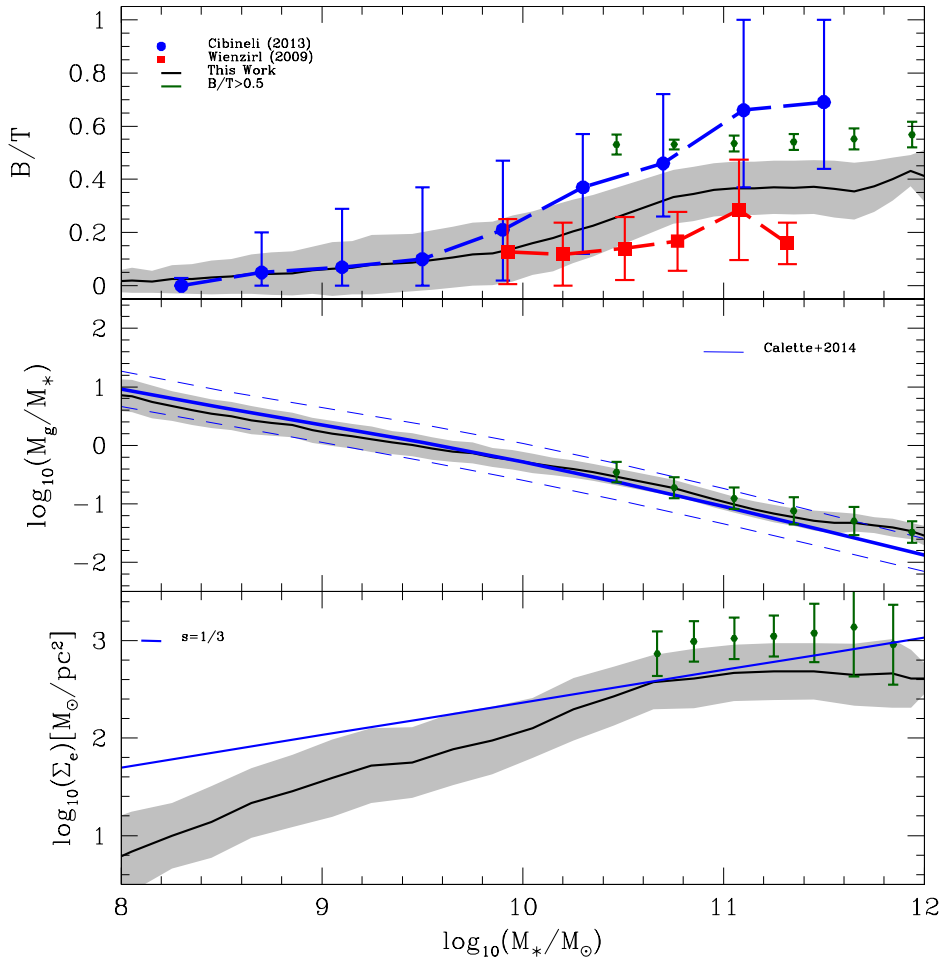


Figure 5.3: *Upper panel:* Bulge-to-total mass ratio vs. M_* for the semi-empirical models (black solid line surrounded by a gray area) compared to some observational determinations (indicated inside the panels). The gray area and the error bars are the standard deviations at each M_* bin. The semi-empirical models and the observations by Weinzierl et al. refer to disk galaxies ($B/T \leq 0.5$). The green solid circles with error bars are the averages and standard deviations corresponding to the models with $B/T > 0.5$. *Medium panel:* Gas-to-stellar mass ratio vs. M_* for the semi-empirical models (black solid line surrounded by a gray area) compared to the empirical correlation inferred in Calette et al. (2014; blue solid line surrounded by the blue dashed lines). The green solid circles with error bars are the averages and standard deviations corresponding to the models with $B/T > 0.5$. *Lower panel:* Effective stellar surface density, Σ_e , vs. M_* for the disk ($B/T \leq 0.5$) semi-empirical models. The blue line indicates a slope of $1/3$ predicted for disk galaxies when f_{bar} and λ are constant.

Our results regarding the $\Sigma_e - M_*$ or $(R_e - M_*)$ correlation show that the shape of the semi-empirical $f_{\text{bar}} - M_h$ relation has an imprint on this correlation. As previous authors have already shown, for pure disks and assuming that $M_* = M_d$, then Σ_e scales as $M_*^{1/3}$ when f_{bar} and λ are constant (e.g., Mo et al., 1998; Avila-Reese et al., 1998, this dependence is indicated with a thin blue solid line in the bottom panel of Fig. 5.1). This is evident from the following dependences for exponential disks:

$$\Sigma_e = \frac{(M_*/2)}{2\pi(1.68R_D)^2} \propto \frac{f_{\text{bar}}M_h}{(\lambda R_h)^2} \propto \frac{f_{\text{bar}}^{2/3}M_*^{1/3}}{\lambda^2}, \quad (5.4)$$

where we have made use of $R_D = g(C)f_{\text{bar}}M_h\lambda$ (see Chapter 2; $g(C)$ is a function that almost does not depend on mass), and $R_h \propto M_h^{1/3}$ for the CDM halos. So, if f_{bar} and λ do not depend on mass, $\Sigma_e \propto M_*^{1/3}$. However, our semi-empirical galaxies were constructed with a baryon fraction and spin parameter that depend on mass. At low masses, roughly $f_{\text{bar}} \propto M_h^{0.4}$ (see Fig. 2.2), and since $M_h = M_*/f_{\text{bar}}$, then $f_{\text{bar}} \propto M_*^{0.4/1.4} = M_*^{0.29}$; λ does not depend on M_h . Therefore, using eq. (5.4) we obtain that at the low-mass end $\Sigma_e \propto M_*^{0.53}$, close to the slope seen in the lower panel of Fig. 5.3.

At the high-mass end, roughly $f_{\text{bar}} \propto M_h^{-0.56}$, then $f_{\text{bar}} \propto M_*^{-0.56/0.44} = M_*^{-1.27}$, and using eq. (5.4), $\Sigma_e \propto M_*^{-0.53}$. However, at high masses, λ decreases with M_h according to our semi-empirical approach: very roughly $\lambda \propto M_h^{-0.22}$ or $\propto M_*^{-0.28}$. Therefore, according to eq. (5.4), $\Sigma_e \propto M_*^{0.03}$, that is the $\Sigma_e - M_*$ correlation flattens in agreement with what is seen in Fig. 5.3. Note that these approximate calculations refer to an exponential stellar disk (no bulge, no gas). The results presented in Fig. 5.3 are for a disk that can contain gas and is not perfectly exponential plus a stellar bulge. In any case, this approximation and our results agree very well.

The conclusion is that the $\Sigma_e - M_*$ correlation of disk galaxies results with a slope steeper than $1/3$ at low masses because the baryonic fraction decreases as M_h (or M_*) is smaller, and it flattens at the largest masses because the baryonic fraction decreases as M_h (or M_*) is larger; actually, the slope of the $\Sigma_e - M_*$ relation can be even negative at the high-mass end if λ keeps constant, however, our semi-empirical model shows that the spin parameter

out of which massive galaxies form should decrease with mass (see above), which compensates the effect of the low values of f_{bar} , making the slope of the $\Sigma_e - M_*$ relation at large masses almost flat. A large survey of galaxies with measured Σ_e values and stellar masses would provide valuable information in the light of the predictions of our semi-empirical approach. The surface density of galaxies is notably affected by the astrophysical processes that coin the $f_{\text{bar}} - M_h$ and $\lambda_{\text{bar}} - M_h$ relations.

5.1.3 The Tully-Fisher relations

The predicted stellar and baryonic TF relations from our (semi-empirical) mock catalog are plotted in Fig. 5.4 (black dashed line surrounded by a gray area) similar as in Fig. 4.2 in Section 4.1. By comparing both figures, we see that the strong steepening of the TF relations at high masses ameliorated a little now. This is mainly because after the formation of larger bulges at high masses here with respect to the models in the previous Chapter (compare Figs. 4.3 and 5.3), the overall mass distribution of the baryons strongly concentrates to the center (the bulge is compact), being the peak of the baryon circular velocity component shifted to the very inner radii. Since the total circular velocity is the sum in quadratures of the halo and the baryon contributions, at the radius where the baryon component has now its maximum, the halo contribution is low in such a way that the quadratic sum of both is yet low. The maximum velocity, V_{max} , is attained at larger radii, where the disk dominates over the bulge, but since the disk is now less massive and more extended, this V_{max} results lower than the one when the bulge was smaller. The net result is that the $V_{\text{max}} - M_{\text{bar}}$ and $V_{\text{max}} - M_*$ relations flatten at large masses. In the case of the $V_{\text{max}} - M_*$ relation, note that M_* also increased slightly as larger is the mass with respect to the models in the previous Chapter; this is because massive galaxies are now more efficient in transforming gas into stars (compare Figs. 4.3 and 5.3).

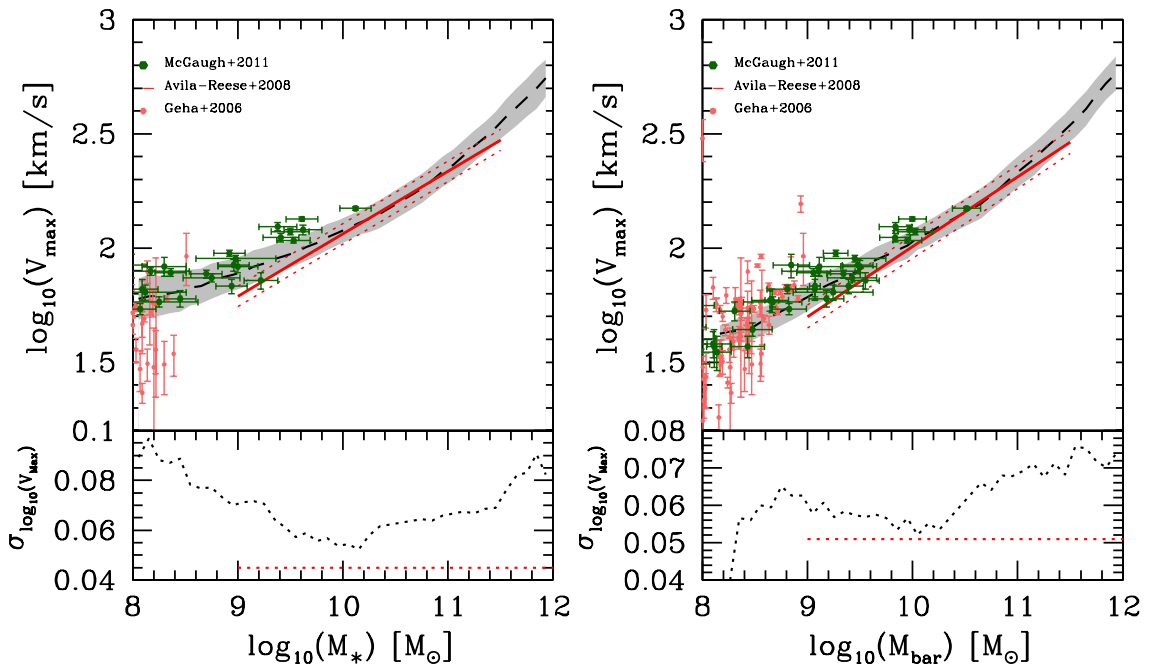


Figure 5.4: Stellar and baryonic TF relations from our (semi-empirical) mock catalog compared to observations (indicated inside the panels). The dashed line and the gray area are the means and standard deviations calculated in small M_* bins. Only galaxies with $B/T \leq 0.5$ are considered.

It is quite encouraging that the predicted TF relations are in good agreement with the observations, confirming this that the Λ CDM cosmology offers a natural explanation for the origin of these relations (see extensive discussions in Avila-Reese et al., 1998, 2008, and more references therein). Note that there is not a problem in the zero-point of both the stellar and baryonic TF relations as it was suggested in the literature² (e.g., Dutton et al., 2007), and, by construction, our initial conditions are in agreement with the galaxy stellar and baryonic mass functions. Recall that the $f_{\text{bar}}-M_h$ relation used as input here, was constrained by using the observed baryonic mass function. In Fig. 5.5, we plot the $f_{\text{bar}}-M_h$ relation and its scatter from our semi-empirical

²The problem was enunciated originally for the semi-analytic models: if their parameters are tuned to fit the observed GSMF, then the modeled galaxies used to have too large V_{max} for their masses (or luminosities) as compared to observations.

models and compare them with the semi-empirical $f_{\text{bar}}-M_h$ relation taken from Calette (2014); the latter relation has been used actually as input to generate our mock catalog. Therefore, this plot is just to show that we have sampled well the input $f_{\text{bar}}-M_h$ relation (see Fig. 2.2 in Chapter 2). In Fig. 5.5, it is also plotted the F_s-M_h relation ($F_s \equiv M_*/M_h$) and its scatter from our models, and it is compared with the semi-empirical inference of this relation for blue galaxies given in Calette (2014); this relation is the one that map the Λ CDM halo mass function to the GSMF of blue galaxies. The overall agreement between our prediction and the semi-empirical inference *implies that our semi-empirical model would map well the observed GSMF.*³

³However, according to Fig. 5.5, at low halo masses, our galaxies have systematically slightly higher F_s values than those in Calette (2014) and the scatter around the F_s-M_h relation significantly increases. This is because in halos smaller than $10^{11} M_\odot$, a fraction of the disk galaxy models are quite stable to the Toomre criterion for gas transformation into stars and form small amounts of stars or not form stars at all. The fraction of purely gaseous galaxies increases as M_h decrease. Some fraction of these pure-gas model galaxies should actually have small stellar masses, which would contribute to lower the average values of F_s at these masses.

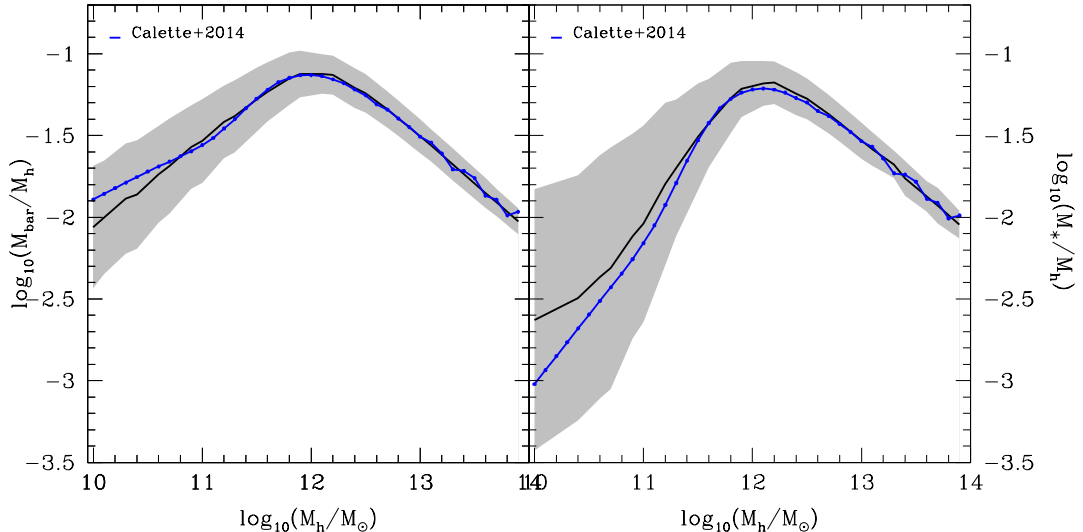


Figure 5.5: Galaxy baryonic and stellar mass fractions as a function of M_h from the (semi-empirical) mock catalog. The means and standard deviations are plotted with solid lines and shaded areas, respectively. The blue lines are the means from the semi-empirical inferences by Calette (2014) for blue/late-type galaxies. Our catalog was generated actually by using as input the $f_{\text{bar}}-M_h$ from these authors, see Fig. 2.2. Only galaxies with $B/T \leq 0.5$ are considered.

The bending of the stellar TF relations at low masses was already discussed in Section 4.1. It is less pronounced for the baryonic TF relation than for the stellar one, in good agreement with observations. Regarding the bending at high masses, it is difficult to say whether observations exhibit also such a systematic bending since very massive disk galaxies are rare, and the fit to observations is just an extrapolation at the largest masses. *It would be interesting to have more observations of massive disk galaxies in order to test this prediction.*

5.1.3.1 The intrinsic scatter around the TF relations

The standard deviations in mass bins of our semi-empirical models in the TF relations (associated to the 1σ intrinsic scatter of these relations), are in general larger than the intrinsic scatter estimated from the observations.⁴ The lower panels of Fig. 5.4 shows the logarithmic standard deviations of the $V_{\max}-M_*$ and $V_{\max}-M_{\text{bar}}$ relations as a function of mass. The semi-empirical models show a minimal scatter at stellar and baryonic masses in between approximately 5×10^9 and $1.5 \times 10^{10} M_{\odot}$. At lower and larger masses, the scatter increases, specially for the stellar TF relation. Even in the mentioned mass range, the model scatter is larger than the estimated from the observations. The dashed horizontal lines in both panels of Fig. 5.4 show the intrinsic scatters inferred from the observations in Avila-Reese et al. (2008). The scatter around the TF relation is a long standing problem of the models in the context of the CDM cosmologies stated originally in Eisenstein and Loeb (1996) and Avila-Reese et al. (1998).

In the next subsection, we will explore the role that the initial parameters play on the scatter of the scaling TF and size-mass relations. We will see that in the case of the TF relations, the scatter is mainly produced by the dispersion in the halo concentration parameter C . At this point, we should mention that the mock catalog was generated by sampling the distributions of the parameters C , λ_{bar} and f_{bar} in the assumption that *they are independent among them*. If these parameters are correlated among them, then the scatter in the TF relations could reduce (or it could increase). We leave for a future work the exploration in detail of these possibilities.

⁴In Avila-Reese et al. (2008), the compiled and homogenized galaxy sample was not pruned to minimize the scatter as other samples do it (the main goal of these samples was to use them for calibrating the TF relation as distance indicator). Avila-Reese et al. (2008) have also subtracted the observational errors in order to estimate the *intrinsic* scatter of the TF relations.

5.2 The source of scatter in the disk scaling relations

The predicted size–mass relations have a large scatter, while the TF relations are much tighter, i.e., they have smaller scatters. We explore further which parameters from the initial conditions are related to the scatters around these disk galaxy ($B/T \leq 0.5$) scaling relations. First, we present how the initial condition parameters, λ_{bar} , f_{bar} , and C , correlate with M_* (left panels of Fig. 5.6). The correlations are actually a result of the input dependences of λ_{bar} , f_{bar} , and C on M_h , shown for completeness in the right panels of Fig. 5.6. However, since our semi-empirical model results agree very well with several of the observed scaling correlations, we can say also that *our models constrain in an empirical fashion the values and how the λ_{bar} , f_{bar} , and C parameters correlate with M_* or M_h .* This was discussed already for the case of the spin parameter in §§5.1.1.

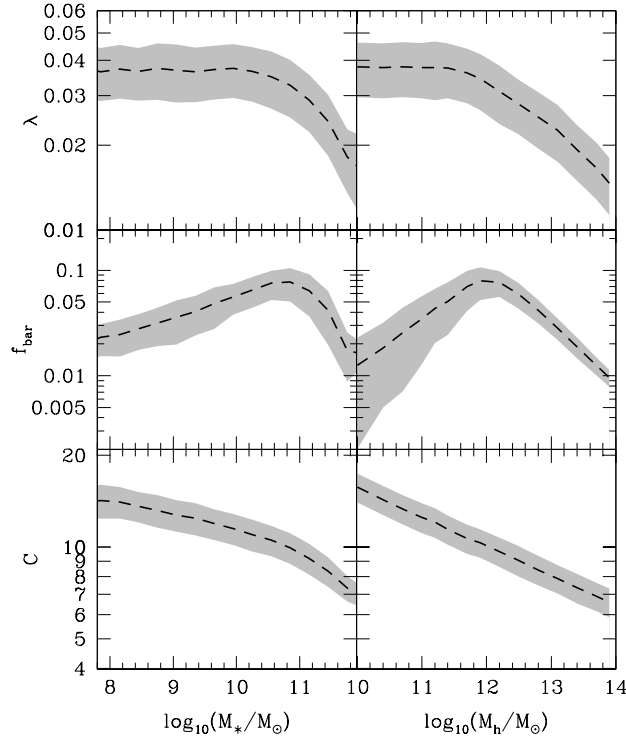


Figure 5.6: Correlations of the model input parameters λ_{bar} , f_{bar} , and C with M_* (left panels) and M_h (right panels) from our (semi-empirical) mock catalog. The dashed lines are the means and the gray shaded areas represent the standard deviations. The correlations of these parameters with M_h are actually a sampling of the *assumed* input relations and their scatters. Only galaxies with $B/T \leq 0.5$ are considered.

In Fig. 5.7, we plot the residuals of the $R_e - M_*$ and $V_{\text{max}} - M_*$ scaling relations vs. the residuals of the dependences of λ_{bar} , C , and f_{bar} on M_* (see Fig. 5.6). This plot shows us how much the “input” parameters affect the intrinsic scatter of the scaling relations of disk galaxies ($B/T \leq 0.5$). The dispersion around the $R_e - M_*$ relation is large and it is produced actually by the three parameters (the residuals of these relations correlate with the residuals of the three parameters). The main source of scatter, at a given M_* , is λ_{bar} : the larger the λ_{bar} , the larger is the galaxy size; the slope of the correlation $\Delta_{\lg} R_e$

vs. $\Delta_{\lg} \lambda_{bar}$ is higher than 1. The second source of scatter is f_{bar} ; the higher the f_{bar} , the smaller is the galaxy size, with a correlation slope around 1. The residuals of the $R_e - M_*$ relation correlate only weakly with the residuals of the $C - M_*$ relation (the scatter is large), in the sense that, for a given M_* , more concentrated halos tend to produce galaxies with smaller R_e , i.e., more concentrated in their stellar mass distributions.

The dispersion around the $V_{max} - M_*$ relation, which is small, is produced mainly by the C parameter. For a given M_* , the higher the halo concentration C , the larger is the galaxy V_{max} . The correlation among the residuals is tight with a slope around 1. The $\Delta_{\lg} V_{max}$ residuals anticorrelate weakly with the $\Delta_{\lg} \lambda_{bar}$ and $\Delta_{\lg} f_{bar}$ residuals. Thus, *the scatter around the TF relation is small because its source is practically only the scatter of the C parameter.*

We have also studied the correlations among the residuals of the baryonic size-mass and TF relations and the residuals of the $\lambda_{bar} - M_{bar}$, $C - M_{bar}$, and $f_{bar} - M_{bar}$ relations. They are actually similar to those of the stellar case discussed above, though more scattered in the case of the size-mass relation and less scattered in the case of the TF relation.

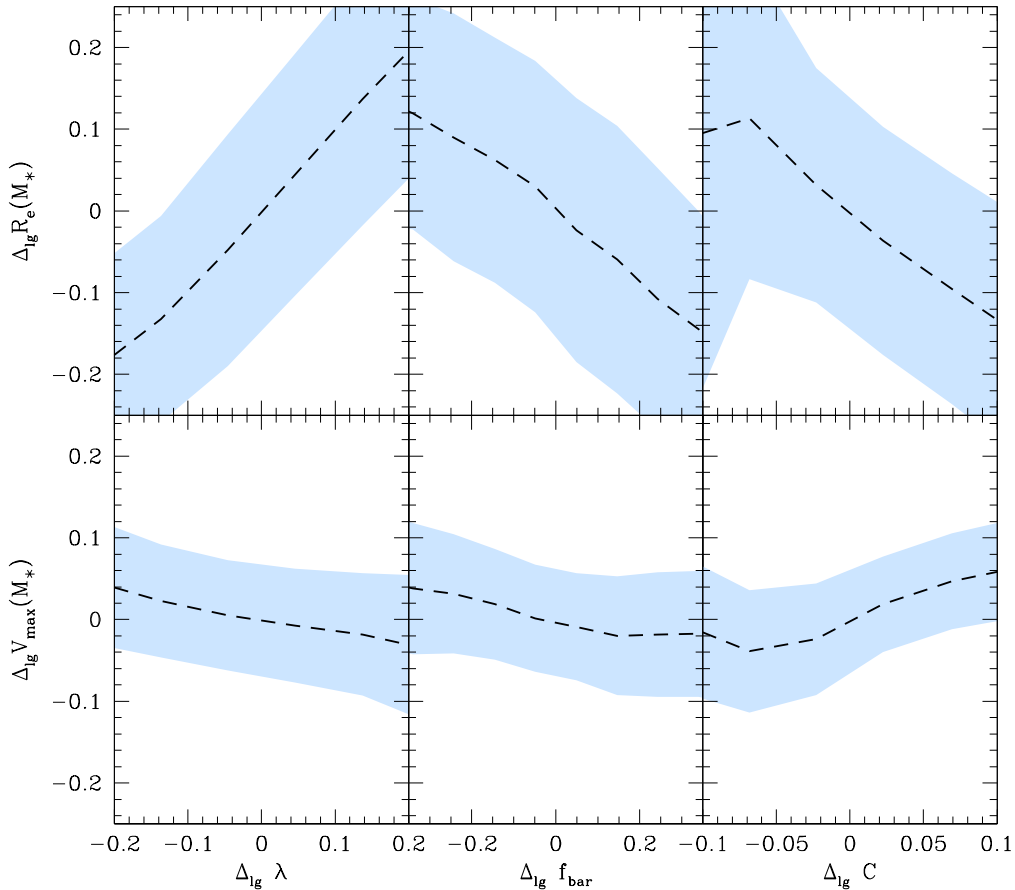


Figure 5.7: Residuals of the stellar TF and $R_e - M_*$ relations vs. the residuals of the $\lambda_{bar}-$, $C-$, and $f_{bar}-M_*$ correlations. The correlations among these residuals show how much the origin of the scatters around the scaling relations depend on the “initial” parameters. Only galaxies with $B/T \leq 0.5$ are considered.

We would like to know whether the scatter around the disk galaxy ($B/T \leq 0.5$) scaling relations is segregated by a given galaxy property. In the upper panels of Fig. 5.8, we present the correlations among the residuals of the $R_e - M_*$ relation and the global galaxy properties R_{gas} , B/T , and effective surface density (bulge + disk), Σ_e . The means (dashed lines) and standard deviations (shaded areas) are shown. As seen, there is not an evident segregation of

the the $R_e - M_*$ relation by the gas mass ratio R_{gas} , while there is a weak but systematical trend with the B/T ratio in the sense that those galaxies that for a given M_* are smaller (more concentrated), have also higher B/T ratios on average. Regarding Σ_e , for the stellar low-surface density galaxies there is not a segregation in the $R_e - M_*$ relation due to Σ_e , but for the high-surface density ones, those that deviate to smaller radii at a given M_* , also are those that have the highest effective surface densities. Note that the low-surface density galaxies are gas dominated (and a significant fraction did not even appear in the plot because they are completely gaseous).

In the lower panels of Fig. 5.8, the correlations among the residuals of the $V_{max} - M_*$ relation and the same global galaxy properties than above are presented. For low-gas content galaxies (which are mostly massive galaxies), there is a trend with in the sense that those that deviate in the stellar TF relation more to the high- V_{max} side have on average smaller gas contents. The opposite happens for the high-gas content galaxies (which are mostly low-mass galaxies); those that more deviate to the the high- V_{max} side have on average higher gas contents, though this trend is very noisy.

The residuals of the stellar TF relation almost do not correlate with the B/T ratio. At intermediate B/T ratios there is a very weak correlation of the residuals with B/T but at larger B/T ratios disappears at all. For intermediate-mass galaxies, the bulge component is not too big but it can contribute significantly to V_{max} ; therefore, those galaxies that have larger B/T ratios, can be also those with larger deviations to high velocities in the TF relation. However, more massive galaxies, in spite that can have larger B/T ratios, their bulges already do not contribute significantly to V_{max} because they tend to be dark matter dominated (see below); therefore, there is not anymore a correlation of the TF relation residual with B/T.

Finally, the TF relation residuals do not correlate with Σ_e for the low-surface density disk galaxies, while for the high-surface density ones, the residuals strongly correlate with Σ_e . Note that the low-surface density galaxies are gas dominated (and a significant fraction did not even appear in the plot because they are completely gaseous). For the high-surface density, it is expected that the more concentrated the bulge-disk system, the more it can contribute to

increase V_{\max} .

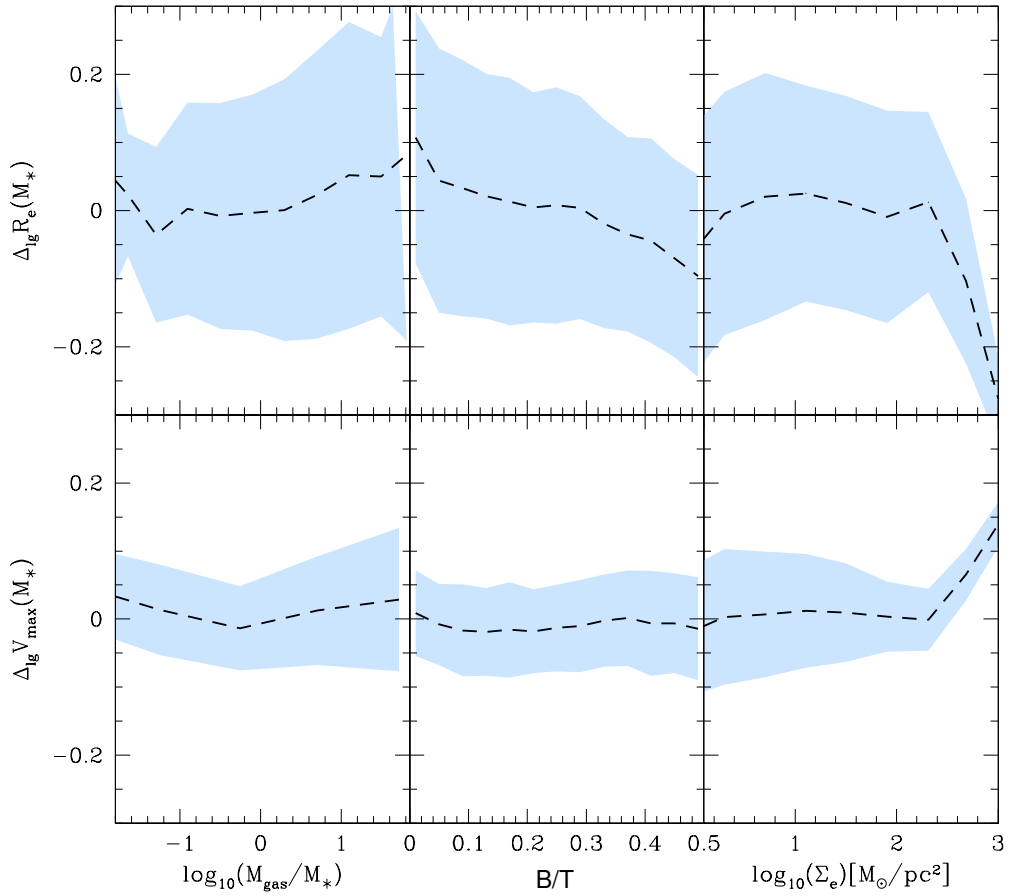


Figure 5.8: Residuals of the stellar TF (upper panels) and $R_e - M_*$ (lower panels) relations vs. disk galaxy properties, namely the gas mass and B/T ratios, and the central stellar surface density. Only galaxies with $B/T \leq 0.5$ are considered.

5.3 On the scatter of the $M_{\text{bar}}-M_h$ and M_*-M_h relations

The results from our semi-empirical mock catalog give a possibility to study the interesting question about the scatter of the $M_{\text{bar}}-M_h$ and M_*-M_h relations of disk galaxies. As discussed in Chapter 2, these relations have been recently inferred from direct and semi-empirical studies. They are relatively tight but some scatter around them is present; see Fig. 5.5. In Fig. 5.9 we explore how the residuals from both relations do correlate with internal galaxy properties.

Our semi-empirical disk galaxies show that the residuals of the $f_{\text{bar}}-M_h$ relation are in some degree segregated by the galaxy properties studied here, mainly by the gas mass ratio $R_{\text{gas}} \equiv M_g/M_*$ and the effective stellar surface density Σ_e : as higher is R_{gas} and Σ_e , the more the galaxies deviate on average to the low- f_{bar} and high- f_{bar} sides of the $f_{\text{bar}}-M_h$ relation, respectively. This means, that those galaxies that in the $f_{\text{bar}}-M_h$ plane are below the mean relation tend also to be those with higher gas mass ratios and lower effective surfaces densities. Regarding the B/T ratio, there is a noisy correlation among the residuals of the $f_{\text{bar}}-M_h$ relation and this ratio: those galaxies with high f_{bar} values with respect to the average relation tend to have roughly large B/T ratios.

In the case of the F_s-M_h relation, similar trends as for the $f_{\text{bar}}-M_h$ relation are seen, though in the detail there are some differences. The residuals get larger in this relation than in the $f_{\text{bar}}-M_h$ relation, specially at high values of R_{gas} and low values of Σ_e and B/T, that is, when the galaxies are less massive (see also Fig. 5.5).

The results presented here are clear predictions that in future empirical and semi-empirical studies will be likely able to test.

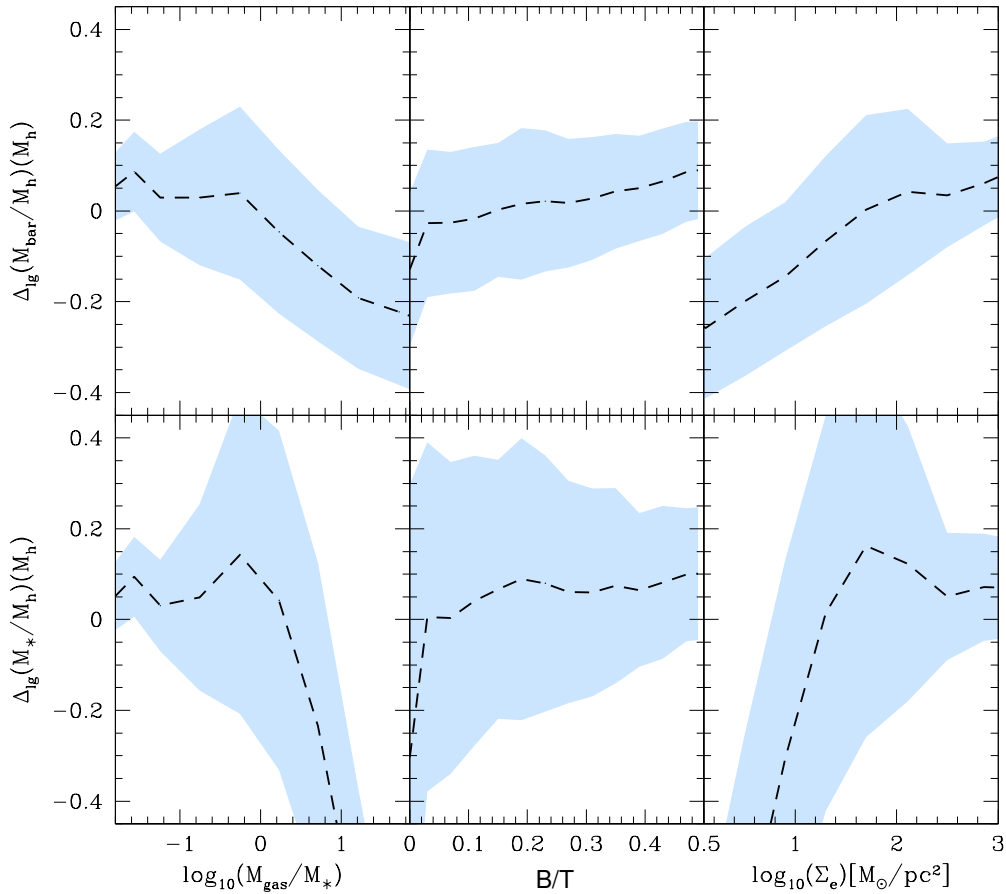


Figure 5.9: Correlations among the residuals of the $f_{\text{bar}}-M_h$ (upper panels) and F_s-M_h (lower panels) relations with some disk galaxy internal properties. The means and standard deviations of the correlations are plotted with dashed lines and blue shaded areas, respectively.

5.4 Correlations among the residuals of the scaling relations

In Fig. 5.10, the correlation among the residuals of the R_e-M_* and $V_{\text{max}}-M_*$ relations (left panel), and among the residuals of the $R_{e,\text{bar}}-M_{\text{bar}}$ and $V_{\text{max}}-$

M_{bar} relations (right panel) are shown. The dashed lines and shaded blue areas correspond to the means and standard deviations. For exponential disks without dark matter, the logarithmic residuals of the radius–mass and V_{max} –mass relations anti-correlate with a slope of -0.5 (Courteau and Rix, 1999, blue line in the panels). This is because for a given mass, the smaller the disk scale radius (the more compact the disk), the higher is V_{max} (the more peaked is the circular velocity rotation). The presence of a dark matter halo, softens this dependence and in the case of dark halo dominion, the dependence may completely disappear: V_{max} is determined by the halo internal mass distribution and it does not depend on the disk component.

Our results show that there is a weak and scattered anti-correlation among the residuals both for the baryonic and stellar scaling relations, implying that the semi-empirical disk galaxies are mostly dark matter dominated already at radii around the one where V_{max} is attained. However, a weak anti-correlation is seen, means that there is a little trend: those galaxies that at a given mass deviate to larger V_{max} values tend to have smaller effective radii. The weak anti-correlations among the residuals of the scaling relations of model galaxies are similar to those inferred from observational samples (e.g., Dutton et al., 2007; Courteau et al., 2007; Avila-Reese et al., 2008). If any, the latter authors have found that the correlation in the baryonic case is slightly stronger and steeper than in the stellar case. These authors interpreted this difference as an compensation effect in the TF and size–mass relations when passing from the baryonic to the stellar quantities (see Firmani and Avila-Reese, 2000). Our results are surprisingly similar to these empirical inferences; the green lines in Fig. 5.10 are the orthogonal linear fits to their data presented in Avila-Reese et al. (2008).

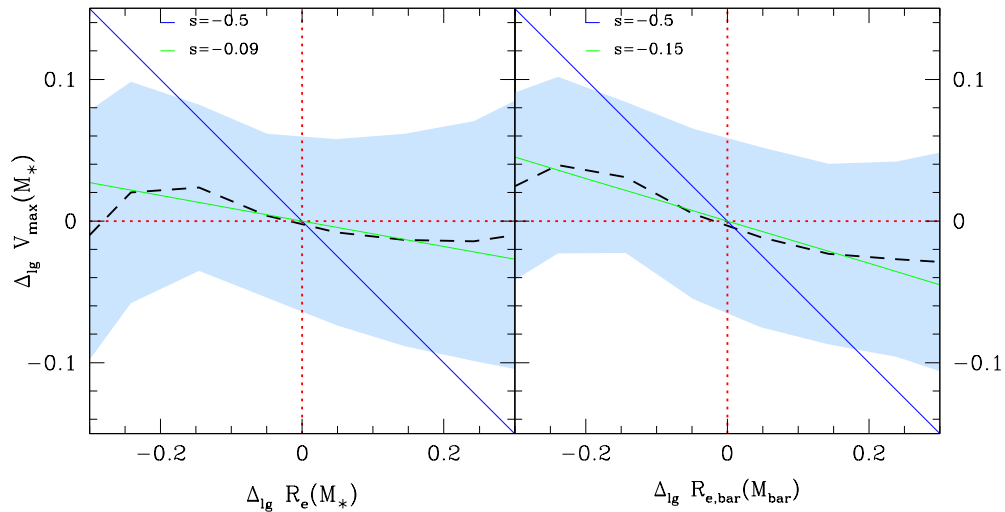


Figure 5.10: Residuals of the stellar and baryonic TF relations vs. the residuals of the respective stellar and baryonic effective radius–mass relations. The residuals are in dex. The blue lines correspond to a slope of -0.5 , valid for exponential disk galaxies without dark halo and bulge. The absence of correlation is indicative of dark matter dominion at radii where V_{\max} is attained. The green lines are the orthogonal linear fits to the observations presented in Avila-Reese et al. (2008). Their slopes are indicated inside the panels.

Chapter 6

The inner mass distributions of the semi-empirical disk galaxies

We have found in Section 5.4 of the previous Chapter a weak and shallow anti-correlation among the residuals of the baryonic and stellar scaling relations, which suggests nearly dark matter dominion at radii where the maximum circular velocity is attained (see Fig. 5.10). Our goal in this Section is to study in more detail the inner mass distributions and dynamics of the galaxy disk-bulge-halo systems build up inside Λ CDM halos. The $f_{\text{bar}}-M_h$ relation used as the "astrophysical" input in our model, and the closely related F_s-M_h relation (Fig. 5.5, recall that $F_s \equiv M_*/M_h$) summarize the key aspects of galaxy formation and evolution of galaxies within the Λ CDM halos. We will explore now *how these relations do project into the inner mass distributions of the disk galaxy systems, within optical radii of the galaxies instead of the hypothetical virial radii.*

6.1 Galaxy-to-total maximum velocity ratios

The ratio of disk (or disk + bulge) to total circular velocity is a quantity related to the "luminous"-to-dark matter ratio. The velocities can be defined (and measured) at a given radius or estimated at their respective maxima (the total one, V_{\max} , comes directly from observations while the disk or disk+bulge

ones are inferred from the observed luminosity mass distributions or from vertical disk dynamics studies).

In Fig. 6.1, we plot three circular velocity ratios vs. some global properties: V_{\max} , the effective stellar (bulge + disk) surface density Σ_e , and M_* . The model results for the disk galaxies ($B/T \leq 0.5$) are shown as the averages and standard deviations calculated in small bins of these properties (dashed lines and shaded areas, respectively). We also show the corresponding means and standard deviations for the “early-type” subsample, i.e. those models with $B/T > 0.5$ (green dots with error bars, respectively). Recall that a significant fraction of the low-mass model galaxies are gaseous, so they can not be plotted in the panels where stellar quantities appear (central and right columns). However, in the first column, they can be included and are plotted with red dots and error bars. The upper panels are for the ratio of disk circular velocity to total circular velocity at $2.2R_D$, where R_D is the baryonic disk scale length (exponential by definition). The medium panels are for the ratio of the maximum circular velocity of the disk component, $V_{D,\max}$, to V_{\max} while the lower panels are for the ratio of the baryonic (bulge + disk) maximum circular velocity, V_{bar} to V_{\max} note that the disk or disk+bulge maximum circular velocity may occur at radii different to the one where the total circular velocity has its maximum.

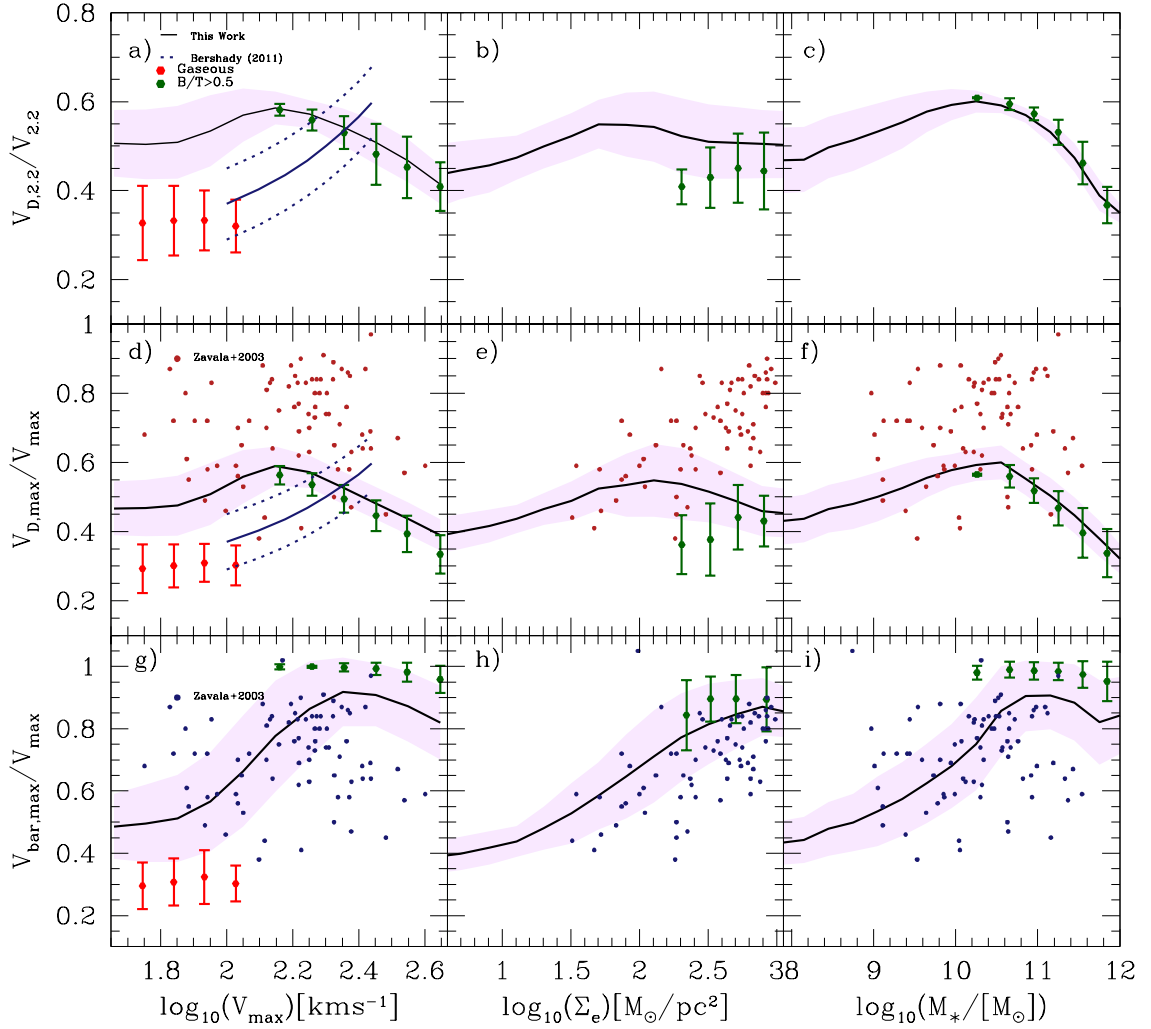


Figure 6.1: Different “luminous”-to-total velocity ratios as a function of V_{\max} , Σ_e and M_* for the semi-empirical mock disk galaxy catalog ($B/T \leq 0.5$); the dashed lines and shaded areas are the means and standard deviations, respectively. Green dots with error bars correspond to the sample of galaxies with $B/T > 0.5$. The red dots with error bars correspond to the sample of purely gas disk galaxies; they can not be plotted in the medium and right panels because they do not have stars. *Upper panels:* Disk-to-total velocity ratio measured at 2.2 scale radii of the baryonic disk. *Medium panels:* Maximum disk-to-maximum total velocity ratio. *Lower panels:* Maximum disk+bulge-to-total velocity ratio.

The $V_{D,2.2}/V_{2.2}$ and $V_{D,\max}/V_{\max}$ ratios of the semi-empirical model galaxies are almost always lower than 0.6, far from the disk-dominated case which has values of 0.75–0.85 (Sackett, 1997) (not taking into account a bulge). At low V_{\max} , Σ_e , and M_* the ratios slightly decrease as lower are these quantities. At $V_{\max} \approx 150$ km/s, $\Sigma_e \approx 200$ M_\odot/pc^2 , and $M_* \approx 2 \times 10^{10}$ M_\odot , these ratios have a shallow maximum, and for larger values the ratios decrease. Determinations of the $V_{D,2.2}/V_{2.2}$ ratio (which is close to the $V_{D,\max}/V_{\max}$ ratio for small-bulge galaxies) with vertical-disk dynamics studies using spectroscopical data were carried out by Bershady et al. (2011). For the small sample these authors present, they infer a correlation of the $V_{D,2.2}/V_{2.2}$ with V_{\max} , which we reproduce with a solid line (the dotted lines show the scatter of their correlation). The low-velocity semi-empirical model galaxies have larger velocity ratios than those of the small observational sample by Bershady et al. (2011). If we include the significant fraction of gaseous model galaxies (red dots and error bars), then the agreement would be better. It is probably that our algorithm for gas transformation into stars based on a simple Toomre instability criterion underpredicts the amount of stars formed at our lowest halo masses. On the other hand, the Bershady et al. (2011) velocity ratios seem to be too low; previous studies with similar techniques showed higher ratios, around 0.6 (e.g., Bottema, 1993). The sample of this author was small, only 12 galaxies, and he did not find a dependence of $V_{D,2.2}/V_{2.2}$ on luminosity or V_{\max} .

At maximum velocities around 200 km/s, the velocity ratios of the Bershady et al. (2011) and (Bottema, 1993) observations are of the order of our predictions. However, for the observational sample from the former authors, it seems that the $V_{D,2.2}/V_{2.2}$ ratio continues increasing with V_{\max} , while in our mock sample, the ratio at these values decreases with V_{\max} . Unfortunately, there are not dynamical observational determinations for galaxies with V_{\max} values larger than ~ 250 km/s.

Zavala et al. (2003) provided estimates of the $V_{D,\max}/V_{\max}$ ratio for 79 disk galaxies, whose properties were compiled from the literature (it is the same sample used in Avila-Reese et al., 2008). Their data are plotted in Fig. 6.1 (color dots). The data do not show a significant correlation with V_{\max} nor with M_* , but a trend of increasing $V_{D,\max}/V_{\max}$ with Σ_e is seen. At low

values of V_{\max} , Σ_e , and M_* the semi-empirical galaxies are in rough agreement with the observational inferences, but at large values of these quantities, the semi-empirical galaxies decrease their $V_{D,\max}/V_{\max}$ ratios with respect to the observational inferences. Recall that that the disk velocity contribution in the massive models becomes smaller in favor of a bulge component that increases the total maximum circular velocity, V_{\max} . So, it could be that when the bulge is significant, too much of the inner disk has been reduced. On the other hand, it should be said that the observational inferences could be contaminated partially by a bulge component at the time of estimating $V_{D,\max}$.

In the lower panels of Fig. 6.1, the disk+bulge velocity component is used. As expected, this component is now higher than in the only disk case, specially for the larger and higher surface density model galaxies. From our results, we see that in general the inclusion of the bulge increases significantly the maximum circular velocities ratios; this is even more notorious for the $B/T > 0.5$ galaxies (green dots with error bars). The circular velocity decompositions into bulge, disk and halo from observations are actually not trivial. On the other hand, the total velocity maxima can be at very different radii than those where the disk or disk+bulge maxima are attained. Therefore, these ratios are not reflecting already the luminous-to-dark matter contents at a given radius, specially for the bulge-dominated or dark-matter dominated galaxies. Unfortunately, observational samples with structural and dynamical information are scarce and do not allow for a full disk-bulge-halo decomposition in such a way that we can get the maximum circular velocities for each component and compare with our predictions.

For all the maximum velocity ratios presented in Fig. 6.1, there is a general trend: these ratios as a function of V_{\max} , Σ_e and M_* follow a bell-shaped dependence; after a maximum, they decrease as smaller/less dense and larger/more dense are the galaxies. The latter behavior could seem unexpected, but, as we will see below, its related to the dependence of f_{bar} on M_h used as an input in our static model of disk galaxies.

6.2 The inner baryon and dark matter mass fractions

In Fig. 6.2, we present the *direct* measures of the baryon (bulge+disk) mass fraction (i.e., the amount of baryon matter with respect to the total one) in the semi-empirical galaxies as a function of V_{\max} , Σ_e and M_* . The solid lines and shaded areas are the means and standard deviations of this fraction, $M_{\text{bar}}/M_{\text{tot}}$, measured up to one stellar effective radius, R_e , for our disk ($B/T \leq 0.5$) nongaseous galaxies. The green dots and error bars correspond to the galaxies with $B/T > 0.5$. The dashed lines are the means of the measured mass fractions at 0.5 , 1.5 and $2.0 R_e$, from top to bottom, respectively. Note that the corresponding *dark matter mass fractions* are $1 - M_{\text{bar}}/M_{\text{tot}}$.

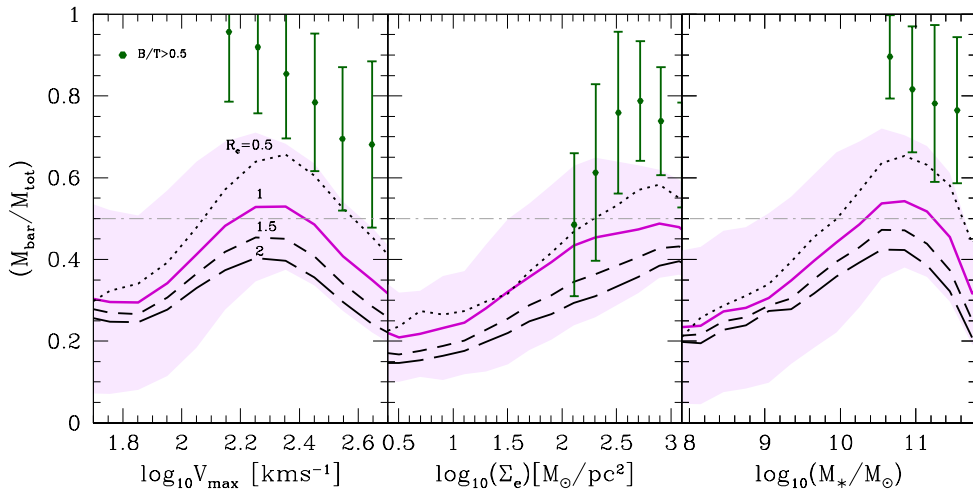


Figure 6.2: Baryon-to-total mass ratio at a given radius, $M_{\text{bar}}/M_{\text{tot}}$, of the semi-empirical galaxies as a function of V_{\max} , Σ_e , and M_* . The solid lines and shaded areas are for measures of this ratio at $1 R_e$ (the means and standard deviations, respectively). The dashed lines, from top to bottom, are the means of the $M_{\text{bar}}/M_{\text{tot}}$ ratio measured at 0.5 , 1.5 , and $2.0 R_e$, respectively. The green dots with error bars are the means and standard deviations of this ratio at $1 R_e$ for the sample of $B/T > 0.5$ galaxies.

From Fig. 6.2, we learn that:

- The baryon mass fraction at $1R_e$ has a maximum on average for galaxies with $V_{\max} \approx 200$ km/s, $\Sigma_e \approx 500 M_\odot/\text{pc}^2$, and $M_* \approx 5 \times 10^{10} M_\odot$. These maximal baryon fractions are slightly above 0.5, i.e. the mentioned above galaxies have a slight dominion of baryon matter over dark matter at $1R_e$. At values lower and higher than these, the mass ratios decrease. The decreasing is more pronounced for the dependence on M_* . Such a behavior of the inner baryon mass fraction is partially a consequence of the global $f_{\text{bar}}-M_h$ relation of disk galaxies used as input in our stationary model. This implies that *the $f_{\text{bar}}-M_h$ relation (or the closely related F_s-M_h relation) has a clear imprint in the inner galaxy and halo mass distributions.*
- As expected, the baryon (dark matter) mass fraction increases (decreases) as the radius is smaller, but for small, low-density galaxies, the differences between 0.5 and $2.0R_e$ are on average very small (the galaxies are already dark matter dominated since $\sim 0.5R_e$), while for larger, higher-density galaxies, the differences are more notorious, being many giant galaxies baryon-matter dominated at $0.5R_e$ but dark-matter dominated already at $2R_e$. It is interesting that our Milky-Way sized galaxies, contain on average 50% of baryons and 50% of dark matter at $1R_e$; at $2R_e$, the proportion change on average to 40% and 60%, respectively.
- The baryon mass fraction at $1R_e$ depends more tightly on Σ_e than on M_* and V_{\max} . This can be seen from the small scatter in the medium panel with respect to the left and right ones. The inner baryon mass fraction in the Λ CDM-based semi-empirical galaxies is determined by both the galaxy surface density (concentration) and the mass, but it dominates the first one.
- For the subsample of bulge-dominated semi-empirical galaxies (green dots with error bars), which are mostly high- V_{\max} , massive galaxies, the baryon mass fractions at $1R_e$ are high, being most of them actually baryon matter-dominated at this radius.

Our results clearly show how are expected to be the “luminous” and dark

matter distributions in disk galaxies formed in Λ CDM halos. An interesting prediction is that very massive, high-surface density galaxies become dark matter dominated already at $1R_e$. The trend of increasing the baryon matter dominion as galaxies are more massive and of higher surface density is broken, and the reason is that the halo baryon fraction, f_{bar} , decreases significantly with M_h for massive halos. Note that massive galaxies could be even more dark matter dominated than we show in Fig. inner-mass if the halo spin parameter λ would have remained the same for the baryons (detailed angular momentum conservation). After introducing here a decreasing of the initial spin parameter out of which galaxies form as M_h is larger (see Chapter 5), the galaxies are more concentrated and hence, increase their contribution to the total mass in the inner regions. But not enough as to dominate over dark matter at radii $\sim 1R_e$.

6.3 The outer slope of the circular velocity curves

A debated question in the literature is the one related to the rotation velocity shape of disk galaxies (e.g., Persic and Salucci, 1997; Catinella et al., 2006). Are the rotation curves described by an universal profile? Do the parameters of this profile depend more on luminosity (or M_*) or in surface brightness or any other galaxy property? The answers to these questions are tightly related to how are distributed the luminous and dark matter mass components.

Here, we focus only on the outer slope of the circular velocity profiles. By outer we understand galaxy radii further away the radius where the luminous (bulge + disk) component attained its maximum. For example, in the case of an exponential disk-dominated system, where the maximum is attained at $\approx 2.2R_D$, or equivalently, $\approx 1.3R_e$, the outer slope could be measured let say at $\sim 3R_D$. Because of our galaxies are composed of bulge, disk and halo, it is not so obvious where is the maximum. If the halo dominates, then the maximum happens typically at radii larger than the one of the disk component. The opposite happens if the bulge dominates. In order to assure a region far

away the maximum of the bulge+disk component, we measure the slope of the circular velocity profile in between 3.0 and $3.5R_D$, α_{out} . This can be considered as an outer radius in the sense of the luminous galaxy. We could measure the slope at even outer radii, but in the hope to compare in the future our results with observational determinations, it is better to keep the measure not too further away. The observational measures of the rotation velocities do not extend typically to much outer radii.

In Fig. 6.3, we plot the dependence of the outer slope of the total circular velocity curves (α_{out}) of our semi-empirical disk galaxies as function of V_{max} , Σ_e , and M_* . According to the figure, α_{out} correlates with these three galaxy properties, but more with Σ_e (the tightest correlation is with this property), implying that outer shape of the circular velocity is mainly determined by the galaxy surface density. In the case of this correlation, we have actually obtained the means and standard deviations for the mock galaxies smaller than $M_* = 5 \times 10^{10} M_\odot$ separate from those larger than this mass. Recall that an important result from our semi-empirical mock galaxy catalog is that the $\Sigma_e - M_*$ correlation flattens at the high-mass end (see subsection 5.1.1 in the previous Chapter) in such a way that increasing M_* , Σ_e almost already does not increase. This behavior in combination with that α strongly increases with M_* at high masses, make that in the $\alpha_{\text{out}} - \Sigma_e$ plane appeared a clear bimodality driven by mass. In order to take into account such a bimodality at the time of obtaining means and standard deviations, we have separated our mock sample into two groups by the mass criterion mentioned above.

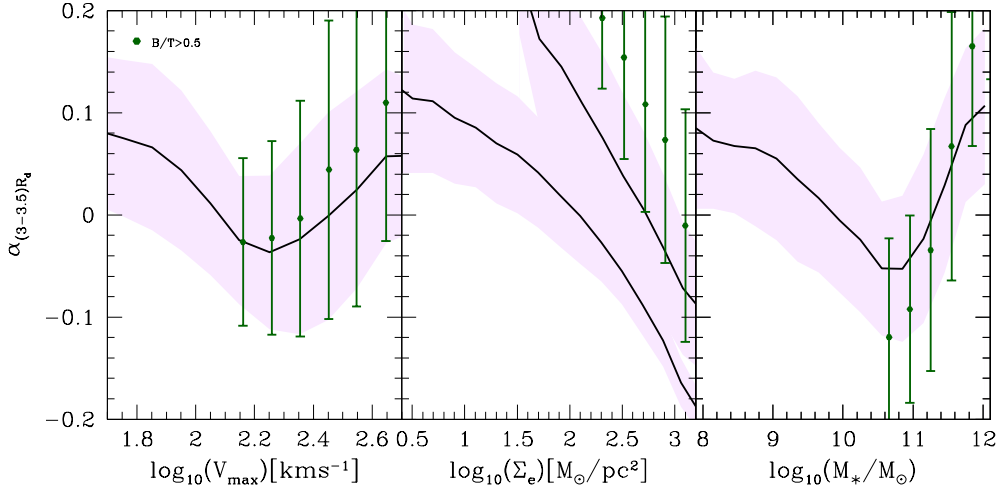


Figure 6.3: Outer slope of the circular velocity of our semi-empirical galaxies as a function of V_{\max} , Σ_e , and M_* . The solid lines and shaded areas are the means and standard deviations. In the case of Σ_e (medium panel), we have calculated these means and standard deviations separated into galaxies smaller and larger than $M_* = 5 \times 10^{10} M_\odot$ because a strong bimodality driven by mass appears in the $\alpha_{\text{out}} - \Sigma_e$ plane. The green dots with error bars are the means and standard deviations for the $B/T > 0.5$ galaxies.

Small, low-surface density galaxies have rising circular velocities ($\alpha_{\text{out}} > 0$) at $3-3.5R_D$, but as the surface density and galaxy size increase, the slope becomes flatter and even decreasing ($\alpha_{\text{out}} < 0$). However, for $M_* \gtrsim 5 \times 10^{10} M_\odot$ ($V_{\max} \gtrsim 200$ km/s) the slope again increases on average; the velocity profiles are rising for the largest disk galaxies. In other words, the baryonic component is sub-dominant for these galaxies and the total circular velocity curve is mainly the one of the dark matter halo at these radii. This is in agreement with the above reported luminous-to-total mass contents at 1.5 and $2R_e$, see Fig. 6.2. The circular velocity profiles of large galaxies are rising at large radii mainly because these galaxies become dark matter dominated, as the low-mass ones. It should be said that the $B/T > 0.5$ galaxies follow the same trends (green dots with error bars).

What about the dependence of α_{out} on Σ_e for high-surface density galaxies?

According to Fig. 6.3, on average α_{out} would continue decreasing up to the largest possible values of Σ_e . When separated by mass, many of the most massive galaxies can have lower values of Σ_e and positive values of α_{out} . A clear bimodality in the $\alpha_{\text{out}}-\Sigma_e$ plane appears. This is why we plot the means and standard deviations in this plane separated by mass.

Our results show that a way to probe the luminous-to-total content of galaxies yet within optical radii, is by the outer shape of the rotation curves. With the advent of large galaxy surveys, large samples of galaxies with rotation curves measured up to $3-3.5R_D$ ($1.5-2R_e$) will be available, and it will be possible then to test whether their outer slopes have the dependences that we have found in our Λ CDM-based semi-empirical disk galaxies. The secondary sample of the MaNGA/SDSS-IV survey (Bundy et al., 2014) is designed to attain $2.5R_e$. Therefore, we will have optical rotation curves at least up to this radius for ~ 1500 galaxies, for which most of the optical properties will be also available.

Chapter 7

Summary and conclusions

El escenario cosmológico Λ CDM proporciona el contexto más adecuado para interpretar la naturaleza, origen y evolución de las galaxias, en particular aquellas que dominan en el Universo local: las galaxias de disco (ver p. ej. Mo et al. 1998; Avila-Reese et al. 1998,2000,2008; Firmani & Avila-Reese 2000; Gnedin et al. 2007; Dutton et al. 2007). En esta tesis nos propusimos explorar la consistencia de dicho escenario con las principales correlaciones observacionales de la población de galaxias de disco locales, tomando en cuenta las recientes inferencias semi-empíricas de la fracción bariónica, $f_{\text{bar}}=M_{\text{bar}}/M_h$, en función de la masa de halo, M_h . Esta relación, $f_{\text{bar}}-M_h$ (o $M_{\text{bar}}-M_h$), contiene la información de los principales procesos astrofísicos que operaron en la evolución de las galaxias en función de la masa como ser la caída y enfriamiento del gas hacia los halos y galaxias, la formación estelar, la retroalimentación de este proceso hacia el medio interestelar así como el de los núcleos galácticos activos, etc. Las relaciones M_*/M_h-M_h y M_{bar}/M_h-M_h , incluyendo su dispersión intrínseca, fue inferida por primera vez por separado para galaxias tardías y tempranas locales (Rodríguez-Puebla et al., 2014; Calette, 2014), siendo éstas diferentes en realidad. En esta tesis se hizo uso de tales inferencias correspondientes a las galaxias azules/tardías (mayormente de disco).

Se implementó como herramienta de trabajo un modelo estático (no evolutivo) de población de galaxias de disco que consiste en cargar discos en equilibrio centrífugo en los halos de Λ CDM, tomando en cuenta la contracción adiabática

que sufre el halo internamente por la galaxia (Mo et al., 1998). Se implementó la posibilidad de calcular la formación de bulbos por inestabilidades intrínsecas del disco así como de transformación de gas en estrellas por inestabilidades tipo Toomre (Dutton et al., 2007). Las condiciones iniciales del modelo estático son las propiedades “cosmológicas” del halo (masa virial M_h , parámetro de giro λ y concentración C) y la relación $f_{\text{bar}}-M_h$ que resume los procesos astrofísicos de incorporación y pérdida de bariones por parte de la galaxia. Cada uno de estos parámetros sigue en realidad una distribución estadística que tomamos en cuenta.

Armados de este modelo semi-empírico, se procedió a generar un catálogo sintético de decenas de miles de galaxias de disco locales cubriendo el intervalo de masa de halo de 10^{10} a $10^{14} M_\odot$. Para ser consistentes en las comparaciones con las observaciones, tomamos en cuenta como galaxias de disco sólo aquellas con el cociente B/T menor o igual a 0.5. La fracción de galaxias con $B/T > 0.5$ es baja ($\approx 11\%$) y aplica sólo para galaxias masivas.¹ Un repaso de las principales conclusiones relacionadas a las relaciones de escala y correlaciones de propiedades galácticas globales con la masa (Capítulos 4 y 5) es como sigue:

- Partiendo de las distribuciones que las simulaciones cosmológicas de N cuerpos dan para los parámetros λ y C , y suponiendo conservación detallada de momento angular, la población de galaxias de disco generada reproduce muy bien las relaciones de escala observadas (radio-masa y TF, tanto estelares como bariónicas) así como correlaciones de propiedades intensivas (B/T, cociente de masa de gas a estelar $-R_{\text{gas}} = M_g / M_*$, densidad estelar superficial efectiva, Σ_e) con la masas estelar M_* . No obstante este acuerdo es válido sólo hasta masas $M_* \approx 3 \times 10^{10} M_\odot$ que corresponde a halos de $M_h \approx 3 - 5 \times 10^{11} M_\odot$. A masas mayores, las galaxias tienen radios y V_{max} mayores a los observados, B/T demasiado pequeños y contenidos de gas muy altos. Además las densidades superficiales de las galaxias masivas decrecen con M_* .

¹Nótese que esta fracción no pretende ser una predicción de la fracción de galaxias tempranas pues desde un principio, se estuvo tratando sólo la población de galaxias azules/tardías. La fracción puede ser más bien interpretada como galaxias azules que de todos modos presentan un bulbo dominante.

- El desacuerdo de los modelos con las observaciones a altas masas es de esperarse: en el escenario Λ CDM los halos masivos han ensamblado sus masas con una fracción importante de fusiones mayores implicando que las galaxias también sufrieron fusiones e interacciones en su evolución reciente (e.g., Avila-Reese et al., 2014). En estos casos la formación de bulbos y la transformación de gas en estrellas en un régimen de inestabilidades intrínsecas (evolución secular) no es suficiente; de igual manera, la suposición de conservación detallada de momento angular deja de ser del todo correcta pues las fusiones son mecanismos de transporte de momento angular, de los bariones del que se forman las galaxias a la materia oscura (Zavala et al., 2008). En vista de esto, nuestros resultados nos indican el rol que las fusiones/interacciones juegan en las principales propiedades de las galaxias de disco actuales: prácticamente ninguno para las de masas menores a $M_* \approx 3 \times 10^{10} M_\odot$ y cada vez mayor a medida que la masa crece a partir de $M_h \approx 3 - 5 \times 10^{11} M_\odot$.
- Operando sobre los parámetros que controlan las inestabilidades del disco para hacerlos “artificialmente” más inestables mientras más masivos son sus halos debido a las fusiones y disminuyendo el parámetro de giro del gas del que se forma la galaxia, logramos que las galaxias de altas masas estén en acuerdo con la relación radio–masa y las correlaciones $B/T-M_*$ y M_g-M_* observadas. Nuestro método puede entenderse a este punto como una manera (semi)empírica sofisticada de determinar el parámetro de giro inicial del que las galaxias de disco observadas se formaron, λ_{bar} en función de M_* y M_h . El resultado es que hasta masas de $M_* \approx 3 - 5 \times 10^{10} M_\odot$, este parámetro es similar en magnitud y distribución (lognormal) al de los halos Λ CDM (λ promedio de 0.036 sin una dependencia con M_h), pero a masas mayores, disminuye con M_h como $\lambda_{bar} \propto -0.0095 \log M_h$ o, en función de M_* , como $\lambda_{bar} \propto -0.0126 \log M_*$; es decir, hay ”pérdida” de momento angular a masas mayores. La dispersión de la distribución ”cosmológica” original se mantiene; con ella se logra reproducir la dispersión observada en las relaciones radio-masa.
- Las relaciones R_e-M_* y $R_{e,D}-M_*$ predichas tienen una dispersión considerable, que aumenta hacia las masas menores; estas dispersiones son

similares a la que se infieren de las observaciones. A paridad de M_* , la dispersión tiene su fuente principalmente en la dispersión de λ_{bar} : a mayor λ_{bar} , radio más grande. Sin embargo, encontramos que también es una fuente de dispersión el parámetro f_{bar} (radio más pequeño en promedio mientras f_{bar} es mayor) y en mucho menor grado, la concentración C (se observa una leve tendencia a que el radio es mayor cuando C es mayor).

- La relación de la densidad superficial estelar efectiva, Σ_e , con M_* que se predice es estrecha. La dependencia inicial de f_{bar} con M_h que usamos tiene su clara huella en esta relación, haciendo que sea más empinada a bajas masas que el caso esperado $\Sigma_e \propto M_*^{1/3}$ (la correlación que medimos va como $M_*^{0.6}$) y que se aplane a las altas masas. De hecho, Σ_e incluso decrecería con M_* a las altas masas (por el hecho de que f_{bar} decrece con la masa en este régimen) si es que λ_{bar} fuese constante. No obstante, λ_{bar} en nuestro modelo decrece con la masa en este régimen como ya se discutió arriba.
- Una vez que a altas masas se reprodujeron las relaciones radio-masa, $B/T - M_*$ y $M_g/M_* - M_*$, las relaciones predichas de TF estelar y bariónica están en excelente acuerdo con las observaciones. En particular, no encontramos ningún problema con el punto cero, siendo que por construcción nuestros modelos están de acuerdo con la función de masa bariónica (y estelar) inferida de las observaciones. A bajas masas, la TF estelar sufre un doblez que aparentemente también lo muestran las galaxias enanas; a nivel de TF bariónica este doblez es mucho menos perceptible. A masas muy altas, los modelos semi-empíricos muestran también un doblez que será interesante comprobar si en las observaciones se da o no.
- La dispersión en las relaciones de TF predichas es moderada y producida casi únicamente por la dispersión en la concentración C de los halos. Los parámetros λ_{bar} y f_{bar} no parecen ser fuente de dispersión y por ende las relaciones de TF son muy robustas a variaciones en estos parámetros. No obstante, la dispersión intrínseca en las relaciones de TF de los modelos semi-empíricos son mayores a la que presentan las observaciones. Este podría ser un potencial problema, aunque hacemos notar que el catálogo fue construido bajo la suposición de que las dispersiones en λ_{bar} , C y f_{bar}

son independientes. En caso de que hubiese cierta correlación entre C y los otros dos parámetros, la dispersión en la TF podría disminuir (o aumentar!).

- Los residuales de la relación $R_e - M_*$ no correlacionan significativamente con R_{gas} , pero sí anticorrelacionan con el cociente B/T (galaxias que se desvían hacia radios menores para su masa, tienden a tener B/T mayores) y con Σ_e (galaxias que se desvían hacia radios menores para su masa, tienden a ser de mayor densidad superficial, aunque esto no se observa en el caso de las galaxias con Σ_e bajos). Los residuales de la relación $V_{max} - M_*$ (TF) prácticamente no correlacionan con el cociente B/T y lo hacen débilmente con R_{gas} : anticorrelacionan con R_{gas} en caso de galaxias poco gaseosas (que son las masivas) pero correlacionan con R_{gas} en caso de galaxias gaseosas (que son poco masivas). Los residuales de la relación TF correlacionan con Σ_e para galaxias de alta densidad superficial pero esta correlación desaparece para densidades superficiales menores.
- Se exploró también los residuales de las relaciones $M_{bar} - M_h$ y $M_* - M_*$, encontrando que hay cierta segregación en estas relaciones con las propiedades galácticas estudiadas aquí: R_{gas} , B/T y Σ_e . Será de interés comprobar en un futuro con las observaciones directas estas segregaciones predichas, mismas que son más evidentes en el caso bariónico.
- Los residuales de las relaciones $R_e - M_*$ y $V_{max} - M_*$ anticorrelacionan muy débilmente con una pendiente mucho menor a -0.5 y en acuerdo a ciertas inferencias observacionales. Algo similar ocurre con los residuales de las relaciones de escala bariónicas, mostrando una anticorrelación ligeramente mayor. La anticorrelación entre los residuales con una pendiente tan baja es evidencia de que la componente disco+bulbo en la velocidad de rotación es poco dominante, es decir, es más importante la componente del halo oscuro.

En el Capítulo 6 estudiamos más en detalle la cuestión de las contribuciones a la velocidad circular por parte del disco y del disco + bulbo, cuestión relacionada directamente con las distribuciones de masa interna en las galaxias de disco. Los principales resultados son:

- El cociente de velocidades de disco a total a $2.2R_D$, $V_{D,2.2}/V_{2.2}$, es casi siempre menor a 0.6, lejos del caso de “disco máximo” (0.75-0.85). Este cociente para las galaxias semi-empíricas decrece en promedio con V_{\max} , Σ_e y M_* en el lado de valores bajos de estas propiedades globales de las galaxias. Alcanza un máximo suave (alrededor de 0.6) a $V_{\max} \approx 150$ km/s, $\Sigma_e \approx 200 M_\odot/pc^2$, and $M_* \approx 2 \times 10^{10} M_\odot$, y para valores mayores, el cociente $V_{D,2.2}/V_{2.2}$ vuelve a decrecer. En comparación con estudios espectroscópios de dinámica vertical en galaxias de disco que infieren estos cocientes para muestras muy pequeñas, nuestros resultados son someramente consistentes dentro de las incertidumbres.
- El cociente de velocidades $V_{D,\max}/V_{\max}$ (donde los máximos pueden ser a diferentes radios) muestra un comportamiento con V_{\max} , Σ_e y M_* similar al mencionado arriba: el cociente crece a medida que estas propiedades aumentan en valor, llega a un máximo y para galaxias más grandes y densas, vuelve a decrecer. Este comportamiento es una huella de la relación $f_{\text{bar}}-M_h$ usada como condición inicial en los modelos semi-empíricos. Cuando se usa la velocidad al máximo del disco + bulbo, el cociente $V_{B+D,\max}/V_{\max}$, se incrementa, en especial para las galaxias más masivas y de altas densidades superficiales. Lamentablemente no hay muchos datos observacionales aún de este tipo como para confrontar con las predicciones.
- Los cocientes de velocidades son importante porque es la manera de explorar observacionalmente la distribución dinámica de la masas de diferentes componentes (bulbo, disco, halo). No obstante, nuestros modelos dan la predicción directa de dichas distribuciones. Ellos muestran que la fracción de masa bariónica (bulbo+ disco) hasta $1R_e$ alcanza su máximo en promedio para galaxias con $V_{\max} \approx 200$ km/s, $\Sigma_e \approx 250 M_\odot/pc^2$, and $M_* \approx 5 \times 10^{10} M_\odot$; estas galaxias son ligeramente dominadas por materia “luminosa”, con fracciones algo superiores a 0.5 en promedio. Para valores de V_{\max} , Σ_e , y M_* menores y mayores a los mencionados, la fracción de masa “luminosa” decrece, es decir domina la masa oscura dentro de $1R_e$ para ellas. Esto es consecuencia de la relación $f_{\text{bar}}-M_h$ usada como condición inicial.

- La fracción de masa “luminosa” aumenta hacia radios más centrales, aunque para galaxias pequeñas y de baja densidad superficial, el aumento es mínimo, por ejemplo a $0.5 R_e$, es decir estas galaxias ya son dominadas por materia oscura a estos radios. Nuestros resultados muestran que una galaxia similar a la Vía Láctea contiene en promedio 50% de bariones y 50% de materia oscura a $1R_e$; a $2R_e$ la proporción cambia en promedio a 40% y 60% respectivamente.
- Una cantidad que se podría obtener observacionalmente para catastros de galaxias y que está relacionada con el cociente de masa “luminosa” a oscura, es la pendiente externa (entre 3 y $3.5R_D$) de la curva de rotación, α_{out} . Calculamos α_{out} para nuestras galaxias semi-empíricas y encontramos que esta pendiente correlaciona con V_{max} , Σ_e y M_* , pero más con Σ_e , implicando esto que es la densidad superficial la que más afecta a la forma externa de las curvas de rotación.
- Galaxias pequeñas, de baja densidad superficial tienen perfiles externos de V_c crecientes ($\alpha_{\text{out}} > 0$). A medida que las galaxias son más masivas y densas, α_{out} decrece en promedio haciéndose negativo (curvas decrecientes), pero para galaxias de $M_* > \sim 5 \times 10^{10} M_\odot$ ($V_{\text{max}} > \sim 200 \text{ km/s}$), la pendiente vuelve a crecer mientras más masivas son las galaxias; las galaxias más masivas tienen curvas crecientes, mismas que están trazando al halo (la contribución luminosa decrece ya a estos radios); es decir son galaxias dominadas por materia oscura a $3-3.5 R_D$. Una vez más, este comportamiento bimodal de α_{out} con la masa (o V_{max}) es debido a la relación $f_{\text{bar}}-M_h$ usada como condición inicial.

Appendix A

The empirical HI-to- M_* and H₂-to- M_* correlations for local late- and early-type galaxies

Calette (2014) have compiled and homogenized from the literatura several samples of local galaxies with reported measures of stellar mass, HI and H₂ masses, as well as morphology type and/or color. By defining the mass ratios $R_{HI} \equiv M_{HI}/M_*$ and $R_{H_2} \equiv M_{H_2}/M_*$, in this work, it is found that the $R_{HI}-M_*$ and $R_{H_2}-M_*$ correlations for blue/late-type (LTG) and red/early-type (ETG) galaxies are better described by a double-power law.

The double power law proposed to fit the R_{HI} vs M_* correlations is:

$$\log_{10}(R_{HI}) = \log_{10}(B) - \log_{10} \left[\left(\frac{M_*}{M^s} \right)^\xi + \left(\frac{M_*}{M^s} \right)^\rho \right], \quad (\text{A.1})$$

where B is the normalization, ξ and ρ are the slopes of the function and M^s is the breakdown mass. In Table A.1, the values of these parameters for both LTGs and ETGs are given.

For the scatter around the determined $R_{HI}-M_*$ correlations, they assume that it is log-normal distributed in agreement with several previous studies (see Calette 2015 for the references). The lognormal intrinsic scatter is proposed

Galaxy population	Parameters.			
ETG	$\log_{10}(B)$	ξ	ρ	$\log_{10}(M^s)$
	-0.82	0.20	1.86	9.50
LTG	$\log_{10}(B)$	ξ	ρ	$\log_{10}(M^s)$
	0.06	0.20	0.85	9.50

Table A.1: Parameters of the R_{HI} - M_* two-power law relations

to slightly depend on M_* as:

$$\sigma_{\log_{10} R_{HI}} = A + \varphi \log_{10} \left(\frac{M_*}{M^s} \right). \quad (\text{A.2})$$

In Table A.2, the values of A and φ for the two galaxy populations are reported.

Galaxy population	Parameters	
ETG	A	φ
	0.70	0.00
LTG	A	φ
	0.41	-0.04

Table A.2: Parameters for the scatters around the R_{HI} - M_* relations

The double-power law proposed to fit the R_{H_2} vs M_* correlations is:

$$\log_{10} (R_{H_2}) = \log_{10}(C) - \log_{10} \left[\left(\frac{M_*}{M^s} \right)^\beta + \left(\frac{M_*}{M^s} \right)^\gamma \right], \quad (\text{A.3})$$

where C is the normalization, β and γ are the slopes of the function and M^s is the breakdown mass. In Table A.3 are given the values of these parameters.

Galaxy population.	Parameters.			
ETG	$\log_{10}(C)$	β	γ	$\log_{10}(M^s)$
	-1.52	0.0	1.50	9.50
LTG	$\log_{10}(C)$	β	γ	$\log_{10}(M^s)$
	-0.5	0.34	0.78	9.50

Table A.3: Parameters of the R_{H_2} - M_* double power-law correlations

Regarding the intrinsic scatter around the R_{H_2} - M_* relations, again, Calette (2015) assumes that it is log-normally distributed. The width of this distribu-

tion, in the case of LTGs, which are mostly star-forming objects, is expected to be close to the width of the specific star formation rate (sSFR) vs. M_* relation, the so-called “main sequence”¹. The observations of local galaxies show that the scatter around this relation is 0.3 – 0.5 dex, increasing slightly to lower masses (e.g., Salim et al., 2007). Based on this reasoning as well as on the scatter that observations show in the largest compiled samples in Calette (2015), he finds that a good description for the intrinsic scatter of LTGs is:

$$\sigma_{\log_{10} R_{H_2}} = A' + \varphi' \log_{10} \left(\frac{M_*}{M^s} \right). \quad (\text{A.4})$$

with $A' = 0.37$ and $\varphi' = -0.01$.

In the case of ETGs, the intrinsic scatter seems to be larger than for LTGs. The former are in general passive, devoid of gas reservoirs, but probably a fraction of them can acquire some gas and trigger star formation during interactions and mergers. Then, the amount of H_2 depends on the kind of merger and on the conditions to transform the atomic gas to molecular one. The range of possibilities is huge, hence, the scatter around the R_{H_2} – M_* relation should be large. Calette (2015) assumes the width of the log-normal distribution to be $\sigma_{\log_{10} R_{H_2}} = 0.7$ dex and constant with mass.

¹The sSFR is a measure of the efficiency of current SFR of a galaxy with respect to its past average efficiency. Since star formation proceeds in molecular clouds, the fraction of H_2 in a galaxy with respect to its size (M_*), is expected to correlate with the sSFR

Bibliography

- Abazajian, K. N., Adelman-McCarthy, J. K., Agüeros, M. A., Allam, S. S., Allende Prieto, C., An, D., Anderson, K. S. J., Anderson, S. F., Annis, J., Bahcall, N. A., and et al. (2009). The Seventh Data Release of the Sloan Digital Sky Survey. *ApJs*, 182:543–558.
- Avila-Reese, V. (2006). Understanding Galaxy Formation and Evolution. *ArXiv Astrophysics e-prints*.
- Avila-Reese, V., Carrillo, A., Valenzuela, O., and Klypin, A. (2005). Secular evolution of galactic discs: constraints on phase-space density. *MNRAS*, 361:997–1004.
- Avila-Reese, V. and Firmani, C. (2000). Properties of Disk Galaxies in a Hierarchical Formation Scenario. *RevMexAA*, 36:23.
- Avila-Reese, V., Firmani, C., and Hernández, X. (1998). On the Formation and Evolution of Disk Galaxies: Cosmological Initial Conditions and the Gravitational Collapse. *ApJ*, 505:37–49.
- Avila-Reese, V., Zavala, J., Firmani, C., and Hernández-Toledo, H. M. (2008). On the Baryonic, Stellar, and Luminous Scaling Relations of Disk Galaxies. *AJ*, 136:1340–1360.
- Avila-Reese, V., Zavala, J., and Lacerna, I. (2014). The growth of galactic bulges through mergers in Λ cold dark matter haloes revisited - II. Morphological mix evolution. *MNRAS*, 441:417–430.
- Baldry, I. K., Driver, S. P., Loveday, J., Taylor, E. N., Kelvin, L. S., Liske, J., Norberg, P., Robotham, A. S. G., Brough, S., Hopkins, A. M., Bamford,

- S. P., Peacock, J. A., Bland-Hawthorn, J., Conselice, C. J., Croom, S. M., Jones, D. H., Parkinson, H. R., Popescu, C. C., Prescott, M., Sharp, R. G., and Tuffs, R. J. (2012). Galaxy And Mass Assembly (GAMA): the galaxy stellar mass function at $z < 0.06$. *MNRAS*, 421:621–634.
- Baldry, I. K., Glazebrook, K., and Driver, S. P. (2008). On the galaxy stellar mass function, the mass-metallicity relation and the implied baryonic mass function. *MNRAS*, 388:945–959.
- Behroozi, P. S., Conroy, C., and Wechsler, R. H. (2010). A Comprehensive Analysis of Uncertainties Affecting the Stellar Mass-Halo Mass Relation for $0 < z < 4$. *ApJ*, 717:379–403.
- Behroozi, P. S., Wechsler, R. H., and Conroy, C. (2013). The Average Star Formation Histories of Galaxies in Dark Matter Halos from $z = 0\text{--}8$. *ApJ*, 770:57.
- Bell, E. F. and de Jong, R. S. (2001). Stellar Mass-to-Light Ratios and the Tully-Fisher Relation. *ApJ*, 550:212–229.
- Bell, E. F., McIntosh, D. H., Katz, N., and Weinberg, M. D. (2003). The Optical and Near-Infrared Properties of Galaxies. I. Luminosity and Stellar Mass Functions. *APJS*, 149:289–312.
- Bernardi, M., Meert, A., Sheth, R. K., Vikram, V., Huertas-Company, M., Mei, S., and Shankar, F. (2013). The massive end of the luminosity and stellar mass functions: dependence on the fit to the light profile. *MNRAS*, 436:697–704.
- Bernardi, M., Meert, A., Vikram, V., Huertas-Company, M., Mei, S., Shankar, F., and Sheth, R. K. (2012). Systematic effects on the size-luminosity relation: dependence on model fitting and morphology. *ArXiv e-prints*.
- Bernardi, M., Shankar, F., Hyde, J. B., Mei, S., Marulli, F., and Sheth, R. K. (2010). Galaxy luminosities, stellar masses, sizes, velocity dispersions as a function of morphological type. *MNRAS*, 404:2087–2122.

- Bershady, M. A., Martinsson, T. P. K., Verheijen, M. A. W., Westfall, K. B., Andersen, D. R., and Swaters, R. A. (2011). Galaxy Disks are Submaximal. *ApJ*, 739:L47.
- Berta, Z. K., Jimenez, R., Heavens, A. F., and Panter, B. (2008). The role of spin in the formation and evolution of galaxies. *MNRAS*, 391:197–204.
- Bett, P., Eke, V., Frenk, C. S., Jenkins, A., Helly, J., and Navarro, J. (2007). The spin and shape of dark matter haloes in the Millennium simulation of a Λ cold dark matter universe. *MNRAS*, 376:215–232.
- Blanton, M. R., Eisenstein, D., Hogg, D. W., Schlegel, D. J., and Brinkmann, J. (2005a). Relationship between Environment and the Broadband Optical Properties of Galaxies in the Sloan Digital Sky Survey. *ApJ*, 629:143–157.
- Blanton, M. R., Geha, M., and West, A. A. (2008). Testing Cold Dark Matter with the Low-Mass Tully-Fisher Relation. *ApJ*, 682:861–873.
- Blanton, M. R. and Roweis, S. (2007). K-Corrections and Filter Transformations in the Ultraviolet, Optical, and Near-Infrared. *AJ*, 133:734–754.
- Blanton, M. R., Schlegel, D. J., Strauss, M. A., Brinkmann, J., Finkbeiner, D., Fukugita, M., Gunn, J. E., Hogg, D. W., Ivezić, Ž., Knapp, G. R., Lupton, R. H., Munn, J. A., Schneider, D. P., Tegmark, M., and Zehavi, I. (2005b). New York University Value-Added Galaxy Catalog: A Galaxy Catalog Based on New Public Surveys. *AJ*, 129:2562–2578.
- Blanton, M. R., Schlegel, D. J., Strauss, M. A., Brinkmann, J., Finkbeiner, D., Fukugita, M., Gunn, J. E., Hogg, D. W., Ivezić, Ž., Knapp, G. R., Lupton, R. H., Munn, J. A., Schneider, D. P., Tegmark, M., and Zehavi, I. (2005c). New York University Value-Added Galaxy Catalog: A Galaxy Catalog Based on New Public Surveys. *AJ*, 129:2562–2578.
- Blumenthal, G. R., Faber, S. M., Flores, R., and Primack, J. R. (1986). Contraction of dark matter galactic halos due to baryonic infall. *ApJ*, 301:27–34.
- Bottema, R. (1993). The Stellar Kinematics of Galactic Disks. *A&A*, 275:16.

- Bruce, V. A., Dunlop, J. S., Cirasuolo, M., McLure, R. J., Targett, T. A., Bell, E. F., Croton, D. J., Dekel, A., and et al. (2012). The morphologies of massive galaxies at $1 < z < 3$ in the CANDELS-UDS field: compact bulges, and the rise and fall of massive discs. *MNRAS*, 427:1666–1701.
- Bruzual, G. and Charlot, S. (2003). Stellar population synthesis at the resolution of 2003. *MNRAS*, 344:1000–1028.
- Buitrago, F., Trujillo, I., Conselice, C. J., and Häußler, B. (2013). Early-type galaxies have been the predominant morphological class for massive galaxies since only $z \sim 1$. *MNRAS*, 428:1460–1478.
- Bundy, K., Bershady, M. A., Law, D. R., Yan, R., Drory, N., MacDonald, N., Wake, D. A., Cherinka, B., Sánchez-Gallego, J. R., Weijmans, A.-M., Thomas, D., Tremonti, C., Masters, K., Coccato, L., Diamond-Stanic, A. M., Aragón-Salamanca, A., Avila-Reese, V., Badenes, C., Falcón-Barroso, J., Belfiore, F., Bizyaev, D., Blanc, G. A., Bland-Hawthorn, J., Blanton, M. R., Brownstein, J. R., Byler, N., Cappellari, M., Conroy, C., Dutton, A. A., Emsellem, E., Etherington, J., Frinchaboy, P. M., Fu, H., Gunn, J. E., Harding, P., Johnston, E. J., Kauffmann, G., Kinemuchi, K., Klaene, M. A., Knapen, J. H., Leauthaud, A., Li, C., Lin, L., Maiolino, R., Malanushenko, V., Malanushenko, E., Mao, S., Maraston, C., McDermid, R. M., Merrifield, M. R., Nichol, R. C., Oravetz, D., Pan, K., Parejko, J. K., Sanchez, S. F., Schlegel, D., Simmons, A., Steele, O., Steinmetz, M., Thanjavur, K., Thompson, B. A., Tinker, J. L., van den Bosch, R. C. E., Westfall, K. B., Wilkinson, D., Wright, S., Xiao, T., and Zhang, K. (2014). Overview of the SDSS-IV MaNGA Survey: Mapping Nearby Galaxies at Apache Point Observatory. *ArXiv e-prints*.
- Calette, A. R. (2014). Conexión halo-galaxia: Fracción bariónica de galaxias rojas y azules. Master's thesis, Universidad Nacional Autónoma de México.
- Capaccioli, M. (1989). In *The World of Galaxies*.
- Carollo, C. M., Cibinel, A., Lilly, S. J., Miniati, F., Norberg, P., Silverman, J. D., van Gorkom, J., Cameron, E., Finoguenov, A., Peng, Y., Pipino, A., and Rudick, C. S. (2013). The Zurich Environmental Study of Galaxies

- in Groups along the Cosmic Web. I. Which Environment Affects Galaxy Evolution? *ApJ*, 776:71.
- Catinella, B., Giovanelli, R., and Haynes, M. P. (2006). Template Rotation Curves for Disk Galaxies. *ApJ*, 640:751–761.
- Cebrian, M. and Trujillo, I. (2014). The effect of the environment on the stellar mass - size relation of present-day galaxies. *ArXiv e-prints*.
- Cervantes-Cota, J. L., Rodríguez-Meza, M. A., and Nuñez, D. (2007). Flat rotation curves using scalar-tensor theories. *Journal of Physics Conference Series*, 91(1):012007.
- Cervantes-Sodi, B., Hernandez, X., Park, C., and Kim, J. (2008). Environment and mass dependencies of galactic λ spin parameter: cosmological simulations and observed galaxies compared. *MNRAS*, 388:863–872.
- Chabrier, G. (2003). Galactic Stellar and Substellar Initial Mass Function. *PASP*, 115:763–795.
- Christodoulou, D. M., Shlosman, I., and Tohline, J. E. (1995). A new criterion for bar-forming instability in rapidly rotating gaseous and stellar systems. 1: Axisymmetric form. *ApJ*, 443:551–562.
- Cibinel, A., Carollo, C. M., Lilly, S. J., Miniati, F., Silverman, J. D., van Gorkom, J. H., Cameron, E., Finoguenov, A., Norberg, P., Peng, Y., Pipino, A., and Rudick, C. S. (2013). The Zurich Environmental Study (ZENS) of Galaxies in Groups along the Cosmic Web. II. Galaxy Structural Measurements and the Concentration of Morphologically Classified Satellites in Diverse Environments. 776:72.
- Ciotti, L. (1991). Stellar systems following the $R^{-1/m}$ luminosity law. *AAP*, 249:99–106.
- Colless, M., Dalton, G., Maddox, S., Sutherland, W., Norberg, P., Cole, S., Bland-Hawthorn, J., Bridges, T., Cannon, R., Collins, C., Couch, W., Cross, N., Deeley, K., De Propris, R., Driver, S. P., Efstathiou, G., Ellis, R. S., Frenk, C. S., Glazebrook, K., Jackson, C., Lahav, O., Lewis, I., Lumsden, S.,

- Madgwick, D., Peacock, J. A., Peterson, B. A., Price, I., Seaborne, M., and Taylor, K. (2001). The 2dF Galaxy Redshift Survey: spectra and redshifts. *MNRAS*, 328:1039–1063.
- Colless, M., Peterson, B. A., Jackson, C., Peacock, J. A., Cole, S., Norberg, P., Baldry, I. K., Baugh, C. M., Bland-Hawthorn, J., Bridges, T., Cannon, R., Collins, C., Couch, W., Cross, N., Dalton, G., De Propris, R., Driver, S. P., Efstathiou, G., Ellis, R. S., Frenk, C. S., Glazebrook, K., Lahav, O., Lewis, I., Lumsden, S., Maddox, S., Madgwick, D., Sutherland, W., and Taylor, K. (2003). The 2dF Galaxy Redshift Survey: Final Data Release. *ArXiv Astrophysics e-prints*.
- Courteau, S., Dutton, A. A., van den Bosch, F. C., MacArthur, L. A., Dekel, A., McIntosh, D. H., and Dale, D. A. (2007). Scaling Relations of Spiral Galaxies. *ApJ*, 671:203–225.
- Courteau, S. and Rix, H.-W. (1999). Maximal Disks and the Tully-Fisher Relation. *ApJ*, 513:561–571.
- De Rijcke, S., Zeilinger, W. W., Hau, G. K. T., Prugniel, P., and Dejonghe, H. (2007). Generalizations of the Tully-Fisher Relation for Early- and Late-Type Galaxies. *ApJ*, 659:1172–1175.
- de Rossi, M. E., Tissera, P. B., and Pedrosa, S. E. (2010). Impact of supernova feedback on the Tully-Fisher relation. *A&A*, 519:A89.
- Dekel, A. and Birnboim, Y. (2008). Gravitational quenching in massive galaxies and clusters by clumpy accretion. *MNRAS*, 383:119–138.
- deSouza, R. E., Gadotti, D. A., and dos Anjos, S. (2004). BUDDA: A New Two-dimensional Bulge/Disk Decomposition Code for Detailed Structural Analysis of Galaxies. *ApJS*, 153:411–427.
- Dutton, A. A. and van den Bosch, F. C. (2009). The impact of feedback on disc galaxy scaling relations. *MNRAS*, 396:141–164.
- Dutton, A. A., van den Bosch, F. C., Dekel, A., and Courteau, S. (2007). A Revised Model for the Formation of Disk Galaxies: Low Spin and Dark Halo Expansion. *ApJ*, 654:27–52.

- Dutton, A. A., van den Bosch, F. C., Faber, S. M., Simard, L., Kassin, S. A., Koo, D. C., Bundy, K., Huang, J., Weiner, B. J., Cooper, M. C., Newman, J. A., Mozena, M., and Koekemoer, A. M. (2011). On the evolution of the velocity-mass-size relations of disc-dominated galaxies over the past 10 billion years. *MNRAS*, 410:1660–1676.
- Eisenstein, D. J. and Loeb, A. (1996). Can the Tully-Fisher Relation Be the Result of Initial Conditions? *ApJ*, 459:432.
- Eke, V. R., Baugh, C. M., Cole, S., Frenk, C. S., Norberg, P., Peacock, J. A., Baldry, I. K., Bland-Hawthorn, J., Bridges, T., Cannon, R., Colless, M., Collins, C., Couch, W., Dalton, G., de Propris, R., Driver, S. P., Efstathiou, G., Ellis, R. S., Glazebrook, K., Jackson, C., Lahav, O., Lewis, I., Lumsden, S., Maddox, S., Madgwick, D., Peterson, B. A., Sutherland, W., and Taylor, K. (2004). Galaxy groups in the 2dFGRS: the group-finding algorithm and the 2PIGG catalogue. *MNRAS*, 348:866–878.
- Elmegreen, B. G. (2011). Gravitational Instabilities in Two-component Galaxy Disks with Gas Dissipation. *ApJ*, 737:10.
- Eskridge, P. B., Frogel, J. A., Pogge, R. W., Quillen, A. C., Berlind, A. A., Davies, R. L., DePoy, D. L., Gilbert, K. M., Houdashelt, M. L., Kuchinski, L. E., Ramírez, S. V., Sellgren, K., Stutz, A., Terndrup, D. M., and Tiede, G. P. (2002). Near-Infrared and Optical Morphology of Spiral Galaxies. *APJS*, 143:73–111.
- Firmani, C. and Avila-Reese, V. (2000). Disc galaxy evolution models in a hierarchical formation scenario: structure and dynamics. *MNRAS*, 315:457–472.
- Fisher, D. B. and Drory, N. (2008). The Structure of Classical Bulges and Pseudobulges: the Link Between Pseudobulges and Sérsic Index. *AJ*, 136:773–839.
- Fisher, D. B. and Drory, N. (2010). Bulges of Nearby Galaxies with Spitzer: Scaling Relations in Pseudobulges and Classical Bulges. *ApJ*, 716:942–969.

- Fisher, D. B. and Drory, N. (2011). Demographics of Bulge Types within 11 Mpc and Implications for Galaxy Evolution. *ApJL*, 733:L47.
- Fisher, D. B., Drory, N., and Fabricius, M. H. (2009). Bulges of Nearby Galaxies with Spitzer: The Growth of Pseudobulges in Disk Galaxies and its Connection to Outer Disks. *ApJ*, 697:630–650.
- Freeman, K. C. (1970). On the Disks of Spiral and so Galaxies. *ApJ*, 160:811.
- Frenk, C. S. and White, S. D. M. (2012). Dark matter and cosmic structure. *Annalen der Physik*, 524:507–534.
- Gadotti, D. A. (2009). Structural properties of pseudo-bulges, classical bulges and elliptical galaxies: a Sloan Digital Sky Survey perspective. *mnras*, 393:1531–1552.
- Geha, M., Blanton, M. R., Masjedi, M., and West, A. A. (2006). The Baryon Content of Extremely Low Mass Dwarf Galaxies. *ApJ*, 653:240–254.
- Gnedin, O. Y., Kravtsov, A. V., Klypin, A. A., and Nagai, D. (2004). Response of Dark Matter Halos to Condensation of Baryons: Cosmological Simulations and Improved Adiabatic Contraction Model. *ApJ*, 616:16–26.
- Gnedin, O. Y., Weinberg, D. H., Pizagno, J., Prada, F., and Rix, H.-W. (2007). Dark Matter Halos of Disk Galaxies: Constraints from the Tully-Fisher Relation. *ApJ*, 671:1115–1134.
- Gottlöber, S., Klypin, A., and Kravtsov, A. V. (2001). Merging History as a Function of Halo Environment. *ApJ*, 546:223–233.
- Graham, A. W. and Driver, S. P. (2005). A Concise Reference to (Projected) Sérsic $R^{1/n}$ Quantities, Including Concentration, Profile Slopes, Petrosian Indices, and Kron Magnitudes. *PASA*, 22:118–127.
- Guo, Q., White, S., Boylan-Kolchin, M., De Lucia, G., Kauffmann, G., Lemson, G., Li, C., Springel, V., and Weinmann, S. (2011). From dwarf spheroidals to cD galaxies: simulating the galaxy population in a Λ CDM cosmology. *MNRAS*, 413:101–131.

- Hernquist, L. (1990). An analytical model for spherical galaxies and bulges. *ApJ*, 356:359–364.
- Hoffmann, V. and Romeo, A. B. (2012). The effect of ISM turbulence on the gravitational instability of galactic discs. *MNRAS*, 425:1511–1520.
- Hopkins, P. F., Bundy, K., Croton, D., Hernquist, L., Keres, D., Khochfar, S., Stewart, K., Wetzel, A., and Younger, J. D. (2010). Mergers and Bulge Formation in Λ CDM: Which Mergers Matter? *ApJ*, 715:202–229.
- Kauffmann, G., Heckman, T. M., White, S. D. M., Charlot, S., Tremonti, C., Brinchmann, J., Bruzual, G., Peng, E. W., Seibert, M., Bernardi, M., Blanton, M., Brinkmann, J., Castander, F., Csabai, I., Fukugita, M., Ivezić, Z., Munn, J. A., Nichol, R. C., Padmanabhan, N., Thakar, A. R., Weinberg, D. H., and York, D. (2003a). Stellar masses and star formation histories for 10^5 galaxies from the Sloan Digital Sky Survey. *MNRAS*, 341:33–53.
- Kauffmann, G., Heckman, T. M., White, S. D. M., Charlot, S., Tremonti, C., Peng, E. W., Seibert, M., Brinkmann, J., Nichol, R. C., SubbaRao, M., and York, D. (2003b). The dependence of star formation history and internal structure on stellar mass for 10^5 low-redshift galaxies. *MNRAS*, 341:54–69.
- Kennicutt, Jr., R. C., Lee, J. C., Funes, José G., S. J., Sakai, S., and Akiyama, S. (2008). An $\mathrm{H}\alpha$ Imaging Survey of Galaxies in the Local 11 Mpc Volume. *APJS*, 178:247–279.
- Knebe, A., Pearce, F. R., Lux, H., Ascasibar, Y., Behroozi, P., Casado, J., Moran, C. C., Diemand, J., Dolag, K., Dominguez-Tenreiro, R., Elahi, P., Falck, B., Gottlöber, S., Han, J., Klypin, A., Lukić, Z., Maciejewski, M., McBride, C. K., Merchán, M. E., Muldrew, S. I., Neyrinck, M., Onions, J., Planelles, S., Potter, D., Quilis, V., Rasera, Y., Ricker, P. M., Roy, F., Ruiz, A. N., Sgró, M. A., Springel, V., Stadel, J., Sutter, P. M., Tweed, D., and Zemp, M. (2013). Structure finding in cosmological simulations: the state of affairs. *MNRAS*, 435:1618–1658.
- Kormendy, J. (2013). *Secular Evolution in Disk Galaxies*, page 1.

- Kormendy, J. and Kennicutt, Jr., R. C. (2004). Secular Evolution and the Formation of Pseudobulges in Disk Galaxies. *ARA&A*, 42:603–683.
- Kravtsov, A., Vikhlinin, A., and Meshcheryakov, A. (2014). Stellar mass – halo mass relation and star formation efficiency in high-mass halos. *ArXiv e-prints*.
- Kroupa, P., Tout, C. A., and Gilmore, G. (1993). The distribution of low-mass stars in the Galactic disc. *MNRAS*, 262:545–587.
- Li, C., Kauffmann, G., Jing, Y. P., White, S. D. M., Börner, G., and Cheng, F. Z. (2006). The dependence of clustering on galaxy properties. *MNRAS*, 368:21–36.
- Maller, A. H., Berlind, A. A., Blanton, M. R., and Hogg, D. W. (2009). The Intrinsic Properties of SDSS Galaxies. *ApJ*, 691:394–406.
- Marleau, F. R. and Simard, L. (1998). Quantitative Morphology of Galaxies in the Hubble Deep Field. *ApJ*, 507:585–600.
- Masters, K. L., Mosleh, M., Romer, A. K., Nichol, R. C., Bamford, S. P., Schawinski, K., Lintott, C. J., Andreescu, D., Campbell, H. C., Crowcroft, B., Doyle, I., Edmondson, E. M., Murray, P., Raddick, M. J., Slosar, A., Szalay, A. S., and Vandenberg, J. (2010). Galaxy Zoo: passive red spirals. *MNRAS*, 405:783–799.
- McGaugh, S. S. (2005). The Baryonic Tully-Fisher Relation of Galaxies with Extended Rotation Curves and the Stellar Mass of Rotating Galaxies. *ApJ*, 632:859–871.
- McGaugh, S. S. (2011). Novel Test of Modified Newtonian Dynamics with Gas Rich Galaxies. *Physical Review Letters*, 106(12):121303.
- Mo, H. J., Mao, S., and White, S. D. M. (1998). The formation of galactic discs. *mnras*, 295:319–336.
- Mortlock, A., Conselice, C. J., Hartley, W. G., Ownsworth, J. R., Lani, C., and et al. (2013). The redshift and mass dependence on the formation of the Hubble sequence at $z > 1$ from CANDELS/UDS. *MNRAS*, 433:1185–1201.

- Mosleh, M., Williams, R. J., and Franx, M. (2013). On the Robustness of $z = 0\text{--}1$ Galaxy Size Measurements through Model and Non-parametric Fits. *ApJ*, 777:117.
- Moster, B. P., Naab, T., and White, S. D. M. (2013). Galactic star formation and accretion histories from matching galaxies to dark matter haloes. *MNRAS*, 428:3121–3138.
- Muñoz-Cuartas, J. C., Macciò, A. V., Gottlöber, S., and Dutton, A. A. (2011). The redshift evolution of Λ cold dark matter halo parameters: concentration, spin and shape. *MNRAS*, 411:584–594.
- Peng, C. Y., Ho, L. C., Impey, C. D., and Rix, H.-W. (2002). Detailed Structural Decomposition of Galaxy Images. *AJ*, 124:266–293.
- Peng, Y.-j., Lilly, S. J., Renzini, A., and Carollo, M. (2012). Mass and Environment as Drivers of Galaxy Evolution. II. The Quenching of Satellite Galaxies as the Origin of Environmental Effects. *ApJ*, 757:4.
- Perez, J., Valenzuela, O., Tissera, P. B., and Michel-Dansac, L. (2013). Clumpy disc and bulge formation. *MNRAS*, 436:259–265.
- Persic, M. and Salucci, P. (1997). VizieR Online Data Catalog: Spiral galaxies rotation curves (Persic+ 1995). *VizieR Online Data Catalog*, 209:90501.
- Petric, A. O. and Rupen, M. P. (2007). H I Velocity Dispersion in NGC 1058. *AJ*, 134:1952–1962.
- Planck Collaboration, Ade, P. A. R., Aghanim, N., Armitage-Caplan, C., Arnaud, M., Ashdown, M., Atrio-Barandela, F., Aumont, J., Baccigalupi, C., Banday, A. J., and et al. (2013). Planck 2013 results. XVI. Cosmological parameters. *ArXiv e-prints*.
- Rodríguez-Puebla, A., Avila-Reese, V., and Drory, N. (2013). The Galaxy-Halo/Subhalo Connection: Mass Relations and Implications for Some Satellite Occupational Distributions. *ApJ*, 767:92.

- Rodríguez-Puebla, A., Avila-Reese, V., Yang, X., Foucaud, S., Drory, N., and Jing, Y. P. (2014). The stellar-to-halo mass relations of local galaxies segregated by color. *ArXiv e-prints*.
- Rodríguez-Puebla, A., Drory, N., and Avila-Reese, V. (2012). The Stellar-Subhalo Mass Relation of Satellite Galaxies. *ApJ*, 756:2.
- Romeo, A. B. and Wiegert, J. (2011). The effective stability parameter for two-component galactic discs. *MNRAS*, 416:1191–1196.
- Sackett, P. D. (1997). Does the Milky Way Have a Maximal Disk? *ApJ*, 483:103–110.
- Salim, S., Rich, R. M., Charlot, S., Brinchmann, J., Johnson, B. D., Schiminovich, D., Seibert, M., Mallory, R., Heckman, T. M., Forster, K., Friedman, P. G., Martin, D. C., Morrissey, P., Neff, S. G., Small, T., Wyder, T. K., Bianchi, L., Donas, J., Lee, Y.-W., Madore, B. F., Milliard, B., Szalay, A. S., Welsh, B. Y., and Yi, S. K. (2007). UV Star Formation Rates in the Local Universe. *ApJs*, 173:267–292.
- Schawinski, K., Lintott, C., Thomas, D., Sarzi, M., Andreescu, D., Bamford, S. P., Kaviraj, S., Khochfar, S., Land, K., Murray, P., Nichol, R. C., Radnick, M. J., Slosar, A., Szalay, A., Vandenberg, J., and Yi, S. K. (2009). Galaxy Zoo: a sample of blue early-type galaxies at low redshift. *MNRAS*, 396:818–829.
- Sérsic, J. L. (1963). Influence of the atmospheric and instrumental dispersion on the brightness distribution in a galaxy. *Boletin de la Asociacion Argentina de Astronomia La Plata Argentina*, 6:41.
- Sersic, J. L. (1968). *Atlas de galaxias australes*.
- Shadmehri, M. and Khajenabi, F. (2012). On the gravitational stability of a galactic disc as a two-fluid system. *MNRAS*, 421:841–846.
- Shen, S., Mo, H. J., White, S. D. M., Blanton, M. R., Kauffmann, G., Voges, W., Brinkmann, J., and Csabai, I. (2003). The size distribution of galaxies in the Sloan Digital Sky Survey. *mnras*, 343:978–994.

- Shen, Y. and Lou, Y.-Q. (2003). Axisymmetric stability criterion for two gravitationally coupled singular isothermal discs. *MNRAS*, 345:1340–1350.
- Sheth, R. K. and Tormen, G. (1999). Large-scale bias and the peak background split. *MNRAS*, 308:119–126.
- Simard, L., Willmer, C. N. A., Vogt, N. P., Sarajedini, V. L., Phillips, A. C., Weiner, B. J., Koo, D. C., Im, M., Illingworth, G. D., and Faber, S. M. (2002). The DEEP Groth Strip Survey. II. Hubble Space Telescope Structural Parameters of Galaxies in the Groth Strip. *APJS*, 142:1–33.
- Tamburro, D., Rix, H.-W., Leroy, A. K., Mac Low, M.-M., Walter, F., Kennicutt, R. C., Brinks, E., and de Blok, W. J. G. (2009). What is Driving the H I Velocity Dispersion? *AJ*, 137:4424–4435.
- Toomre, A. (1964). On the gravitational stability of a disk of stars. *ApJ*, 139:1217–1238.
- Tully, R. B. and Fisher, J. R. (1977). A new method of determining distances to galaxies. *A&A*, 54:661–673.
- van den Bosch, F. C. (2000a). Semianalytical Models for the Formation of Disk Galaxies. I. Constraints from the Tully-Fisher Relation. *ApJ*, 530:177–192.
- van den Bosch, F. C. (2000b). Semianalytical Models for the Formation of Disk Galaxies. I. Constraints from the Tully-Fisher Relation. *ApJ*, 530:177–192.
- van den Bosch, F. C., Abel, T., Croft, R. A. C., Hernquist, L., and White, S. D. M. (2002). The Angular Momentum of Gas in Protogalaxies. I. Implications for the Formation of Disk Galaxies. *ApJ*, 576:21–35.
- van Zee, L. and Bryant, J. (1999). Neutral Gas Distribution and Kinematics of the Nearly Face-on Spiral Galaxy NGC 1232. *AJ*, 118:2172–2183.
- Weinzirl, T., Jogee, S., Khochfar, S., Burkert, A., and Kormendy, J. (2009). Bulge n and B/T in High-Mass Galaxies: Constraints on the Origin of Bulges in Hierarchical Models. *ApJ*, 696:411–447.

- Wyse, R. F. G., Gilmore, G., and Franx, M. (1997). Galactic Bulges. *ARA&A*, 35:637–675.
- Zavala, J., Avila-Reese, V., Firmani, C., and Boylan-Kolchin, M. (2012). The growth of galactic bulges through mergers in Λ CDM haloes revisited - I. Present-day properties. *MNRAS*, 427:1503–1516.
- Zavala, J., Avila-Reese, V., Hernández-Toledo, H., and Firmani, C. (2003). The luminous and dark matter content of disk galaxies. *A&A*, 412:633–650.
- Zavala, J., Okamoto, T., and Frenk, C. S. (2008). Bulges versus discs: the evolution of angular momentum in cosmological simulations of galaxy formation. *MNRAS*, 387:364–370.